UNIVERSITY OF OKLAHOMA

GRADUATE COLLEGE

ENHANCING PERFORMANCE AND REDUCING EMISSIONS IN NATURAL GAS ASPIRATED ENGINES THROUGH MACHINE LEARNING ALGORITHM

A THESIS

SUBMITTED TO THE GRADUATE FACULTY

in partial fulfillment of the requirements for the

Degree of

MASTER OF SCIENCE

By

MOHAMMED AMEER MOINUDDIN ANSARI

Norman, Oklahoma

2023

ENHANCING PERFORMANCE AND REDUCING EMISSIONS IN NATURAL GAS ASPIRATED ENGINES THROUGH MACHINE LEARNING ALGORITHM

A THESIS APPROVED FOR THE
SCHOOL OF AEROSPACE AND MECHANICAL ENGINEERING

BY THE COMMITTEE CONSISTING OF

Dr. Pejman Kazempoor, Chair

Dr. Wilson E. Merchan-Merchan

Dr. Iman Ghamarian

Acknowledgments

Firstly, I am deeply grateful for the guidance and support provided by my advisor, Dr. Pejman Kazempoor, whose expertise and mentorship have been invaluable throughout my research journey. His encouragement and wisdom have not only shaped this work but have also been instrumental in my personal and professional growth.

My sincere appreciation extends to the committee members, Dr. Wilson E. Merchan-Merchan and Dr. Iman Ghamarian, for their insightful feedback and the valuable time they dedicated to enriching my thesis.

I owe a profound debt of gratitude to my parents, whose unwavering support and belief in my abilities have been the cornerstone of my career. Their love and encouragement have been my guiding light, providing strength and inspiration at every step.

A special acknowledgment goes to my sister, who has been nothing short of a backbone throughout this journey. Her steadfast support, unwavering faith, and invaluable encouragement have been my constant source of motivation. In her, I found not just a sister but a mentor and a friend. "She is not just a sister, but a star that brightens my world."

I extend my thanks to all my colleagues at the Sustainable Energy and Carbon Management Center (SECM) at the University of Oklahoma. I am particularly grateful to team members Hafiz Ahmad Hassan, Carlos de Castro Pena, Matthew D. Hartless, Tu Nguyen, Raelin B. Lane, and our Lab manager James D. Lynch, for their collaboration, camaraderie, and shared commitment to our collective goals.

Each of you has played a pivotal role in this journey, and for that, I am eternally grateful.

Abstract

In an era where the global energy landscape is increasingly defined by the dual imperatives of efficiency and sustainability, the natural gas sector stands at a crucial juncture. The engines powering this sector, especially Natural Gas Fired Reciprocating Engines (NGFRE), are well known for their performance as well as considerable emissions, posing a stark challenge to environmental sustainability goals. This thesis addresses this pivotal issue, presenting a machine learning-based solution to optimize NGFRE performance while substantially reducing their environmental footprint.

The research is anchored in an experimental framework involving the AJAX DPC-81 engine compressor, evaluated across a spectrum of operational loads from 40% to 75%. The study leverages an extensive array of sensors to collect detailed real-time data on engine performance, emissions, and vibration parameters. Central to the methodology is the strategic adjustment of the Air Management System (AMS), varying air/fuel ratio to explore their impact on engine dynamics and emissions. The study also incorporates a comprehensive vibration analysis, providing critical insights into the engine's operational stability under different load conditions. Machine Learning (ML) techniques, including Linear Regression, Artificial Neural Networks (ANN), and Support Vector Machines (SVM), are integrated with a Programmable Logic Controller (PLC). This integration not only facilitates a nuanced analysis of the collected data but also enables the accurate prediction of engine performance, paving the way for real-time adaptive control systems.

The findings of this research are both revealing and impactful. A notable instance is observed at a 40% engine load with a 70% bypass valve opening, where emissions of methane (CH_4) plummet by 64%, nitrogen oxides (NOx) by 52%, and Volatile Organic Compounds (VOC) by 50%. This substantial decrease highlights the effectiveness of the ML-driven approach in curbing harmful

emissions. Further, the study unveils the manipulation of the bypass valve position can lead to enhanced fuel efficiency and improved engine stability. For example, at a 75% engine load, the research demonstrates that optimal emission reduction is achieved with a mere 10% bypass valve opening, illuminating the delicate interplay between engine load parameters and environmental emissions.

In conclusion, the study demonstrates the effectiveness of ML in enhancing NGFRE performance. It sets a foundation for developing intelligent engine systems that can self-adjust for optimal performance and minimal environmental impact, forging a path to a future where the two are seamlessly integrated.

Table of Contents

Abbreviations

NG:	Natural gas	ITE:	Indicated thermal efficiency
AFR:	Air-to-fuel ratio	N_2:	Nitrogen
BDC:	Bottom-dead-center	NSPS:	New Source Performance Standards
BTE:	Brake thermal efficiency	NOx:	Nitrogen oxides
BSFC:	Brake-specific fuel consumption	O_2:	Oxygen
CNG:	Compressed natural gas	PM:	Particulate matter
CO:	Carbon monoxide	VOCs:	Volatile organic compounds
CO_2:	Carbon dioxide	FFT:	Fast fourier transform
COV:	Coefficient of variation	MSE:	Mean square error
COx:	Carbon oxides	RMSE:	Root mean square error
EPA:	Environmental Protection Agency	MAE:	Mean absolute error
EGR:	Exhaust gas recirculation	R^2:	R-squared
H_2:	Hydrogen		
H_2S:	Hydrogen sulfide		
HC:	Hydrocarbon		
HRR:	Heat release rate		
ICE:	Internal combustion engine		
IMEP:	Indicated means effective pressure		
SIE:	Spark ignition engine		
SOx:	Sulfur oxides		
TDC:	Top-dead-center		

List of Figures

List of Tables

Chapter 1: Introduction

1.1 Background

Energy serves as the foundation for economic growth and development. Energy stands as the bedrock of economic vigor and advancement. The discovery of large reserves of natural gas in various countries as well as improved distribution of gas has made possible a wide variety of uses. Presently, fossil fuels predominantly fulfill the global energy demand with over 80%. Nevertheless, the technologies associated with fossil fuel extraction, transportation, processing, and, notably, their utilization especially combustion have adverse consequences on the environment, leading to both direct and indirect detrimental effects on the economy [1-6].

Natural Gas (NG) has served as a fuel for more than a century. It underwent significant advancements, particularly during the oil crises of 1974 and 1980 [7]. In the past two decades, reserves of NG varied from 123.5 trillion cubic meters (Tcm) in 1996 to 186.6 Tcm in 2016, increasing by 51.1% [8]. However, NG has emerged as a highly favored energy source that effectively addresses engine-related combustion issues while matching energy density [9]. Various countries consider NG a prime candidate for powering vehicles due to its abundant availability, cost-effectiveness, lower emissions, and compatibility with traditional diesel and gasoline engines. Notably, among fossil fuels, NG combustion yields the most minor greenhouse gas emissions and minimal suspended particles [10].

NG refers to hydrocarbon-rich gas as a gaseous fossil fuel that is found in oil fields and natural gas fields. It occasionally contains carbon dioxide (CO_2), nitrogen (N_2), and helium (He) depending on factors such as climate, location, or processing [11, 12]. While it is commonly grouped with

other fossil fuels and sources of energy, many characteristics of NG make it unique. The term NG is often extended to gases and liquids from the recently developed shale formations [13-16] as well as gas (biogas) produced from biological sources [17-19]. Along with these newer uses, there has been an increased need not only for the compositional analysis of natural gas but also for analytical data that provide other information about the behavior of natural gas. Consequently, the utilization of natural gas as a vehicle fuel has gained substantial traction in recent years, and this trend is anticipated to persist [20].

NG is considered a promising fuel for both sustainability and alternative fuels due to its interesting chemical properties with a high H/C ratio and high research octane number (about 130) [21]. It also has relatively wide flammability limits [22]. The lower peak combustion temperatures under ultra-lean conditions in comparison to stoichiometric conditions lead to a lower knock tendency of NG engines, allowing a higher power for the same engine displacement by increasing the boost pressure level [23].

Engines powered by NG and engineered for high compression ratios, lean-burn conditions, or extensive exhaust gas recirculation are positioned to potentially exceed the performance metrics of gasoline engines in terms of torque and power [24, 25]. These engines also show promise in significantly reducing emissions and improving thermal efficiency [25]. NG engines have been demonstrated to emit less CO_2 than diesel engines at equivalent air-fuel ratios while maintaining similar levels of thermal efficiency in very lean conditions [26, 27]. Exceptionally low levels of nitrogen oxide (NO_x) and carbon Monoxide (CO) emissions have been achieved at lean equivalence ratios [12]. Moreover, unburned hydrocarbon (HC) emissions can also be reduced below the corresponding levels for gasoline engines, [28]. However, NG engines produce lower power than gasoline engines and have higher combustion instability in lean burn conditions [29].

Despite these challenges, the trend toward increased production and utilization of NG is on the rise [30]. This is highlighted by the widespread consumption across various sectors, as depicted in Figure 1, signaling NG's critical role in the current energy paradigm and accentuating the pressing need to prioritize advancements in this field.

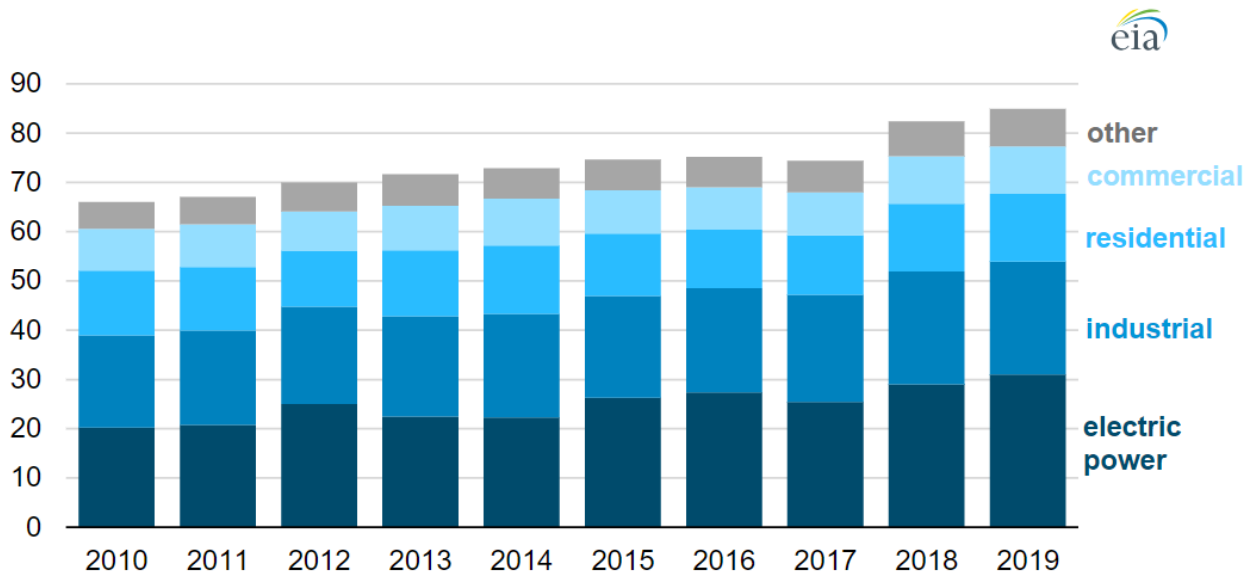

Figure 1. U.S. Natural Gas Consumption by Sector from 2010 to 2019(billion cubic feet per day).[www.eia.gov]

Reciprocating engines are pivotal in the processing and transportation of NG. Their ability to achieve substantial pressure ratios makes them indispensable in settings such as oil refineries, power generation facilities, and compressed natural gas (CNG) stations [31-34]. Although these compressors are designed for steady, rated loads, they often operate under fluctuating demands, deviating from ideal conditions. This variability has notable implications, especially in the Transmission and Storage (T&S) sector of the natural gas industry, where methane (CH_4) emissions are a significant concern, accounting for approximately one-third of the sector's methane emissions [35].

Two-stroke reciprocating engines are lauded for their impressive power-to-weight ratio, straightforward design, and compact nature, outpacing their four-stroke counterparts. However, this advantage is offset by their higher fuel consumption and emissions profile [36]. Among the environmental concerns is the release of CH_4 when NG is used as fuel. Methane's global warming potential towers over that of CO_2, being 25 to 30 times more impactful over a century [37-39]. This issue is particularly acute in two-stroke engines where the design of their ports and the resultant scavenging losses elevate the amount of unburned fuel, further exacerbating methane emissions [12]. Therefore, mitigating methane emissions from two-stroke Natural Gas Fired Reciprocating Engines (NGFREs) becomes critically important. Adding to the challenge, NG combustion in these engines tends to be less stable under partial-load operations, presenting another front in the quest for efficient and environmentally friendly engine technology [29, 40].

The NG gathering sector in the United States is a vast network, boasting over 5,200 gathering stations [41]— hubs responsible for the compression and enhancement of natural gas quality—linked by an extensive web of approximately 407,000 miles of pipelines [42]. A decent number of compressors that are used in the compression stations are NGFRE's. The specialty of these integral engines is that the engine and compressor relate to the same crankshaft. The engine studied in this research is also an NGFRE which is discussed later in the methodology section in detail.

Typically, NGFREs are engineered for harsh operation, pausing only for oil changes, unforeseen downtime, or during the few months intervals of scheduled maintenance. Yet, the challenge lies in harnessing advanced technology to elevate their performance and minimize emissions—a task complicated by the remote locations of some compressors. These sites are often beyond the reach of regular monitoring, not due to a lack of will, but rather due to logistical and technological constraints [43].

1.2 Formation Processes and Hazards of Emissions

Nitrogen oxides (NOx), Carbon monoxide (CO), CH_4, and volatile organic compounds (VOCs) exert detrimental effects on both human health and the environment. Therefore, it is imperative to mitigate their release into the atmosphere [44]. Different emissions gasses are discussed below. Figure 2 shows the relationship between the equivalence ratio of a fuel-air mixture and various exhaust gas components typically measured in internal combustion engines. The equivalence ratio is a measure of the air-fuel mixture, with a value of 1.0 representing a stoichiometric mixture (the exact chemical balance between fuel and oxygen). Ratios below 1.0 indicate a fuel-lean mixture (excess air), while ratios above 1.0 indicate a fuel-rich mixture (excess fuel). The curve for NOx peaks just before the equivalence ratio of 1.0, suggesting that NOx emissions are highest near the stoichiometric ratio and decrease in both fuel-rich and fuel-lean conditions. The HC curve, on the other hand, shows higher concentrations in fuel-rich conditions and drops as the mixture becomes leaner. The CO curve peaks in fuel-rich conditions (indicating incomplete combustion) and decreases towards leaner mixtures. The O_2 curve shows the remaining oxygen in the exhaust, which is higher in lean conditions due to excess air and lower in rich conditions as more oxygen is consumed during combustion [45].

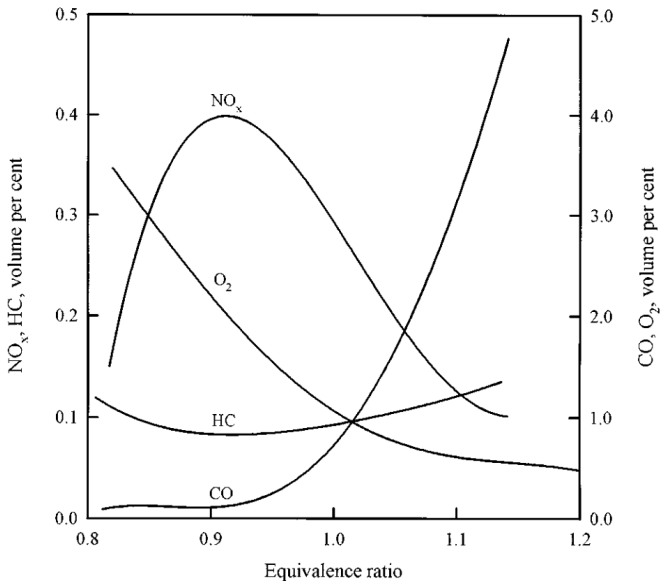

Figure 2. Spark-ignition engine emissions for different fuel/air ratios adapted from Stone, 1991[45]

1.2.1 NOx

NO_2 is distinguished by a reddish-brown hue and is toxic and corrosive, becoming visibly noticeable when present in substantial ambient quantities [46]. NOx constitutes a group of emissions of significant concern in spark-ignition (SI) engines, encompassing several compounds such as nitric oxide (NO), NO_2, nitrous oxide (N_2O), dinitrogen trioxide (N_2O_3), and dinitrogen tetroxide (N_2O_4). Predominantly, NO and NO_2 are encountered, with the latter compounds occurring in relatively minor quantities [47]. Kinetic equations [1,2,3] represent the basic steps of the Zeldovich mechanism [48-50].

$$N_2+O\rightarrow NO+N \quad (1)$$

$$N+O_2\rightarrow NO+O \quad (2)$$

$$N+OH\rightarrow NO+H \quad (3)$$

The genesis of NOx in spark ignition (SI) engines is primarily through the oxidation of nitrogen molecules within the engine cylinders, a process that intensifies at elevated temperatures [51]. The factors influencing the formation of NOx include the availability of oxygen, the peak combustion temperature, the fuel-to-air ratio, and the duration available for the reaction between atmospheric oxygen and nitrogen [52, 53]. An effective strategy for NOx mitigation centers on precise engine control. In contrast to other emissions like CO, CH_4, and VOCs, where enhanced combustion efficiency yields notable reductions, NOx reduction demands targeted control measures due to its unique formation mechanisms during combustion.

1.2.2 CO

Carbon monoxide (CO), an invisible and odorless gas, poses a significant risk to human health. It can stealthily bind to hemoglobin in the blood, leading to oxygen deprivation. This insidious interaction can cause symptoms of suffocation even at low concentrations, highlighting the necessity for stringent controls on CO emissions [44]. The production of CO is intricately linked to the combustion process within an engine's cylinders. It is primarily the result of incomplete fuel burning, where the availability of unburnt fuel and the temperature within the combustion chamber dictate the decomposition and subsequent partial oxidation of fuel molecules [54-56]. Figure 3 shows the variation of CO in the engine.

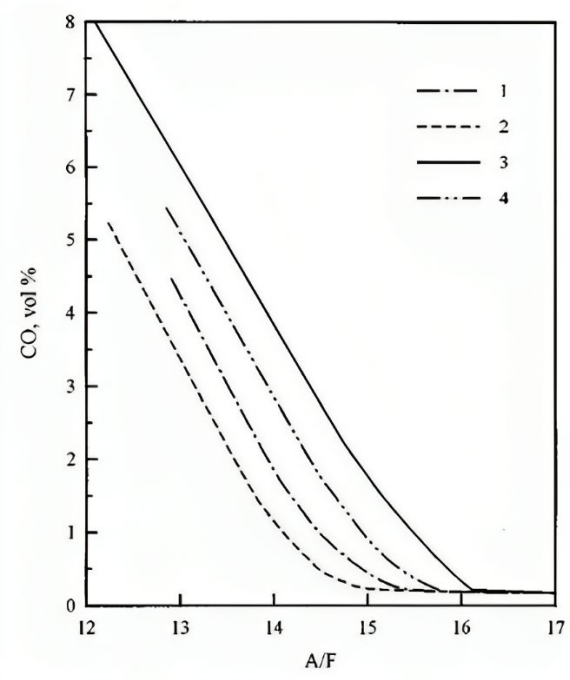

Figure 3. Variation of Carbon monoxide in SI engine with air/fuel ratio (adapted from Novak and Blumberg, 1978 [57])

The concentration of CO emissions is closely related to the air-to-fuel ratio during combustion. For fuel-lean mixtures, the CO levels tend to remain relatively constant, despite the variation in air-to-fuel ratios. However, CO can still be produced from fuel-lean mixtures due to factors such as suboptimal mixing, and localized pockets of rich fuel [58]. Notably, non-road vehicles and machinery account for a considerable portion of CO emissions, highlighting the broader environmental impact of this pollutant [59, 60].

1.2.3 VOCs

VOCs are a diverse group of carbon-based chemicals. VOCs are primarily formed during incomplete combustion when fuel is not fully oxidized [61, 62]. They can originate from a range of precursors within the natural gas itself, and their formation is influenced by various factors one of them being incomplete combustion with the presence of higher hydrocarbons [44]. The control of VOC emissions from natural gas engines is crucial due to their environmental and health

impacts, including their role in the formation of ground-level ozone and their potential to contribute to the greenhouse effect [63].

1.2.4 CH_4

CH_4 is the primary component of natural gas and a potent greenhouse gas with a global warming potential significantly higher than carbon dioxide over 100 years [64, 65]. In natural gas engines, methane is released during incomplete combustion processes, particularly under lean burn conditions or when misfires and incomplete fuel-air are mixed [66]. The formation of CH_4 is attributed to lower oxygen combustion temperatures. The engine design and operating conditions, such as the timing of ignition and the quality of the air-fuel mixture, can influence methane emissions. The hazards of methane extend beyond its immediate flammability and asphyxiation risks; its release into the atmosphere contributes considerably to climate change, making its mitigation in the exhaust systems of natural gas engines a critical environmental goal [67, 68].

Regarding other emissions like sulfur oxides (SO_x) and particulate matter (PM), they hold minimal importance for natural gas-fired engines. SO_x emissions are contingent on the sulfur content of the fuel, which is exceedingly low in natural gas fuels. Conversely, PM is a concern primarily for engines utilizing liquid fuels [69].

Table 1 shows the emission standards set by the Environmental Protection Agency (EPA) for a stationary NGFRE.

Table 1. New Source Performance Standards for Stationary Engines [70]

Engine type and fuel	Maximum engine power	Manufacture date	Emission standards (ppmvd ref. 15% O_2)		
			NOx	CO	VOCs
Non-emergency SI NG and non-emergency SI lean-burn LPG (except lean-burn 500 ≥ HP < 1350)	HP < 500	7/1/2008	220	610	80
		7/1/2011	150	610	80

1.3 Challenges to Reduce Emissions from Natural Gas Engines

In the pursuit of environmental sustainability and compliance with stringent regulatory standards, reducing emissions from natural gas engines presents a multi-faceted challenge. This section explores the inherent difficulties faced by the industry and the scientific community in mitigating emissions, underscoring the significance of the research objectives outlined in previous sections.

1.3.1 Technical Challenges

The technical complexity of natural gas engines is a primary barrier. The intricate balance required between combustion efficiency and emission formation is a delicate one. Achieving complete combustion, while simultaneously minimizing NOx, CO, CH_4, and VOCs, demands precise control over the combustion process [71]. Factors such as combustion chamber design [72, 73], fuel quality [74, 75], air-to-fuel ratio (AFR) [44], ignition timing [21], and exhaust gas recirculation [76] rates must all be optimized, often conflicting with one another in terms of desired outcomes.

Furthermore, the transient nature of engine operations, particularly in the oil and gas industry where engines often run at varying loads, exacerbates the difficulty of maintaining optimal combustion conditions. The lag in response times of current feedback and control systems may lead to periods of suboptimal performance, where emissions could spike beyond acceptable levels [77].

1.3.2 Operational Challenges

Operational practices also contribute to the challenge of emissions reduction. The variability in engine loads, the fluctuation of fuel composition, and the maintenance of engine components play significant roles in emissions profiles. Furthermore, the retrofitting of older equipment to meet new standards often requires significant capital investment and can lead to operational inefficiencies.

Furthermore, the integration of machine learning algorithms within existing Programmable Logic Controllers (PLCs) presents its own set of challenges. While PLCs are widely used in industrial control systems, they are traditionally not designed for the complex data processing required by sophisticated machine learning applications. Upgrading these systems to handle advanced analytics involves not just hardware and software changes, but also a rethinking of the operational protocols and data management practices [78].

In addressing these operational challenges, the research seeks to develop a comprehensive understanding of real-world engine operation and the factors influencing emissions. Such as the usage of sensors such as suction pressure, discharge pressure, speed, etc. This understanding is crucial for designing a predictive model that can account for the variability and unpredictability of operational conditions. The thesis aims to leverage real-time sensor data to inform machine

learning algorithms, enabling them to predict and adjust engine performance on the fly, thereby ensuring emission reductions even under the most challenging operational scenarios.

1.3.3 Regulatory Challenges

Regulatory frameworks continue to evolve, often outpacing the ability of industry stakeholders to comply. The gap between regulatory expectations and technological capabilities can lead to a situation where the available technology is not sufficient to meet the new standards, thereby requiring substantial research and development efforts.

Regulatory challenges represent a significant obstacle to the implementation of emission reduction strategies in NG engines. Compliance with environmental regulations requires constant vigilance and adaptation from operators in the oil and gas industry. The landscape of regulatory standards is both complex and dynamic, with variations not only at national levels but also across regional and local jurisdictions. The stringent emission standards set by bodies such as the Environmental Protection Agency (EPA) and the International Maritime Organization (IMO) necessitate the deployment of advanced technologies and practices to limit the output of NOx, CO, CH_4, and VOCs.

1.3.4 Monitoring and Prediction Challenges

Accurate monitoring and prediction of emissions are crucial for effective control strategies. However, the variability in operating conditions, coupled with the limitations of current sensing technologies, poses significant challenges in acquiring real-time, accurate emissions data. Furthermore, predictive models often require extensive data for training, which can be difficult and costly to obtain.

1.3.5 Research and Development Challenges

There is a need for an integrated approach that combines advanced modeling techniques, experimental data, and real-world operational insights to develop solutions that are both effective and pragmatic.

Engine Load is a parameter commonly used as a performance parameter to represent the amount of work done by the Engine. In the previous research Casting et al. [79] focused on modeling engine operation with a particular emphasis on volumetric, isentropic, and effective efficiencies. These efficiencies were found to be primarily dependent on two key parameters: the dead volumetric ratio, significantly affecting volumetric efficiency. Elhaj et al. [80] conducted a numerical study of a two-stage reciprocating engine, expanding diagnostic capabilities for predictive condition monitoring. comparison of detection and diagnosis techniques showed discrepancies with the vibration and acoustics sensors. However, the pressure measurement produced through that model is intrusive. Additionally, the accuracy is highly dependent on the usage of additional devices. Winandy et al. [81] presented a simplified model of an open-type reciprocating engine, revealing the key processes that influence mass flow rate, compressor power, and discharge temperature. A simplified steady-state model was proposed to determine the ambident losses and exhaust temperate, however, there is no utilization of this model on industrial compressors to prove its robustness. Farzaneh-Gord et al. [82] performed a thermodynamic optimization of design parameters for reciprocating air compressors, utilizing a mathematical model based on mass conservation. Although, the study revealed the area ratio of suction to discharge valve. There is no account for the engine's health and performance, which make a massive impact on the prediction of any parameter. Hennigsson et al. [83] predicted emissions such as NO_x using cylinder pressure data by using data-mining techniques. Although the prediction

accuracy was decent the research lacked in in utilizing the model in real-world scenarios because the model was validated using the static model. Yap et al. [84] presented a simulation-based work using an Artificial Neural Network (ANN) to optimize engine parameters to reduce emissions, however, the data collection was a huge concern. Additionally, the study was done on the steady AFR ratio which makes a dramatic difference in the combustion stability

To address these challenges, the current thesis endeavors to advance the understanding of emission processes and develop innovative solutions through the integration of real-time sensor data and machine learning algorithms into engine control systems. This research contributes to the broader goal of reducing the environmental impact of the oil and gas industry and advancing toward a more sustainable future.

1.4 Objectives of the Research

The objectives of this research encompass several key areas. First, it seeks a thorough comprehension of the variable to determine the optimum bypass valve position by analyzing the Air Management System (AMS) across different loads and bypass valve positions through performance and combustion analysis. Second, the study aims to explore the correlation between the engine load and the vibrations associated with it, this would determine whether the vibration can be used as a parameter to predict the engine performance. Finally, a precise machine learning algorithm is introduced, powered by real-time sensor data from the

, aimed at delivering precise predictions of engine performance. The primary goal is to reduce emissions from the engine, collectively contributing to performance enhancement and minimizing environmental impact within the oil and gas (O&G) sector.

1.5 Summary of Chapter One

In this chapter, the crucial role of emissions in the oil and gas industry has been discussed. NG remains a significant fossil fuel resource, especially in the context of reciprocating engines used for T&S. However, these engines pose a substantial challenge due to their significant contribution to methane and other emissions. The literature review revealed that there is less study on the utilization of real-time sensors to predict engine performance. This research sheds light on performance prediction and reduction of emissions from the industrial engine.

Chapter 2: Literature Review

In this section, the role of reciprocating engines in the natural gas industry is discussed. Different performance testing devices and research related to prediction of the engine performance are reviewed.

2.1 Industrial Engines and their Challenges

The United States has experienced an NG boom due to the development of unconventional wells development. The U.S. Energy Information Administration has forecasted natural gas production to increase by 56% by 2040 [85]. Much of this increase is a consequence of major added resources that have become accessible for commercial production due to advances in hydraulic fracturing and horizontal drilling. During this same period, the U.S. has seen an increased demand for NG in the stationary electricity generation and transportation sectors [41]. With the increasing energy demand, the use of NG to support these needs is also increasing at a great pace. It is also important to make sure that while the demands are met are focused on the harm it causes to the environment [41, 86]. Figure 4 shows the NG compression stations all over the U.S. and it is fascinating that a decent number of engines are used to meet the demand in the U.S.

Many of such engines used in the compression stations are NGFREs. What makes these integral engines unique is that the engine and compressor are connected to the same crankshaft. The engine used for the study is an NGFRE at SECM at the University of Oklahoma, which will be discussed in detail in the methodology section.

Reciprocating internal combustion engines, a well-established technology, are utilized extensively for various applications including power generation, transportation, and a multitude of industrial processes. Annually, the production of these engines on a global scale surpasses, underscoring

their prevalence and the scale of their use [87]. In the context of combined heat and power (CHP) installations, reciprocating engines offer a versatile range of capacities, extending from modest 10 kW units to substantial 10 MW single units. Moreover, by synchronizing multiple engines, it is possible to achieve even greater capacities, exceeding the 10 MW mark within a single power generation facility [88].

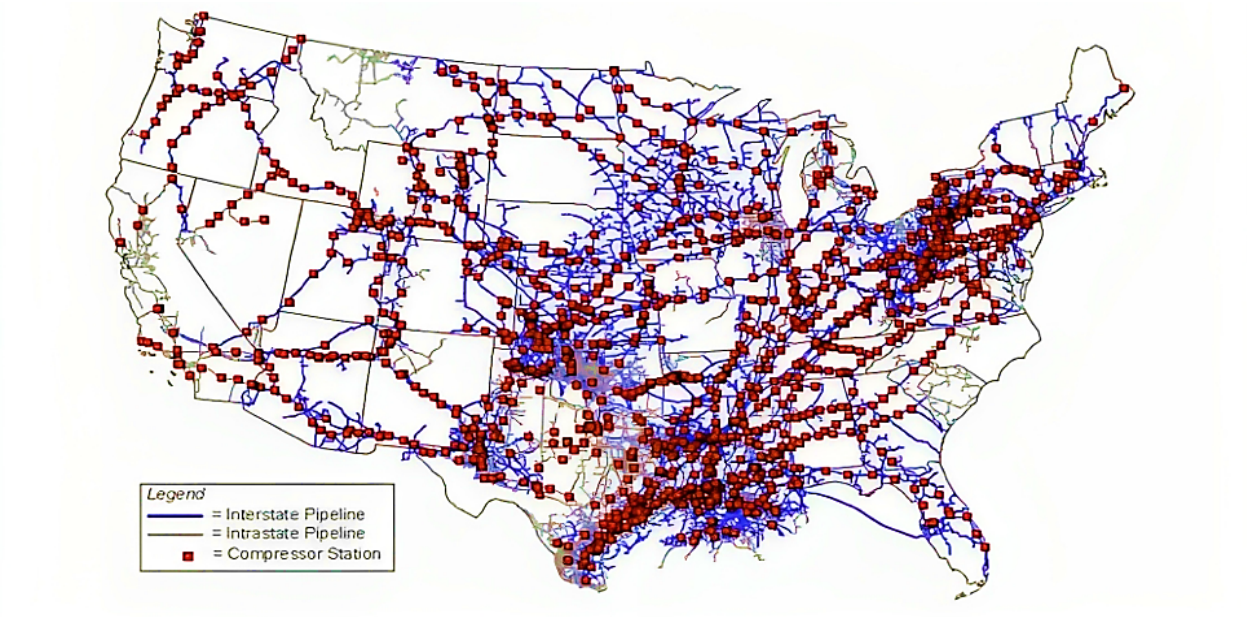

Figure 4. Natural Gas Compressor Station in the U.S (Map courtesy of U.S. Energy Information Administration (EIA))

NG, chiefly composed of methane, is typically both invisible and odorless, making its detection in upstream operations a challenge. Currently, methane stands as the second most prevalent greenhouse gas globally, contributing to 20% of worldwide greenhouse gas emissions [89]. Recognized for its potency and relatively short atmospheric lifetime compared to carbon dioxide, methane exerts a significant immediate impact on climate change [90, 91]. Indirectly, it also affects human health and plays a role in the atmospheric breakdown of various substances [92]. Notably, energy-related activities are responsible for approximately 20% of anthropogenic methane emissions, with the oil and gas sector being the predominant source within this category [93][5].

Numerous manufacturers provide these engines specifically for distributed power generation. Due to their operational efficiency and adaptability, natural gas-fueled reciprocating engines are particularly favored for Combined Heat Power CHP operations. They are designed for continuous operation and are only halted for reasons such as oil pumping malfunctions, unforeseen engine downtime, or scheduled maintenance, the latter of which typically occurs at multi-month intervals [94]. Figure 5 represents the different segments of methane emissions.

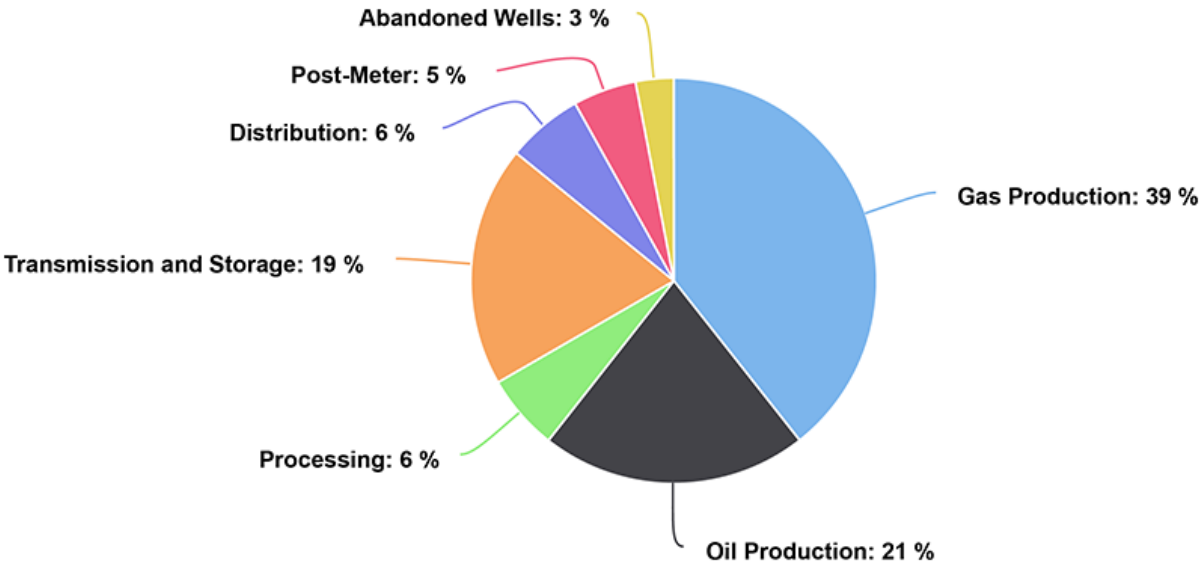

Figure 5. Methane Emission by Segments. Source (www.eia.com)

This underscores the sector's critical responsibility in the concerted efforts to reduce emissions and mitigate climate change. Within the spheres of regulation and operations, emissions of NG are categorized as either vented or fugitive. Emissions are deliberate discharges that occur under controlled conditions during standard operational processes. The patterns of NG emissions are notably inconsistent, displaying significant variations across both location and time [95-97], which complicates their predictability [98, 99]. On the other hand, fugitive emissions arise from

unintended releases due to equipment malfunctions, such as compromised valves or flange connections. However, when the combustion of the NG is involved in industrial engines, it tends to give more emissions.

This robust and continuous service profile underscores the importance of operational reliability and the need for effective emission management strategies, given the substantial role these engines play in the energy sector. The frequent and prolonged operation of these engines highlights the potential environmental impact they have, particularly in terms of CH_4 emissions, and the importance of developing and implementing emissions reduction technologies.

2.2 Techniques for Mitigating Emissions

In the realm of emission reduction strategies for SI engines, they can be broadly categorized into two distinct approaches: pre-combustion methods, involving adjustments to combustion parameters that effectively reduce emissions, and post-combustion methods, which center on treating exhaust gases independently after the combustion process has taken place. An explanation of different methods and their feasibility for the test engine was discussed.

2.2.1 Exhaust Gas Recirculation (EGR)

Exhaust Gas Recirculation (EGR) is recognized as an effective mechanism for mitigating the emission of NO_x, which are significant pollutants emitted by combustion engines [16]. EGR operates by recirculating a portion of an engine's exhaust gas back into the combustion chamber. This recycled gas acts as an inert buffer, mixing with the intake air and thereby reducing the overall oxygen content available for combustion. The result is a lower combustion flame temperature, which directly impacts the formation of NOx[100, 101].

The relationship between flame temperature and NOx production is critical; even modest decreases in temperature can lead to a substantial reduction in NOx levels due to the exponential relationship between temperature and NOx formation [102]. Through the application of EGR, the engine can maintain optimal combustion conditions and mitigate NOx emissions effectively without the need to retard injection timing. However, EGR can lead to increased fuel consumption and the potential for soot contamination in the engine's lubricating oil. Additionally, this technology is still in development for natural gas-burning engines, and due to substantial alterations required in the air intake and exhaust systems, it currently poses challenges in terms of cost-effectiveness [103].

2.2.2 Spark Retardation

In spark ignition engines, the formation of flame, premature burning, and behaviors of emissions are all influenced by ignition timing [55]. The impact of timing for spark on the combustion of an engine fueled with hydrogen was studied by Shi et al. [104]. They discovered that with the advanced spark ignition angle, the brake thermal efficiency initially increases followed by a decline. NO_X, HC, and CO emissions also decreased with retarded spark timing. NO_X emissions increase as the fraction of hydrogen volume increases, whereas HC and carbon monoxide are reduced. The impact of adding a high percentage of hydrogen on the performance of engines fueled by hydrogen–gasoline blends was studied by Elsemary et al. [105]. The finding was that at an ignition timing of 30 °CA BTDC, the consumption of fuel is reduced, and the thermal efficiency improves. Zhang et al. [106] studied the impact of a spark-timing hydrogen/methanol engine on combustion and emissions with the coefficient of excess air at 1.20 and discovered that with increased spark advance angles, after the initial increase, the indicated thermal efficiency begins to decline. Along with the more advanced ignition timing, the flame production time lengthens while the flame propagation period shortens. This technique is low-cost and easier to implement.

However, it does not provide convenient real-time access to altering combustion parameters while the engine operates.

2.2.3 Catalysts

In the operation of internal combustion engines, the exhaust stroke plays a pivotal role by expelling combusted gases through the exhaust system. These gases, comprising unburned hydrocarbons, nitrogen oxides (NO_x), and carbon monoxide (CO), are then routed through a device that resembles a muffler in appearance but serves a far more critical function—the catalytic converter [107, 108]. This component is essential in transforming harmful emissions into less hazardous substances via catalysis, a process of accelerated chemical reactions induced by catalysts. Given the crucial role of the catalytic converter, engine, and exhaust system design must be meticulously calibrated to ensure that emissions are effectively neutralized before release into the atmosphere [108].

The application of catalytic converters extends well beyond the realm of automotive emissions control. They are increasingly utilized across various industrial sectors, notably in processes such as hydrogen production and methane autothermal reforming, to curtail the emission of noxious gases [109]. In these settings, catalytic converters facilitate the reduction of complex pollutants into simpler, environmentally benign components, thereby contributing to cleaner production methods and adherence to stringent environmental regulations.

2.2.4 Fuel Blends

The concept of fuel blending involves the addition of alternative fuels to a primary fuel source to enhance engine performance and reduce emissions. Various blends have been explored for their efficacy in improving engine operation.

The integration of ethanol into fuel for spark-ignition engines, for instance, has been shown to improve thermal efficiency. This improvement is due to ethanol's compatibility with higher compression ratios, which enhances combustion without causing engine knock, thus enabling engines to operate more efficiently [5].

In another study, Tu et. al investigated the effects of hydrogen blending in NGFRE. They discovered that the addition of hydrogen stabilized engine performance, particularly when combined with the Air Management System (AMS). At higher loads, the engine demonstrated enhanced efficiency. An increase in indicated thermal efficiency (ITE) was also observed with hydrogen use. The researchers identified optimal operational conditions for the engine: a load of 60% with a bypass valve position of 60% and a hydrogen blend of 40%. These findings suggest that strategic blending of hydrogen with natural gas can lead to both stabilized engine performance and improved efficiency. However, despite the advantages offered by fuel blending, economic feasibility remains a significant concern. Many alternative fuels, including those that have shown promise in enhancing engine performance, are currently more expensive than conventional fuels. This cost barrier can limit the widespread adoption and routine use of alternative fuel blends. Additionally, some major concerns with the addition of hydrogen as a fuel include the high NO_x emissions and the in-cylinder temperature [110]

2.2.5 Air Management System (AMS)

In prior investigations, Hassan [44] showcased the effective regulation of the Air-Fuel Ratio (AFR) in an NGFRE using an AMS. The emissions, such as NO_x, CO, and VOCs, from a spark ignition engine were demonstrated to be highly contingent on the AFR. The complexity of controlling AFR in two-stroke engines was underscored, primarily due to the ratio of the mass of participating air in the combustion process to the mass of fuel, known as the actual or trapped AFR [111]. Hence,

achieving the optimal AFRs was accomplished indirectly through an AMS. During typical engine operation, as the piston approaches the top dead center (TDC), intake air is introduced through a stuffing box and a scavenging/reed valve into the non-combustion zone of the cylinder. The reed valve facilitates unidirectional airflow, permitting intake while closing during air escape attempts. As the piston moves towards the bottom dead center (BDC), this trapped air begins migrating towards the combustion zone through the opening generated between the piston and cylinder wall due to piston motion. The AFR is the ratio of the mass flow rate of air to the mass flow rate of fuel as given below.

$$AFR = \frac{\dot{m}_{air}}{\dot{m}_{fuel}}$$

Were,

$\dot{m}_{air} = mass\ flow\ rate\ of\ air$

$\dot{m}_{fuel} = mass\ flow\ rate\ of\ fuel$

The AMS encompasses a proportional butterfly valve, referred to as a bypass valve, which is orchestrated by a PLC. The optimal valve positions are ascertained experimentally by correlating the bypass valve position with the concentration of pollutant gases in the exhaust stream. Additionally, a two-way catalyst is positioned downstream in the exhaust system, effectively transforming CO and VOCs into CO_2 and H_2O, further ameliorating pollutant emissions. These concepts are later shown in the experimental section.

The effectiveness of utilizing the AMS at various loads is mentioned here. At 40% load, the bypass valve significantly reduced CH_4 and NOx emissions by 84% and 63%, respectively, enhancing combustion stability and ITE by 4.2%. These improvements were observed at a full 100% bypass

valve position. At 60% load, the optimal emission reduction for CH_4 and VOCs occurred at a 60% bypass valve opening, while for NOx, the ideal setting was at 40%. A 70% bypass valve opening resulted in a notable 68% reduction in CH_4 emissions and a substantial 3.8% ITE improvement. During a 75% load, the most effective reduction in CH_4 and NO_x emissions was achieved at a 40% bypass valve opening, with minimal changes in VOCs, and a modest 1.5% increase in ITE [44].

2.3 Devices for Performance Testing

To determine engine performance special devices are used which help in evaluating the performance of the engine. Some devices are discussed below.

2.3.1 Integral Compressor

A reciprocating compressor is a machine that does mechanical work on a gas to raise its pressure and make it a useful and convenient power source for industry. The purpose of a compressor is to move air (or other gases) from one place to another [112]. A working cycle of the compressor commonly consists of four successive thermodynamic processes: suction (d-f-a), compression (a-b), discharge (b-c), and expansion (c-d), as shown by the dashed lines in Figure 6. The occurrence of the expansion process is due to the residual high-pressure gas in the dead volume V_0 at the end of the discharge process (i.e., Point c), assuming that there is no gas pressure drop through the suction and discharge valves, that intake and discharge are constant pressure processes, and that no gas is left inside the cylinder at the end of the discharge step [113].

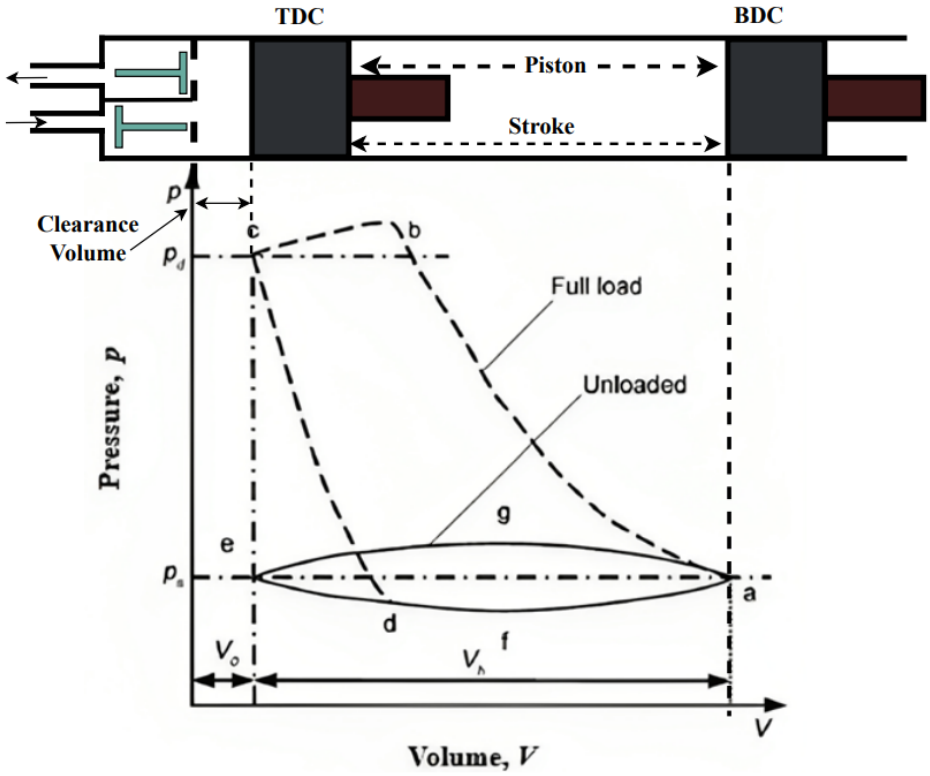

Figure 6. Piston stroke position superimposed on P-V diagram for single-stage compressor [113]

The advantages of a reciprocating compressor over a centrifugal machine are:

1. Greater flexibility in capacity and pressure range
2. Higher compressor efficiency and lower power cost
3. Capability of delivering higher pressures
4. Capability of handling smaller volumes
5. Less sensitive to changes in gas composition and density

With the numerous advantages of reciprocating compressors, these are commonly employed for natural gas T&S as discussed in the previous sections. The engine under study is also an NGFRE which comprises an integral engine-compressor, this compressor acts as a load on the engine. Figure 7 shows the overall components of the compressor. The crankshaft is indeed connected

with the engine on the other side of the compressor frame known as the integral engine-compressor.

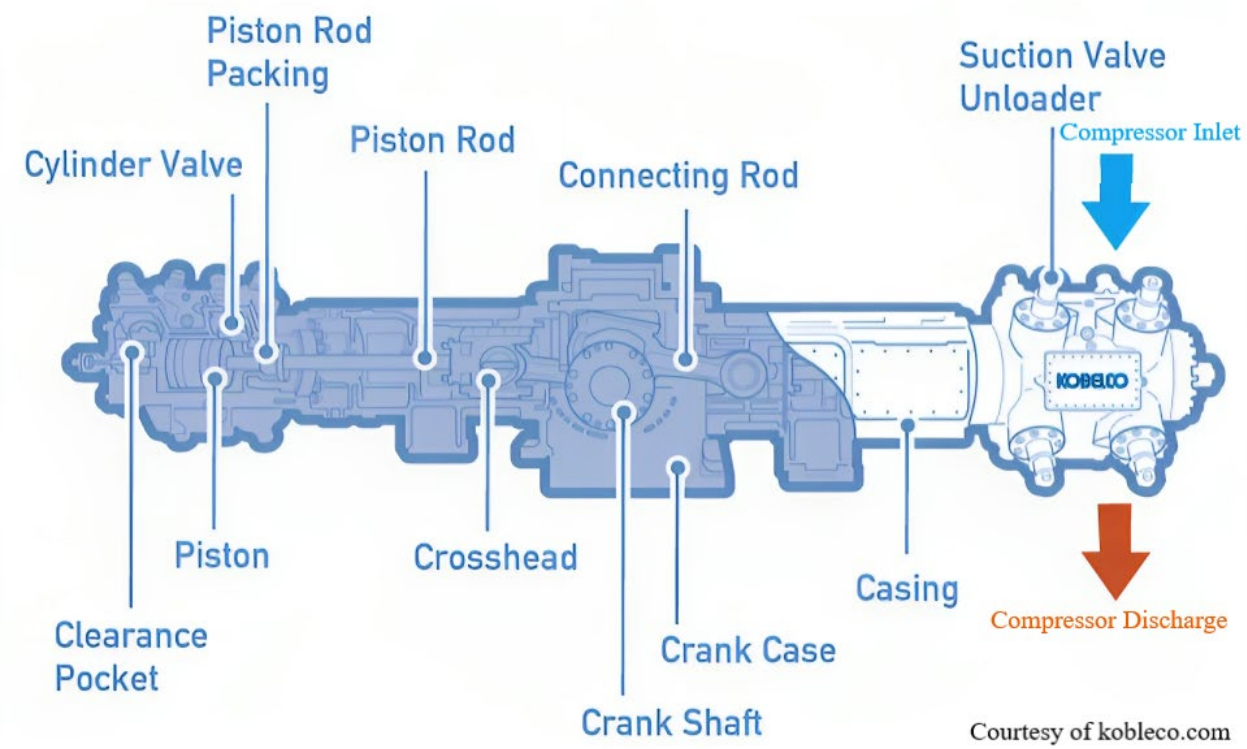

Figure 7. Overview of Integral compressor

The safety of reciprocating compressors managing hazardous materials is dominated by their piston rod sealing systems. These require appropriate design, maintenance, and operator attention [114].

2.3.1 Dynamometer

The power generated by a rotating shaft needs to be measured to get the power that can be generated. The measuring instrument used is called a dynamometer. The brake power of the rotating shaft is obtained after the result of the torque value [115]. A dynamometer is a critical tool for measuring the power output of an engine. It works by applying resistance (load) to the engine and measuring the force the engine can produce against this resistance. This resistance can be

created through various means, such as hydraulic fluids or electromagnetic fields, depending on the type of dynamometer used. The data collected can then be analyzed to understand the engine's performance characteristics, such as power and torque [116, 117]. Figure 8 shows a water brake dynamometer.

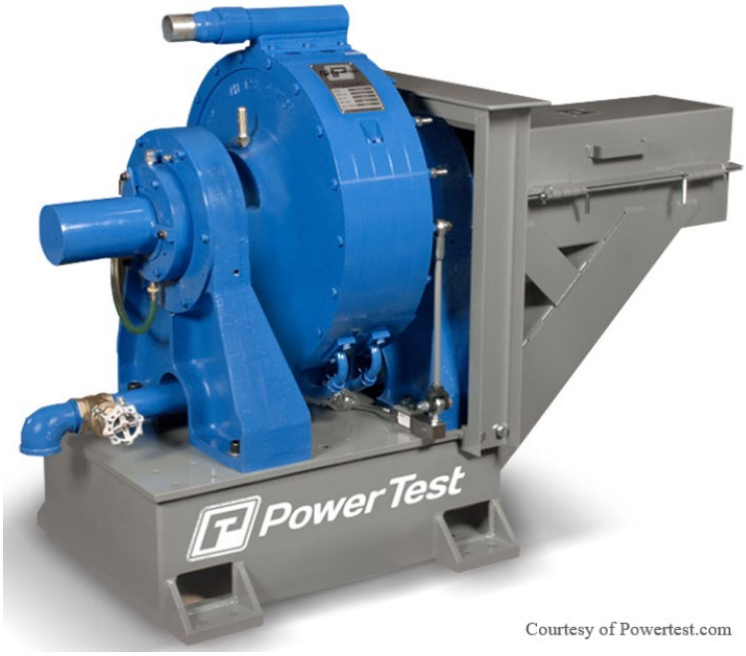

Figure 8. Water Brake Dynamometer

However, the use of dynamometers presents several challenges. Calibration of these devices must be exact and often, which can be both time-consuming and costly. Additionally, they must be able to accurately simulate the real-world conditions under which the engines operate, which can be complex given the variety of environments engines are exposed to. There is also the issue of heat management, as the resistance applied can generate significant heat, which must be dissipated effectively to prevent damage to both the engine and the dynamometer.

2.3.2 Generator

A generator is a device that transforms motion-based energy (including both potential and kinetic energy) or fuel-based energy (derived from chemical sources) into electrical power intended for utilization in an external electrical circuit. This conversion process allows for the measurement of electrical output as a proxy for engine performance. They are capable of being made such that they are reliable in starting and operation, capable of being started automatically; they work on readily available fuel which presents few problems in storage and handling; however, there are a wide range of types and ratings available worldwide [118]. Figure 9 shows the electric generator powered by the engine.

Figure 9. Electric generator by Caterpillar

Challenges arise in the use of generators for performance testing due to their efficiency variance at different power levels and under different loading conditions [119-121]. The precision of measuring electrical output as a representation of mechanical performance can also be affected by factors such as ambient temperature and generator wear over time. Moreover, generators may not

capture the transient behaviors of the engine under rapidly changing loads, which can lead to a less accurate portrayal of engine capabilities [122].

2.3.3 Other Techniques Used to Measure Performance:

2.3.3.1 Chassis Dynamometers

While traditional dynamometers measure engine performance directly, chassis dynamometers are designed to assess the performance of a vehicle's drivetrain, including the engine. The vehicle is driven onto rollers which measure the power output of the drivetrain wheels, thus providing a system-level performance assessment that includes losses through the transmission and drive shafts.

2.3.3.2 Engine Test Cells

Engine test cells are specialized rooms designed for safe and efficient engine testing. They are acoustically insulated and equipped with advanced ventilation systems to manage exhaust gases, temperature, and humidity. Test cells typically house an engine test stand and all necessary measurement devices and can be automated for various test cycles.

2.3.3.3 Torsional Vibration Measurement Systems

These systems are dedicated to measuring the torsional vibrations of the crankshaft and other rotating components. Torsional vibrations can indicate issues with engine balance, alignment, and overall mechanical integrity, which are all crucial for performance.

2.3.3.4 Fuel Consumption Meters

Fuel consumption meters are designed to measure the amount of fuel used by the engine in real-time. They provide direct feedback on the engine's fuel efficiency and are essential for tuning and optimizing fuel maps for better engine performance.

2.3.3.5 Techniques Used in Literature

In gas engine performance monitoring, the effectiveness of the physics-based modeling approach hinges on two performance indicators: the heat loss index and the power deficit index. These metrics gauge performance degradation, with the heat loss index quantifying thermal power wastage relative to optimal engine health, and the power deficit index measuring the shortfall in engine output power caused by deterioration. While offering valuable insights into performance changes and being robust against operational data variability, obtaining these reliable indicators poses challenges. No single measured parameter can fully capture the engine's systemic degradation, and many operational signals may not provide meaningful degradation data. Therefore, there is a necessity to refine methods that aggregate all significant operational data, filtering out non-contributory signals, to develop a comprehensive monitoring approach that accurately tracks performance decline over time, irrespective of the engine's operational conditions [123].

In SI engines the performance was measured using various parameters including brake mean effective pressure (BMEP), brake power (BP), brake specific fuel consumption (BSFC), and brake thermal efficiency (BTE). These parameters were computed based on measurements such as volumetric fuel consumption rate, exhaust gas temperature, exhaust smokiness, and exhaust-regulated gas emissions including nitrogen oxides, carbon monoxide, and total unburned

hydrocarbons. Additionally, the engine brake torque and engine speed (N) were used to calculate the performance quantities. The measurements were conducted at different loads and with different fuel blends to assess the engine's performance under various conditions [124].

Verman et. al [125] measured the performance by conducting tests on a 4-stroke, 4-cylinder spark ignition engine fueled with different blends of ethanol and premium gasoline. The tests were conducted at varying speeds (2200, 3200, 4200 rpm) and loads (5, 10, 15, 20 kg). The performance parameters, including BMEP, brake torque (BT), BP, BTE, and BSFC, were then recorded and analyzed based on the engine's response to the different fuel blends and operating conditions.

2.3.3.6 Vibration

Vibration emerges as a highly promising and reliable medium for the comprehensive monitoring of engines. Beyond its role in monitoring, vibration has convincingly demonstrated its efficacy in being harnessed for the accurate prediction of engine performance.

Vibrations are intrinsic to various facets of our daily experiences, mirroring the fundamental principles seen in the human anatomy—where vocal cords vibrate for voice generation and leg muscles oscillate for coordinated walking. In the context of machinery, vibrations can serve as indicators of performance and potential faults, evident in devices such as pumps or generators. External forces, such as powerful winds affecting improperly constructed structures like suspension bridges, can also induce vibrations. When these external vibrations align with the natural frequencies of a system, resonance occurs, leading to potentially hazardous oscillations [126, 127].

The accelerometer is mostly a piezo-electric accelerometer, and it is considered the standard vibration transducer for machine vibration measurement. Data capture regarding the vibration

emitted by a machine, or other body, begins with the sensor. The accelerometers shown in Figure 10 consist of a piezoelectric crystal that has a mass attached to one of its surfaces. An ICP amplifier is a standard for electronics in transducers that have built-in amplifiers. When the mass is subjected to a vibration signal, the mass converts the vibration (acceleration) to a force, this then being converted to an electrical signal. This is the basis of the "accelerometer". The accelerometer output may then be processed to provide the instantaneous velocity and displacement signals.

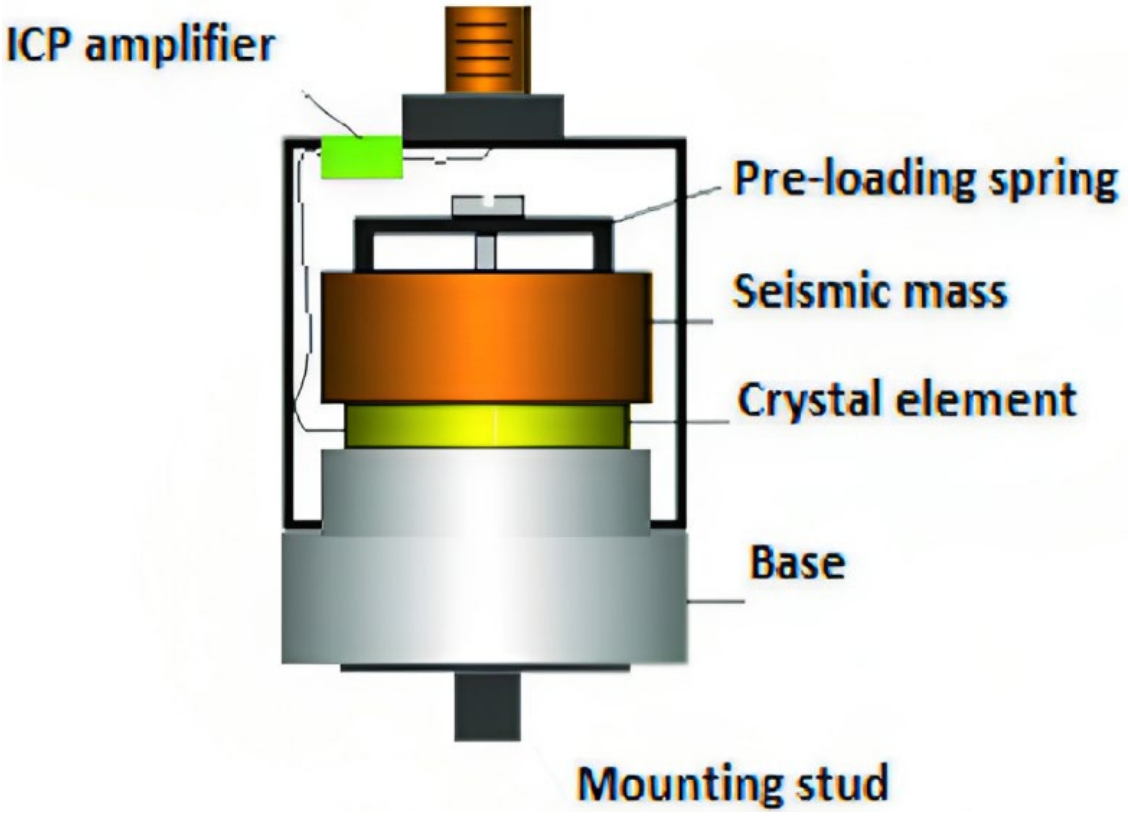

Figure 10. Piezo-Electric accelerometer adapted from Ghemari 2018 [128]

Instances of structural failure, such as the breaking of bridges, turbines, or airplane wings, can be attributed to resonance phenomena [129]. Vibration signals, offering crucial insights, undergo analysis in both the frequency and time domains. In contemporary vibration analysis, the Fast Fourier Transform (FFT) takes center stage, serving as a key component of discrete Fourier

transform and frequency domain analysis. Notably, frequency domain analysis, facilitated by techniques like FFT, proves especially valuable in the study of machines featuring rotating elements, such as bearings [129].

Zhao et.al [130] study explores the importance of accurate combustion parameters for engine control. Challenges in identifying the parameters from engine vibration signals, which include non-combustion-related elements caused by engine dynamics. A mathematical model and pattern recognition are used to extract combustion parameters, with corrections made for discrepancies.

Gravalos et. al [131] explored the vibration behavior of a SI engine fueled with gasoline, ethanol, and methanol blends through experiments. Three fuel types, including unleaded gasoline for comparison, were used with varying blend percentages. Gasoline-ethanol blends yielded intermediate results at both frequencies. An algorithm was developed to reliably identify the fuel type, irrespective of engine speed.

Ghazaly et. al [132] proposed an algorithm based on unsupervised learning and vibration sensors to detect misfires. The behavior of the self-organization map for the engine vibration signals was investigated. the maximum accuracy in detecting the misfire is 93.55% for a 3D vibration signal at 3000 rpm.

The literature above underscores the significance of vibration as a substantial parameter for predicting engine performance. However, there is less study regarding the NGFRE and how the application of vibration can be useful in terms of performance prediction. Therefore, in this research, an investigation into vibration analysis is undertaken to ascertain its correlation with engine performance.

This study endeavors to optimize AMS efficiency by identifying the optimal bypass valve positions through detailed emissions and combustion analyses. It will also examine vibration data across three axes to evaluate whether vibration metrics can serve as viable predictors within a machine learning framework. Ultimately, drawing on the insights from the vibration analysis, a machine learning algorithm is developed to predict engine performance.

In summary, the previous research on AMS has laid a crucial foundation for emissions reduction. The present study is designed to harness the full capabilities of this technology, with the integration of machine learning models aiming to achieve a more effective, automated system that dynamically responds to engine loads, thereby enhancing the performance and environmental benefits of NGFREs.

2.4 Summary

This chapter provides an in-depth exploration of the role of compressors in the NG industry, especially within the context of the U.S. expanding NG production. It emphasizes the increasing demand for NG in electricity generation and transportation, while also addressing the importance of environmental considerations. The focus is on NGFREs used in compressor stations. Furthermore, the review covers techniques for mitigating emissions in spark ignition engines, encompassing methods like Exhaust Gas Recirculation, spark retardation, catalysts, fuel blends, and the AMS. Various devices for performance testing, including dynamometers, generators, and compressors, are discussed, highlighting their significance in assessing engine performance. The AMS's potential for reducing emissions is emphasized, but the need for an optimum bypass position is identified. The importance of vibration analysis is discussed which could be a potential parameter for the performance prediction.

Chapter 3: Methods and Procedure

3.1 Introduction

This research is centered on enhancing efficiency and reducing emissions in NGFRE. A critical component of this study is the optimization of the AMS, pivotal for engine performance. The AMS is analyzed across various operational loads, with a focus on performance and combustion analysis,

The potential of vibration analysis as a tool for predicting engine performance is also assessed, potentially expanding the scope of engine monitoring capabilities. At the heart of this research is the implementation of machine learning algorithms. These algorithms are designed to process real-time data gathered from sensors and interfaced with a PLC, aiming to deliver accurate predictions of engine performance parameters.

The primary objectives are twofold: firstly, to improve the performance of natural gas aspirated engines, and secondly, to significantly reduce their emission output. This contributes to a broader goal of enhancing environmental sustainability within the oil and gas industry.

3.2 Software to Calculate the Engine Performance

The accurate assessment of engine load is a critical component in the operational management of engines, particularly in the energy-demanding oil and gas industry. To this end, PowerFlow software by Cooper Machinery Services emerges as a vital tool in the sector, renowned for its capability to simulate and calculate the load dynamics of compressor-engine systems. PowerFlow integrates the principles of thermodynamics and fluid mechanics to offer a sophisticated simulation environment, which provides a detailed analysis of energy flows within power systems. PowerFlow uses the principles of thermodynamics to model the flow of energy in a compressor-

engine system. The following are the key principles of thermodynamics that are used by PowerFlow:

The First Law of Thermodynamics:

The First Law of Thermodynamics states that energy cannot be created or destroyed, only transformed. This means that the total energy in a system is constant. In a compressor-engine system, the energy is transferred from the engine to the compressor and from the compressor to the air.

The Second Law of Thermodynamics:

The Second Law of Thermodynamics states that entropy always increases over time. Entropy is a measure of the disorder in a system. In a compressor-engine system, entropy increases as the air is compressed and heated.

The Ideal Gas Law

The Ideal Gas Law states that the pressure, volume, and temperature of a gas are related by the following equation:

$$PV/T = N*R$$ [4]

where:

P is the pressure of the gas

V is the volume of the gas

T is the temperature of the gas

N is the number of moles of gas

R is the ideal gas constant

The Ideal Gas Law is used to model the behavior of air in a compressor-engine system.

The Isentropic Efficiency:

The isentropic efficiency of a compressor is a measure of how efficiently the compressor converts the energy of the engine into the energy of the air. The isentropic efficiency is defined as the ratio of the actual work done by the compressor to the ideal work done by the compressor.

The Polytropic Efficiency:

The polytropic efficiency of a compressor is a more general measure of the efficiency of the compressor. It is defined as the ratio of the polytropic work done by the compressor to the adiabatic work done by the compressor.

The principles of thermodynamics are used by PowerFlow to calculate the following:

- The power input to the compressor
- The power output of the compressor
- The efficiency of the compressor
- The pressure ratio of the compressor
- The temperature of the air at the inlet to the compressor
- The temperature of the air at the outlet of the compressor

Figure 10 shows the how the load calculation using the PowerFlow software.

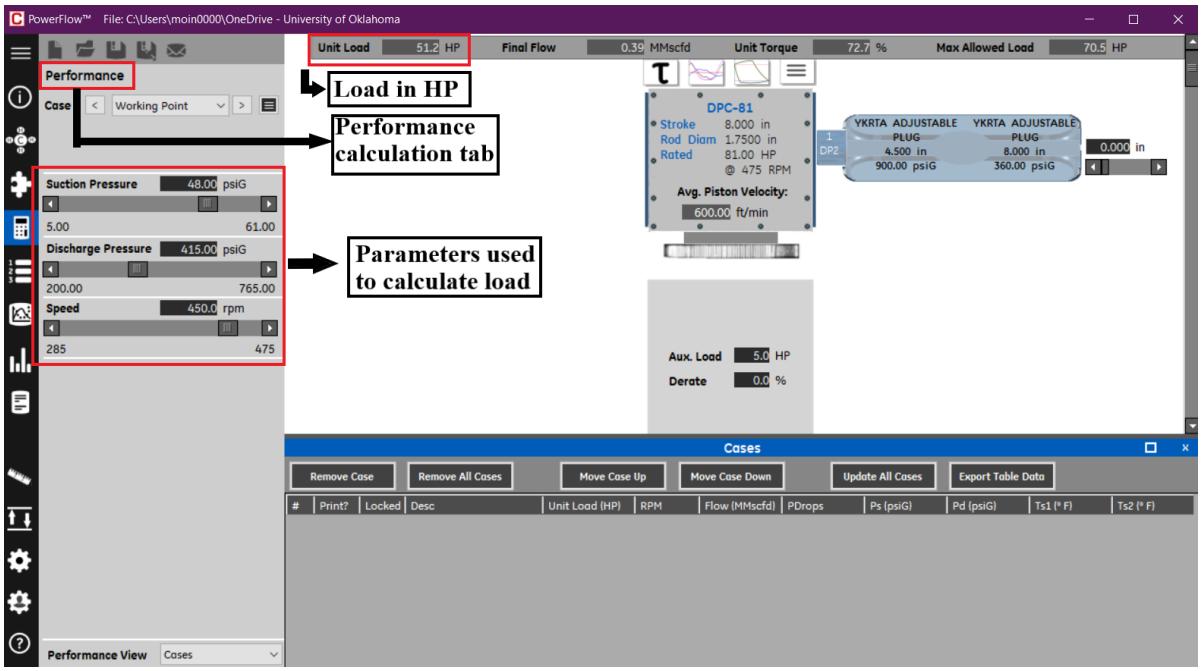

Figure 10. Calculation of engine performance in PowerFlow

While PowerFlow software stands as a robust tool for simulating compressor-engine systems within the oil and gas industry, it is not without its limitations. The software, grounded in the principles of thermodynamics and fluid mechanics, necessitates a deep technical understanding and a substantial investment of both time and resources. Its complexity can impose a steep learning curve and the potential for costly licenses, making it less accessible for some operations. In this context, incorporating additional sensors and Machine Learning algorithms could greatly enhance the efficiency and accessibility of performance prediction. These modern technologies promise to streamline the process, reduce costs, and democratize the ability to optimize engine systems across the industry.

3.3 Sensors Technologies in Engine Performance

In the realm of engine diagnostics and optimization, sensor technology plays an indispensable role. The accurate measurement and monitoring of various engine parameters are critical for

understanding and enhancing engine performance, particularly in the context of reducing emissions and improving efficiency in NGFREs.

3.3.1 Types of Sensors

A variety of sensors play pivotal roles in monitoring and optimizing engine performance. In NGFREs, these sensors are crucial for accurate data collection and subsequent analysis.

Pressure Sensors: Key to the operation of NGFREs, pressure sensors meticulously measure the pressures in various engine parts. They primarily focus on suction and discharge pressures. The suction pressure sensor evaluates the gas entering the cylinder, whereas the discharge sensor measures the pressure after the gas has been compressed. These sensors are fundamental for accurately predicting engine performance by providing insights into the engine's efficiency in compressing and processing the gas, thereby offering a detailed understanding of overall engine performance.

Temperature Sensors: Positioned strategically within the engine, temperature sensors continuously monitor its thermal state. Specifically attached to the exhaust, they play a critical role in preventing overheating and in maintaining the engine within a safe operating temperature range. This is particularly crucial during experimental phases when selecting the optimal bypass valve positions, as it ensures the engine does not exceed its maximum operating temperature of 800 °F.

Flow Meters: Integral to NGFREs, flow meters measure the rate at which fuel and airflow into the engine. This data is vital for calculating the AFR, a key factor in achieving efficient combustion. Understanding AFR is crucial, as it directly influences the combustion quality and, consequently, the engine’s performance and emission levels.

Oxygen and NOx Sensors: These sensors serve dual purposes. Oxygen sensors are utilized to measure the oxygen concentration in the exhaust gases, indicating combustion efficiency. NOx sensors, meanwhile, specifically track the levels of nitrogen oxides in the exhaust, which is critical for managing emissions and ensuring compliance with environmental regulations. Notably, these sensors are affordable, which makes their usage practical and widespread. The data they collect are also used extensively in combustion analysis.

Vibration Sensors: To monitor engine health, vibration sensors are employed, measuring movements along the x, y, and z axes. These sensors are adept at detecting early signs of mechanical failures or deteriorations, making them particularly valuable in the maintenance and monitoring of reciprocating engines. In line with existing literature that highlights the role of vibration analysis in predicting engine performance, this research also utilized vibration sensors for such predictions. These sensors are instrumental in forecasting key performance indicators like engine load. This approach not only corroborates findings from previous studies but also strengthens the methodology used in this research for engine load prediction

Further details and specifications of these sensors, including their placement, operational ranges, and integration with the engine system, are elaborated in the experimental section. The accurate and synchronized functioning of these sensors is foundational for the data-driven analysis that underpins this research, particularly about machine learning-based prediction.

3.3.2 Sensor Used for Performance Measurement

Understanding how sensors contribute to measuring engine performance is essential in the context of NGFREs. In these engines, load is often indicated by the pressure at which the compressor operates. The load is defined as the amount of work done by the engine to compress the gas.

Essentially, the higher the pressure on the compressor, the harder the engine works to compress the gas. The operational load of these engines typically ranges between 40-75%, as recommended by engine manufacturers. Thus, a key performance parameter is measured based on the amount of gas compressed and the engine's operating speed [133].

As discussed earlier, considering the limitations of the software, the research incorporates additional sensors alongside suction pressure, discharge pressure, and speed to advance the technology. This expansion not only elevates the research but also leverages various parameters crucial for load prediction. Furthermore, these parameters have the potential to aid in predictive maintenance, offering broader utility in engine management. In this research, these parameters are used for predicting the load of NGFRE:

1. Suction Pressure: This measures the pressure of the incoming gas to the compressor, defining one aspect of the compressor's functionality.
2. Discharge Pressure: This indicates the pressure of the gas after compression, providing insight into the output side of the compressor.
3. Speed: This parameter, accounting for the engine's operational rate, is crucial for understanding the engine's dynamic performance.
4. Vibration: Vibration sensors attached to the combustion chamber can detect piston movement, aiding load determination.
5. NOx: Measurement of nitrogen oxide emissions offers insights into engine efficiency and environmental impact.
6. O_2: Oxygen levels in the combustion process influence combustion efficiency and emissions.

3.4 Machine Learning

Machine learning (ML) has gained prominence in contemporary technology applications, widely recognized for its ability to train models, make predictions, and automate decision-making processes. Its prevalence in industrial applications is particularly noteworthy, with uses ranging from predictive maintenance to fault detection. Within the context of this research, machine learning is employed as a strategic tool to predict engine performance, particularly focusing on engine load, using various parameters. The following sections delve into several machine learning algorithms that will be explored for their efficacy in enhancing predictive accuracy and operational efficiency in engine management systems.

3.4.1 Introduction

ML is a rapidly expanding domain in every domain with extensive applications, involving the automated detection of meaningful patterns in data. The focus of machine learning tools is on imparting to programs the capability to learn and adapt [134]. In the realm of Information Technology, ML has emerged as a fundamental component, often concealed but central to our lives. Given the continuous surge in data volumes, there is a strong expectation that intelligent data analysis will increasingly establish itself as an essential element for technological advancement [135]. With ML the problems can be solved simply by building a model that is a good representation of a selected dataset.

A taxonomy categorizes machine learning algorithms according to the desired outcome of the algorithm. This categorization comprises: A) Supervised learning, B) Unsupervised learning, and C) Reinforcement learning. The taxonomy of various methods in machine learning is illustrated in

Figure 11. It also demonstrates how the classification is done up to the different algorithms utilized in ML.

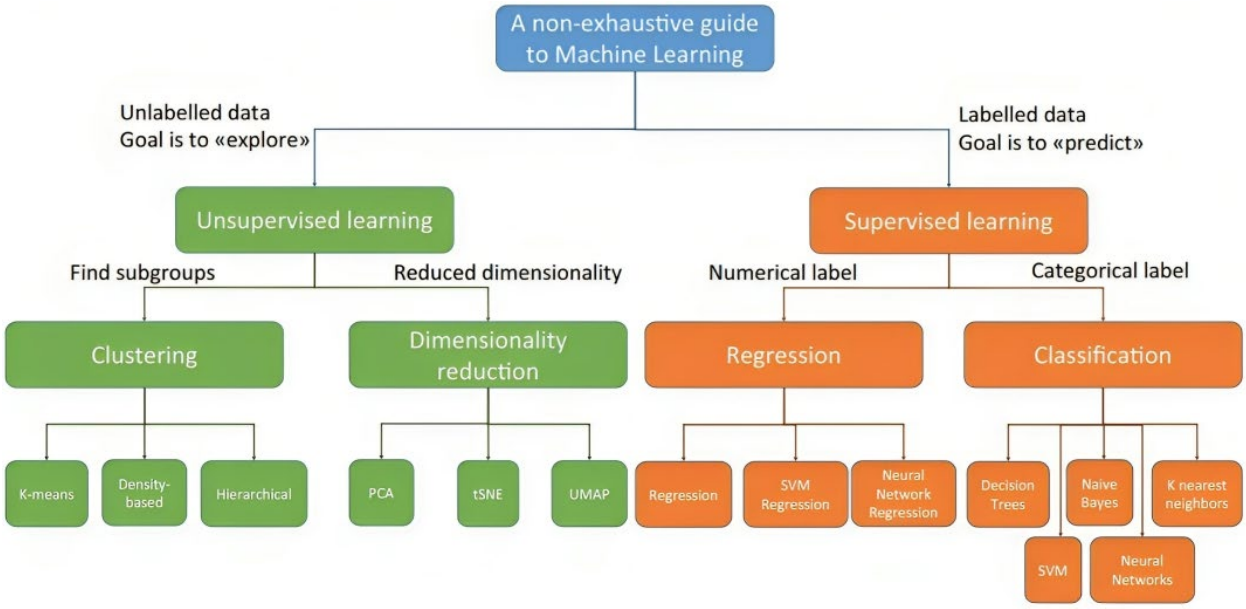

Figure 11. Taxonomy of the different methods presented (adapted from Badillo et al. 2020 [136])

3.4.1.1 Unsupervised Machine Learning Methods

In unsupervised learning, the algorithm is given a set of objects and attempts to group them into classes (Clustering) without any prior knowledge of these classes or any labeled output [137]. Unsupervised machine learning methods are beneficial in description tasks because they aim to find relationships in a data structure without having a measured outcome. This category of machine learning is referred to as unsupervised because it lacks a response variable that can supervise the analysis [138]. Typical clustering algorithms are K-means [139], hierarchical clustering [140], and spectral clustering [141]

Unsupervised learning aims to recognize fundamental dimensions, elements, groups, or paths within a given data framework. Various techniques widely employed in mental health categorization and psychometric studies fall within the domain of unsupervised learning. These

encompass principal components analysis, factor analysis, and mixture modeling, which is one rationale for our emphasis on supervised learning, as elaborated below [142].

It is not possible to directly measure the performance of clustering because the correct output labels are not known as a priority. Instead, the performance depends on whether interesting trends in the data have been captured by the clusters or not.

3.4.1.2 Supervised Machine Learning Methods

In Supervised learning, labeled training data is used to train a function that can be applied to new samples. Feedback on the accuracy of the function is provided by a critic during the training and, if needed, alterations are made to the function to attain the desired result. A function (or model) is constructed by pairing input and desired output with labeled training data in supervised learning. The form of supervision is manifested in the desired output, enabling the adjustment of the function based on its actual performance. Utilizing additional observations (predictions or classifications) after training might yield a valuable output (reaction). The most common supervised learning tasks are regression and classification [138, 140, 143]. The mathematical model created in this study utilizes Linear Regression, Artificial Neural Networks (ANN), and Support Vector Machines (SVM). Figure 12 illustrates supervised machine learning which is the most common technique in the classification problem.

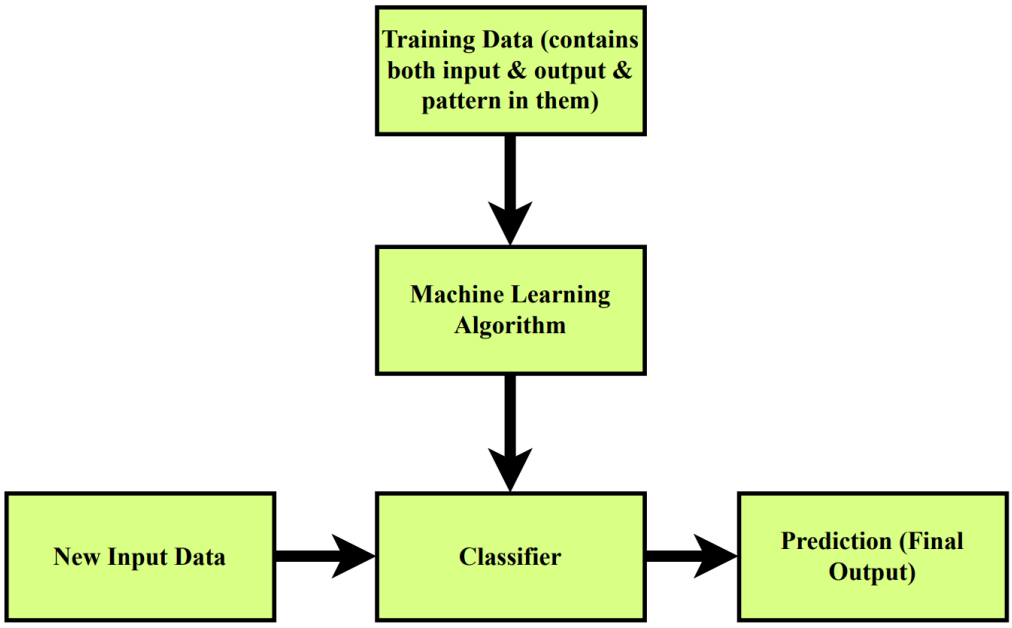

Figure 12. Block Diagram of Supervised Learning Algorithm

3.4.2 Linear Regression

The goal of linear regression, as a part of the family of regression algorithms, is to find relationships and dependencies between variables. It represents a modeling relationship between a continuous scalar dependent variable y (also label or target in machine learning terminology) and one or more (a D-dimensional vector) explanatory variables (also independent variables, input variables, features, observed data, observations, attributes, dimensions, data point, etc.) denoted *X* using a linear function. In regression analysis, the goal is to predict a continuous target variable. It means we train the model on a set of labeled data (training data) and then use the model to predict labels on unlabeled data (testing data) [144, 145]. Linear regression does not have any hyperparameters, however, the advantages and disadvantages are given below to understand the model.

Advantages of linear regression:

1. Simple method for modeling the relationship between a dependent variable and one or more independent variables.
2. Regression is computationally efficient, which makes it fast to run on large datasets.
3. The coefficient of a linear regression model can be interpreted as the estimated effect of each independent variable on the dependent variable. This makes it easy to understand and communicate the results of the model [146, 147].

Disadvantages of linear regression:

1. Linear regression assumes that the relationship between the dependent and independent variables is linear. If the connection is non-linear, the model may not accurately capture the trend in the data.
2. Linear regression is sensitive to outliers, which can have a significant impact on the coefficients of the model.
3. Linear regression is limited to continuous data and cannot handle categorical data or missing data [146, 148].

3.4.3 Artificial Neural Network (ANN)

Artificial Neural Network (ANN) has been a hot topic in artificial intelligence since the 1980s. It abstracts the human brain neural network from the perspective of information processing, establishes a simple model, and composes different networks according to different connections [149]. In engineering and academia, these are often directly referred to as neural networks. A neural network is a computing model, by many nodes (or neurons) connected [150]. The output of

the network varies depending on how the network is connected, the weight value, and the incentive function [151].

In an artificial neural network, a neuron processing unit can represent different objects, such as features, letters, concepts, or some meaningful abstraction pattern. The type of processing unit in the network is divided into three categories: input unit, output unit, and hidden unit. The input unit accepts signals and data from the outside world [152]. The output unit realizes the output of the system processing result which is engine load. A hidden unit is a unit that is located between the input and output units and cannot be observed outside the system [153].

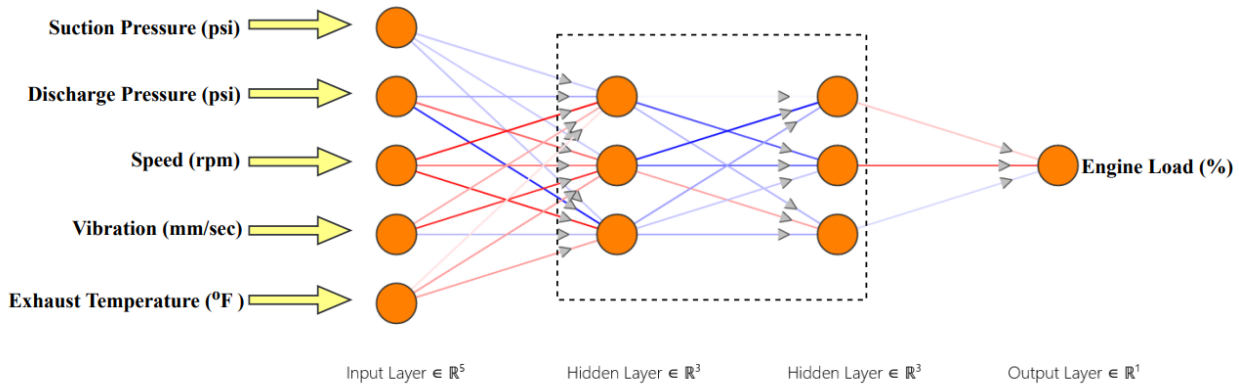

Figure 13. Structure of Artificial Neural Network (ANN)

Figure 13 shows the structure of the ANN. The hyperparameters are generated by the Randomized Search method which is mostly used to find the ideal hyperparameters that tend to have the highest prediction accuracy. The hyperparameters are as follows:

- Activation function: ReLu and Logistic
- Solver: Adam
- Alpha: 0.0001
- Number of Iterations: 500

- Hidden layers: 100 & 200

Advantages of ANN:

1. ANNs can model complex non-linear relationships in data, making them effective for tasks such as image recognition and speech processing.
2. ANNs can adapt and learn from new data, making them suitable for applications where the underlying patterns may change over time, like stock market predictions.
3. ANNs can perform multiple tasks simultaneously, allowing for faster and more efficient data processing [154, 155].

Disadvantages of ANN:

1. Training and fine-tuning ANNs can be a complex and time-consuming process, requiring a large amount of data and computational resources.
2. ANNs are prone to overfitting, where the model fits the training data too closely, leading to poor generalization on unseen data.
3. ANNs are often considered "black boxes," making it challenging to interpret the decision-making process, which can be problematic in applications that require transparency and accountability [156].

3.4.4 Support Vector Machine (SVM)

Support Vector Machine (SVM) is an ML approach that has been used for both classification and regression problems [157, 158]. The goal of SVM is to find the optimal decision boundary that separates the classes which is applicable mostly in classification cases. Similar to all regression methods, the objective of Support Vector Regression (SVR) is to postulate a function on the

input(s) that can help estimate the observed output. As the name suggests, the core concept behind SVR is the ability to objectively choose a subset of training data called support vectors. These support vectors define the model, which is usually a hyperplane in some feature space. To achieve this, several notions need to be introduced. SVR has proven as one of the most powerful machine learning methods that have shown remarkable accuracy in predicting Internal Combustion Engine (ICE) emissions and performance [159-163]. Figure 14 This shows the illustration of SVM and the optimal hyperplane that serves as the idea of SVM.

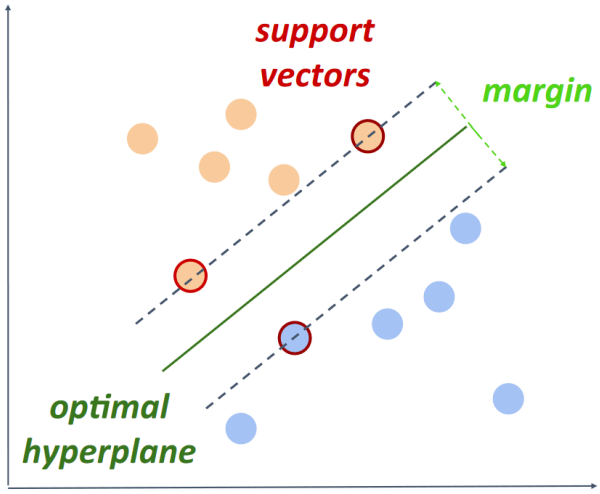

Figure 14 Illustration of Support Vector Machine (SVM) principles adapted from Badillo 2020 [136]

The hyperparameters are generated by Randomized Search which is mostly used to find the ideal hyperparameters that tend to have the highest prediction accuracy. The hyperparameters are as follows:

- Regression Cost (C): 0.01
- Regression loss epsilon: 0.10
- Kernel: Linear

Advantages of SVR:

- Robust Regression: SVR is robust to outliers in the data, as it focuses on minimizing the error within a specified margin.
- Effective in Non-Linear Regression: Like SVM, SVR can manage non-linear regression tasks effectively by using kernel functions.
- Tuning Parameters: SVR provides tuning parameters to control the width of the margin and the tolerance for errors, offering flexibility in model optimization.

Disadvantages of SVR:

- Model Complexity: Fine-tuning an SVR model may be challenging due to the need to select appropriate kernel functions and parameters.
- Computationally Demanding: SVR can be computationally intensive, especially when using non-linear kernels and large datasets.
- Interpretability: SVR models may be less interpretable compared to traditional linear regression models.

3.5 Overview of Data

The data examined in this study included several parameters, such as Suction Pressure, Discharge Pressure, Speed, Exhaust Temperature, NOx, O_2, and Engine load. Figure 15 represents the pairwise correlation plot which shows the relation with the other parameter. This image displays a scatter plot matrix showcasing the relationships between various engine parameters such as Suction Pressure, Discharge Pressure, Speed, Vibration, Exhaust Temperature, NOx, O_2, and Engine Load. Each plot compares two variables, revealing potential correlations. For example, there's a visible positive correlation between Suction Pressure and Discharge Pressure, indicating

that as one increases, so does the other. Conversely, Vibration and Engine Load display a dispersed pattern, suggesting a weak or non-linear relationship. This matrix is a valuable tool for quickly visualizing and assessing the interdependencies within multiple variables of engine performance.

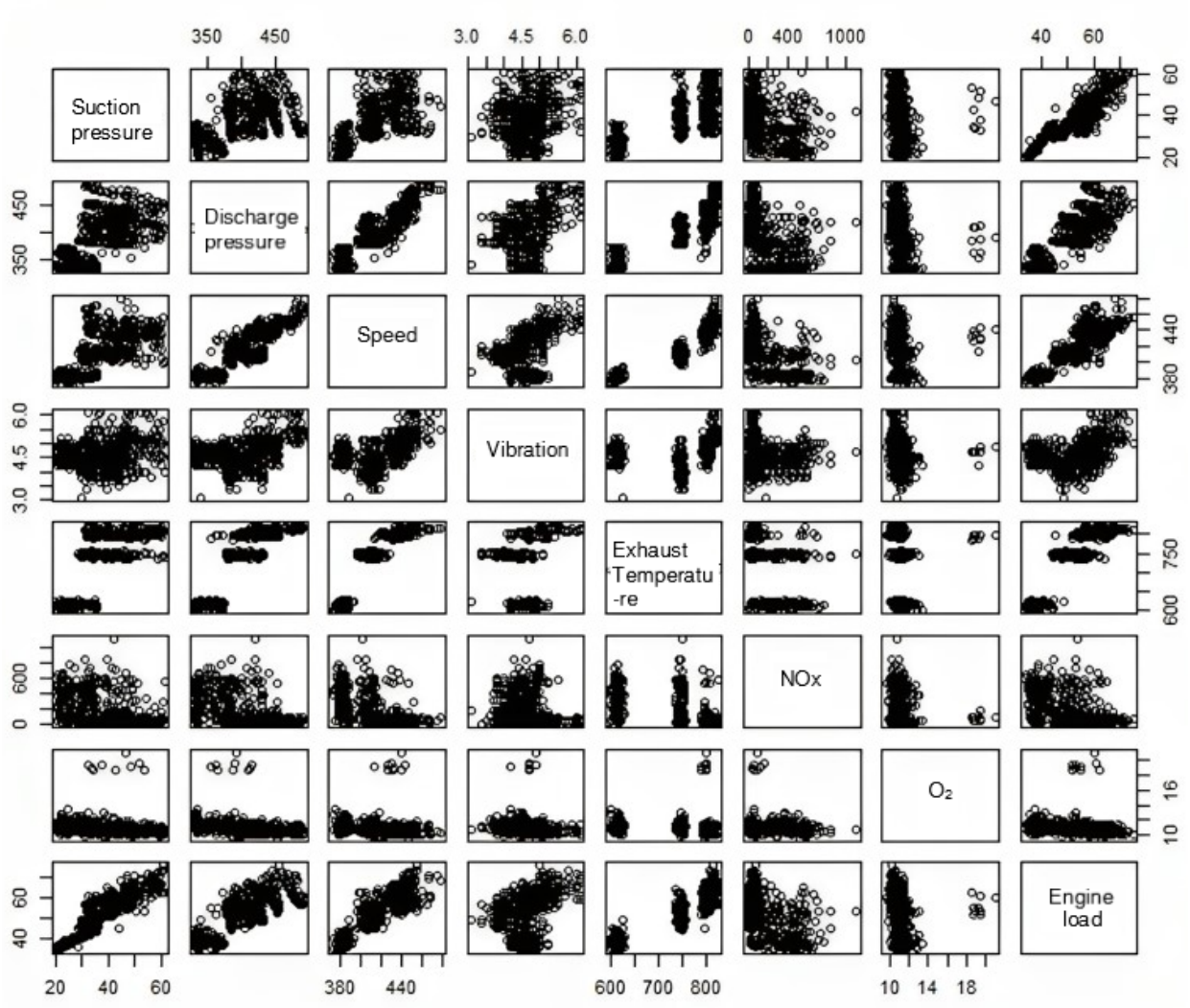

Figure 15. Pairwise correlation plot of the data

Before advancing with the data analysis, an examination is conducted to identify any potential outliers. Through data visualization, certain data points that deviate significantly from the norm are identified and subsequently removed. This process can result in a clean dataset devoid of

outliers, ensuring the accuracy of predictions and eliminating potential data-related errors. Table 2 shows the sample data that is used for the ML algorithms

Table 2 shows the sample data, offering an overview of their characteristics. Additionally, it is evident that NOx had the highest variability compared to the other parameters. As a result, a selection process is conducted to determine which parameters will be considered to predict the engine load in the final load prediction model. This is done to ensure that variations in certain parameters do not significantly impact the accuracy of load predictions.

Table 2. Sample Data for the Machine Learning Algorithm

Suction Pressure (psi)	Discharge Pressure (psi)	Speed (rpm)	Vibration (mm/s)	Exhaust Temperature [°F]	NOx (ppm)	O_2 (%)	Load(%)
27.3	353.0	377.1	4.8	605.1	725.5	11.1	40
23.3	363.7	381.5	4.8	605.1	235.4	11.5	39
35.3	330.0	385.9	4.8	605.6	190.2	11.6	44
43.5	395.5	412	4.2	750	432	10.0	55
35.8	334.9	388	4.8	604.4	10.2	11.0	45

3.6 Summary

The methodology for enhancing efficiency and reducing emissions in NGFREs is detailed. The optimization of the AMS is central to the research, and the potential use of vibration analysis for performance prediction is explored. Machine learning algorithms are employed to process real-time sensor data, to accurately predict engine performance. A variety of sensors, including pressure, temperature, flow, oxygen, NOx, and vibration sensors, are utilized for monitoring, and optimizing engine performance. The focus is placed on the analysis of crucial parameters—Suction Pressure, Discharge Pressure, Speed, Vibration, NOx, and O_2 —which are integrated into a thermodynamic model for load calculation in NGFREs. Various machine learning techniques such as linear regression, ANN, and SVR are discussed for their application in data analysis. The

dataset's preparation and cleansing are highlighted, ensuring the accuracy of machine learning predictions. The foundation for improving NGFRE performance and reducing emissions through advanced monitoring and predictive methods is thus established in this chapter.

Chapter 4 Methodology

4.1 Experimental Setup

4.1.1 AJAX DPC-81 Integral Engine-Compressor

The Sustainable Energy and Carbon Management Center (SECMC) located on the campus of the University of Oklahoma is used for experimental tests. The engine used in this study is an AJAX DPC-81 single-bore, two-stroke, naturally aspirated, natural gas-fired reciprocating lean burn engine designed to operate at a specific AFR, much higher than the stoichiometric AFR. This engine is an integral compressor-engine i.e., a compressor is installed on the same crankshaft as the engine. The engine functions at various load levels determined by three primary parameters: maximum discharge pressure, average suction pressure of the compressor, and engine speed. These specified factors are manually modified to establish the desired engine load. The engine specifications are given in Table 3.

Table 3 AJAX DPC-81 engine specification

Engine type	SI, two-stroke, natural gas aspirated, water-cooled
Rated power	81 BHP
Rated speed	475 rpm
Number of cylinders	1
Bore × stroke	10.5 in. × 12 in.
Swept volume	1039 in^3
Combustion type	Lean burn

The AJAX DPC-81 represents an integrated engine-compressor unit, housing a gas compressor and a reciprocating engine within a unified frame shown in Figure 16. This configuration employs a single crankshaft responsible for driving the pistons in both the power and compressor cylinders. This specific design is particularly favored for field installations due to its emphasis on minimal maintenance, enhanced fuel efficiency, and extended operational lifespan. Mirroring the operational principle of conventional two-stroke engines, the engine cycle commences with air intake into the combustion chamber. Post-compression by the piston, the air-fuel mixture ignites and propels the piston in a rearward direction. This energy is then transmitted through the crankshaft, driving the compressor piston, and facilitating gas compression within the compressor cylinder.

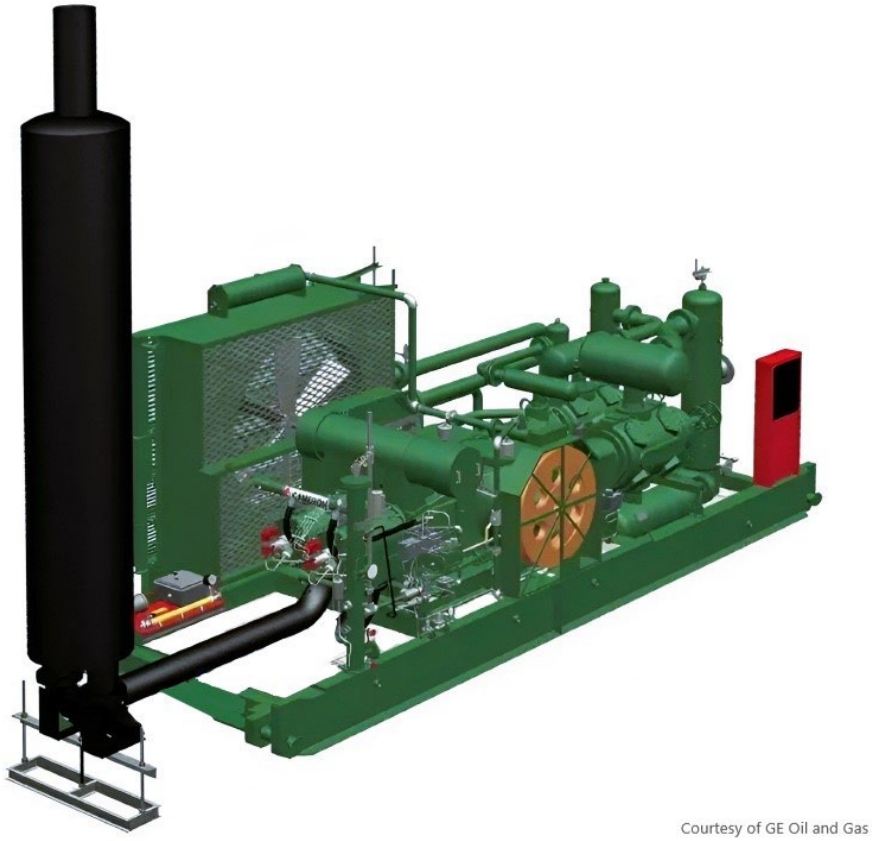

Figure 16. AJAX DPC-81 integral engine compressor

Input parameters for specific engine loads are estimated using PowerFlow sizing software by Cooper Machinery Services, which uses compressor parameters to calculate the engine load. For this experiment, the natural gas is received from city supply lines.

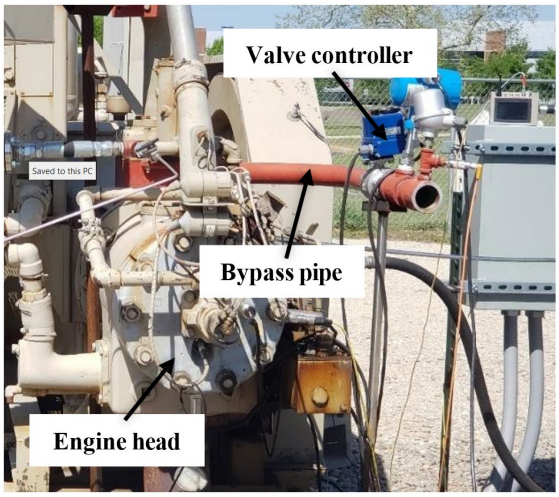

(a)

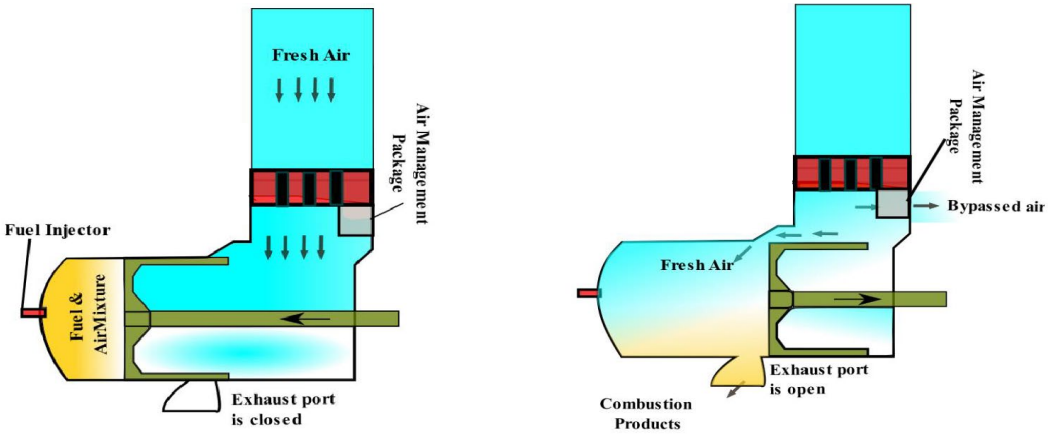

(b) (c)

Figure 17 Air management system (AMS) components and operating mechanism adapted from Ahmad et. al [20] a) Bypass pipe location. B) Bypass pipe closed. C) Bypass pipe opened.

The setup of the experiment's bypass system, consisting of a bypass pipe and a butterfly valve, is observed in Figure 17. The valve permits a portion of the intake air to exit before reaching the combustion chamber. Consequently, a wider opening of the bypass valve results in reduced air in

the combustion chamber, leading to a richer combustion. The bypass mechanism offers a simple means to regulate the AFR during combustion by limiting excess air in the combustion chamber.

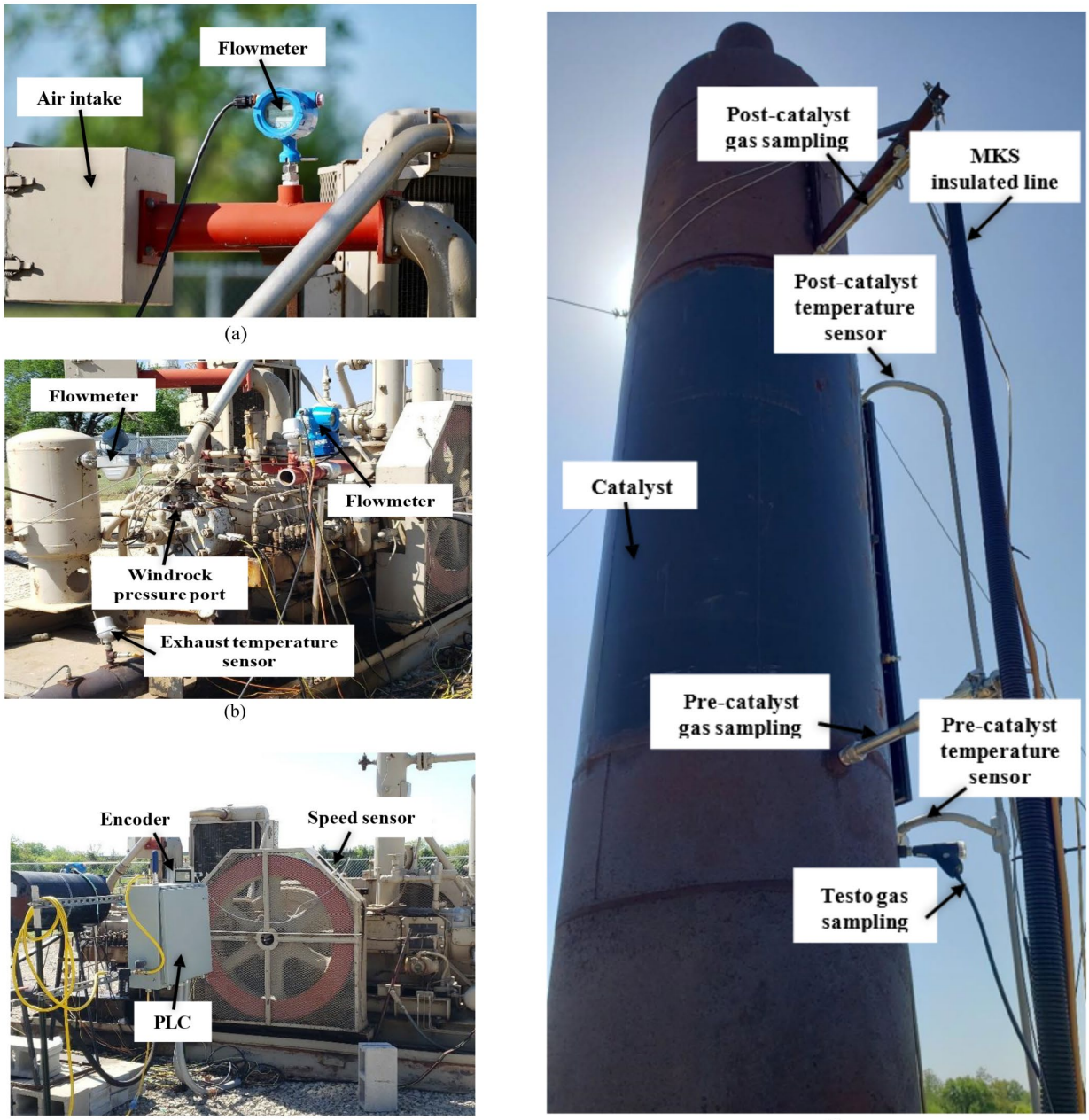

Figure 18 Engine setup. a) Flow meter. b) In-cylinder Pressure setup. c) PLC. d) Exhaust pipe

In Figure 18, an illustrative depiction of the engine and its associated components is presented.

a) The initial segment of Figure 14 displays a flow meter installed immediately after the air intake filter.

b) The subsequent section showcases another flow meter connected after the fuel tank. Additionally, a separate flow meter is affixed post the bypass valve assembly to monitor air bypassing through the system. Moreover, data regarding in-cylinder pressure is gathered via a pressure port affixed to the engine combustion chamber, along with an exhaust temperature sensor.

c) The third part exhibits a speed sensor affixed to the flywheel cover, which collects data from the magnet affixed to the flywheel. Concurrently, data collection is managed by a Programmable Logic Controller (PLC).

d) Lastly, the fourth portion highlights the exhaust system, featuring a catalyst attachment. Furthermore, sensors are positioned both before and after the catalyst to facilitate emissions sampling, utilizing MKS. The exhaust system is also equipped with a Testo gas sampling probe for comprehensive analysis.

The engine is fitted with a catalyst on its exhaust pipe, aimed at transforming harmful emissions into less detrimental substances. A catalyst is a material that facilitates an acceleration in a chemical reaction without undergoing consumption in the process. Essentially, it neither initiates the reaction nor is a resulting product. During catalysis, these catalysts reduce the activation energy, which is the energy needed to initiate a reaction, leading to a faster and more efficient occurrence of the reaction. Consequently, in the catalyst's presence, atoms readily detach from their molecules to generate novel substances.

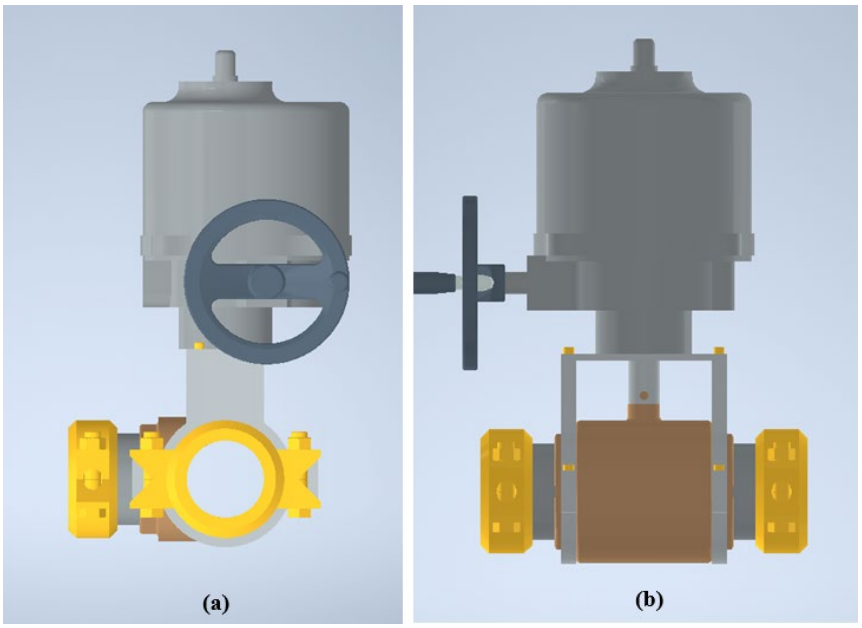

Figure 19 CAD model of the Bypass Valve. (a) Side view, (b) Front view

The bypass valve assembly is a unit affixed to divert air away before it reaches the combustion chamber. This assembly comprises a butterfly valve linked to a motor that can be regulated through the PLC. The operation functions in increments of 10%, allowing a controlled amount of air to bypass as shown in Figure 20. As it opens wider, a greater volume of air is directed away. The maximum aperture achievable is 100%. The functionality is visually detailed in Figure 19.

Three Wilcoxson PC420V-EX series vibration sensors are utilized to collect engine vibration readings. The sensors are designed to endure vibration limitations of 250 g peak and shock limits of 2500 g peak, with a transverse sensitivity of 20mA. The low-frequency response range of these sensors is 10 Hz - 1 kHz, and the high-frequency response range is 4.0 Hz - 2.0 kHz. The installation of vibration modules is conducted using 2 sensors provided by WAGO, which is then affixed to the engine cylinder. Subsequently, they are programmed into the PLC cockpit application for monitoring purposes. The vibration modules are installed on the cylinder head of

the engine to measure vibrations in the x (longitudinal) (mm/s), y (lateral) (mm/s), and z-axis (vertical) (mm/s). The location of these accelerometers is illustrated in Figure 20.

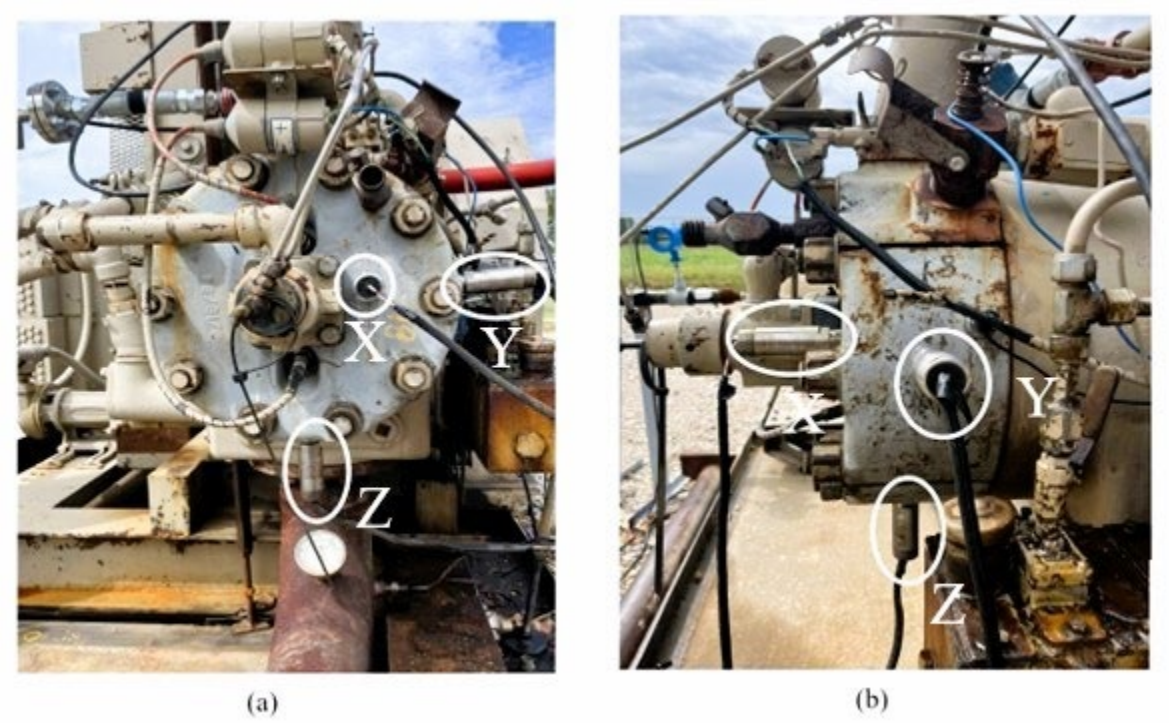

Figure 20 3-Axes vibration sensors setup.
a)Front view. b) Side view

The vibration values in the x, y, and z-axis of the engine are calculated using the RMS (root-mean-square) formula, which involves taking the square root of the arithmetic mean of the squares of these values. The sensors are connected to a Wago 4-channel analog input 4-20 mA to establish a link with the PLC. The output signals from the vibration sensors, along with other data, are immediately logged in the PLC for subsequent analysis. The vibration signals underwent further filtering to eliminate any noise or high-frequency components, ensuring the collected data's reliability and accuracy for precise predictions.

Figure 21 Vibration sensros from Windrock Portable Analyzer. (a) Accelerometer, (b) Velocity probe

Additionally, Figure 21 shows vibration sensors from the Windrock 6400 series, including the (a) Accelerometer and (b) velocity probe, are utilized. Both sensors had a sensitivity of 100 mV/g. The Accelerometer transformed mechanical or physical motion into an electrical signal proportionate to the component's actual movement or vibration. It is placed at various test points on engines. The velocity probe converted mechanical or physical motion into an electronic signal, which the analyzer then processed to reflect actual movement or vibration. The output of the sensor is in inches per second (ips) velocity and could be precisely integrated for measuring components vibrating at lower frequencies, such as frames, cylinders, and skids. The velocity probe is commonly used with FFT data collection.

4.1.2 Data Collection Equipment

Exploring engine performance and emissions required the use of various instruments such as thermocouples, pressure sensors, flow meters, gas analyzers, and engine monitoring devices. Among these, the primary tools are the MKS gas analyzer, Testo gas analyzer, and Windrock engine monitor. Two gas analyzers are employed to capture emission data from the exhaust gas. The MKS 2030 Fourier Transform Infrared Spectroscopy (FTIR) analyzer, specifically engineered for gas analysis tasks like detection and measurement, played a crucial role. Its capability spans a wide range of gases, encompassing NOx, COx, CH_4, and VOCs, through the analysis of their infrared spectra. However, it cannot measure highly concentrated gases like oxygen or nitrogen. As the measurement of oxygen is crucial for combustion optimization, a Testo 300 combustion analyzer is specifically used for this purpose. Additionally, to evaluate engine performance and combustion stability, the Windrock 6400 engine analyzer is employed. This device records in-cylinder pressure about the crank angle, captures flywheel speed, and monitors the engine's primary ignitions. Figure 22 illustrates the equipment used for data collection.

Courtesy of MKS.com

(a)

Courtesy of Testo.com

(b)

Courtesy of ChampionX.com

(c)

Figure 22 Data collection equipment's. a) MKS gas analyzer. b) Testo mobile gas analyzer. c) Windrock engine monitor.

4.2 Experimental Setup

Based on specific operational needs, the engine can operate within a load range of 40% to 75%. The engine's performance varies at each load level within this range. This range, often termed the rated load range, is carefully managed and the engine demonstrates optimal operation within these specified percentages.

In well sites, gas compressors are employed to lift gas from the production well and convey it to transportation pipelines. The compressor's operating load is contingent on the well's gas volume, optimizing efficiency. In contrast, compressors at stations operate at fixed loads to uphold gas pressure and ensure a steady flow in pipelines for end-users. The research replicated the functioning of AJAX compressors, typical in this scenario. While replicating an actual well site or compressor station is unfeasible, the study utilized city pipeline natural gas to power the compressor. To minimize gas wastage, the compressor is integrated into a circuit configuration, as depicted in Figure 23.

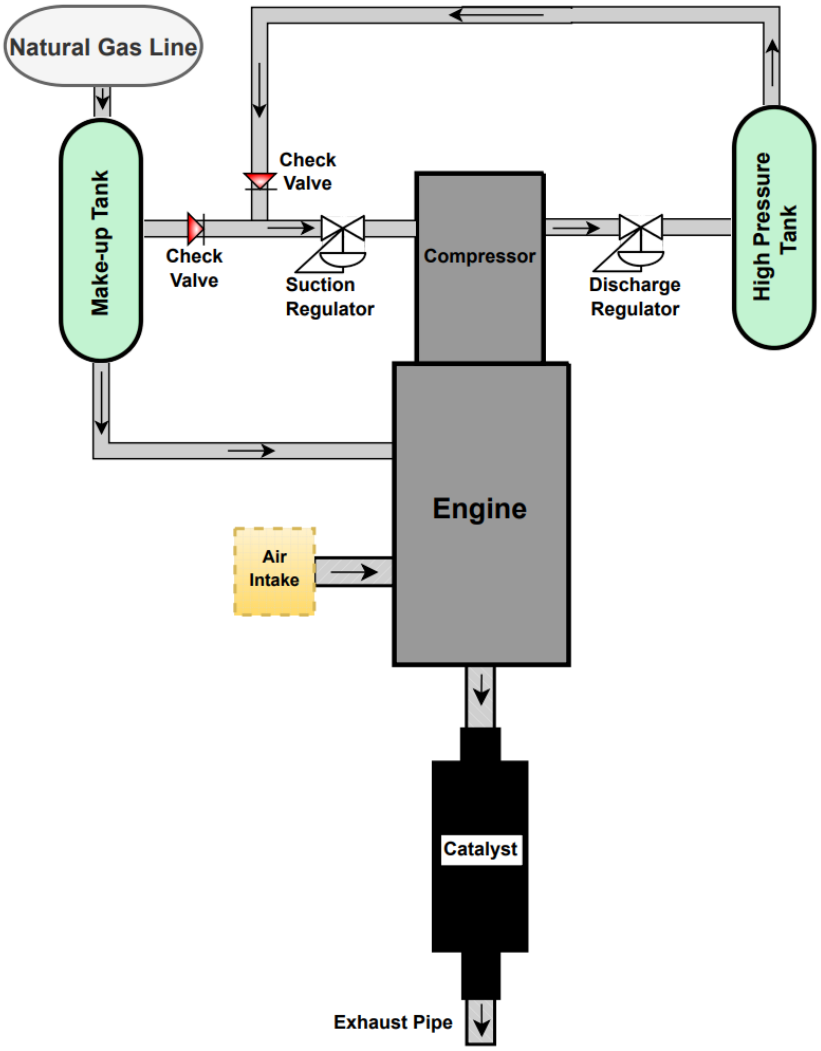

Figure 23 Schematic diagram of engine setup

Figure 24 shows the schematic of the experimental setup. The engine component of AJAX utilizes natural gas from a make-up tank sourced from the city's gas pipeline. This make-up tank, along with a compressor and a high-pressure tank, is interconnected within a circuit. Gas from the make-up tank is compressed by the compressor and pressurized within the high-pressure tank. When the pressure reaches a certain level, the compressor ceases to draw gas from the make-up tank. A suction regulator between the compressor and the make-up tank ensures continuous natural gas cycling within the circuit. Additionally, a check valve prevents gas from backflow into the make-up tank while allowing the tank to supply-more gas to the circuit if the pressure drops too low. Both the suction regulator and discharge regulator are utilized to establish the desired suction and discharge pressures at various loads.

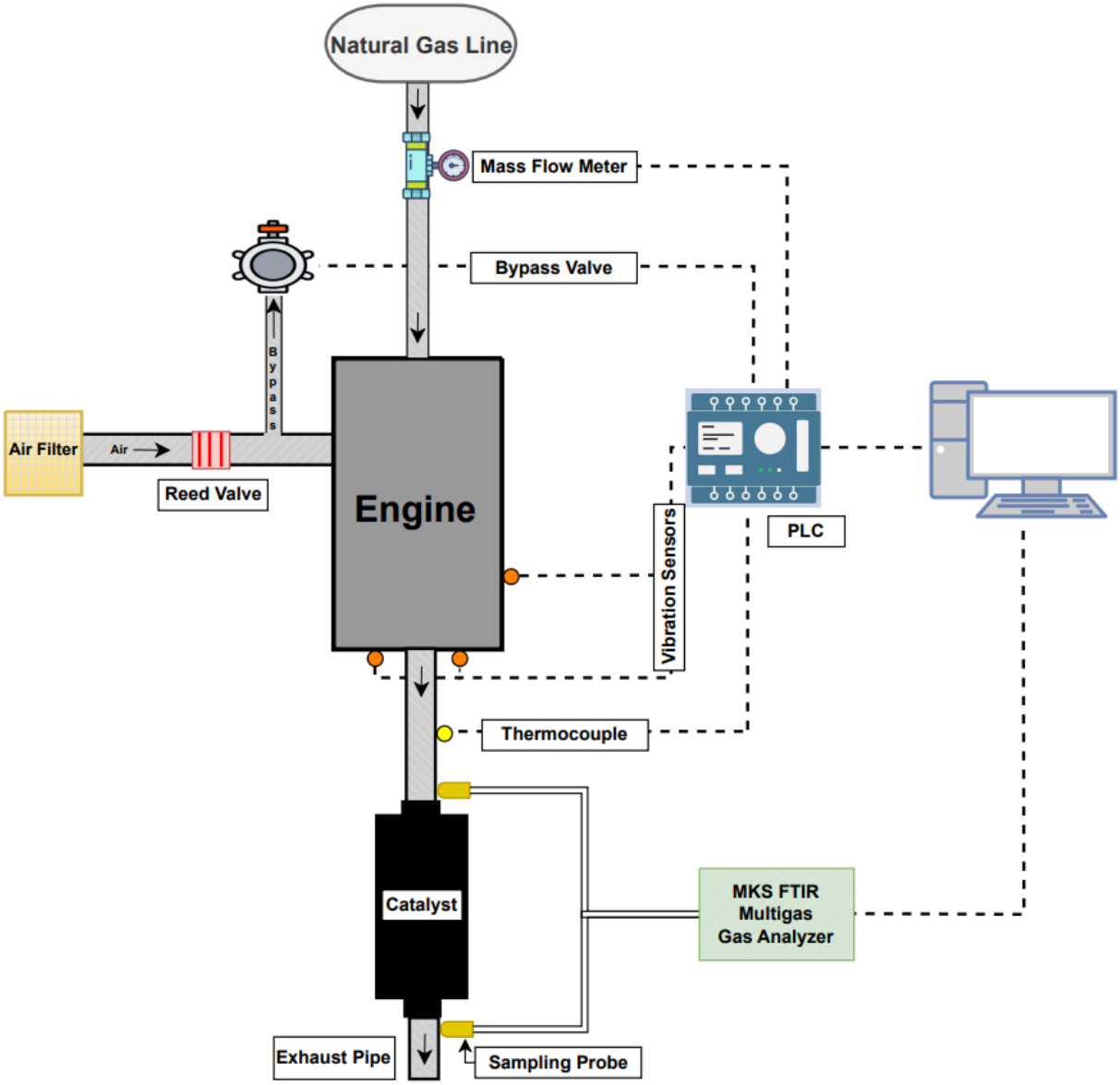

Figure 24 Schematic of Experimental Setup

4.3 Experimental Procedure

The AJAX DPC-81 engine is tested across a load range from 40%, translating to 32.4 BHP, up to 75%, equivalent to 60.8 BHP. However, due to its configuration, the engine cannot operate at a 100% load, with 75% being the maximum attainable load during this study. The operating conditions for different loads are outlined in Table 4.

Table 4 Operating conditions of AJAX DPC-81

	Operating parameters							
Engine Load (%)	40%	45%	50%	55%	60%	65%	70%	75%
Power (BHP)	32	37	41	45	49	53	57	61
Max discharge pressure (psi)	30	36	40	45	50	52	55	60
Average suction pressure (psi)	420	425	430	440	450	455	520	550
Engine speed (rpm)	350	365	380	400	410	435	430	450
Bypass valve position varied (%)	0-80	0-80	0-70	0-70	0-60	0-60	0-20	0-20

The experiment comprised of utilizing the bypass valve. For each load starting from 40% the bypass is incremented at 10% till the exhaust temperature reaches its limit. The same method is followed for the remaining engine loads. Emission data is post-catalyst, along with in-cylinder pressure and primary ignition for combustion analysis.

4.4 Analytical Methods

4.4.1 Emission Analysis

To mitigate the influence of moisture on gas commodities and ensure more dependable data, the compositions are transformed to a dry volume basis. Additionally, considering the engine's operation across various oxygen levels rather than a consistent one, a reference point is necessary to standardize the exhaust gas measurements. Hence, the emission data obtained from the MKS analyzer is adjusted to a dry basis and standardized to a 15% O_2 level for comparison with the emission standards for stationary spark ignition engines set by the New Source Performance Standards(NSPS).

$$x = \mathrm{x}_{exhaust}\left(\frac{21-15}{21-\ \mathrm{O}_{2\ exhaust}}\right) \qquad 5$$

$$\text{ppm} = \text{ppmvw}\left(\frac{100}{100 - \%\ of\ \mathrm{H_2O}_{exhaust}}\right) \qquad 6$$

Were,

x: normalized mole fraction of the gas in ppm

$x_{exhaust}$: mole fraction of the gas measured in ppm

ppm: parts per million of the gas on a dry basis

ppmvw: parts per million of the gas on a wet basis

H_2O: water composition in exhaust gas measured in percentage

O_2%: oxygen composition in exhaust gas measured in percentage

4.4.2 Combustion Analysis

To assess engine combustion stability concerning cycle-to-cycle variability (CCV), the Standard Deviation of peak pressure ($\sigma peak$) is measured. Pressure values for each crank angle (CA) are gathered over 250 cycles, and corresponding calculations are performed. $\sigma peak$ is considered a robust indicator of CCV [164]. These values hold particular significance for part-load conditions, as lean-burn engines often exhibit high CCV under partial load. Additionally, the Indicated Mean Effective Pressure (IMEP) is computed across 250 cycles and graphically represented. IMEP plots offer valuable insights into CCV. The IMEP is determined using the formula [165]. Furthermore, the Coefficient of Variation (COV) for IMEP is also calculated.

$$IMEP = \frac{\oint pdV}{V_{swept}} \quad (7)$$

$$COV = \frac{\sigma_{IMEP}}{\overline{IMEP}} \quad (8)$$

Were,

P = in-cylinder pressure at a particular CA

V_{swept} = swept volume of the cylinder

σ_{IMEP} = standard deviation of IMEP for 250 cycles

$\overline{IMEP}$ = average IMEP for 250 cycles

Furthermore, the Indicated Thermal Efficiency (ITE) is computed for the external bypass system at every 20% increment of the bypass valve position and compared with the ITE of the original operation. The ITE of the engine is determined using the provided formula.

$$ITE = \frac{IMEP \,.\, V_{swept} \,.\, RPM}{60 \,.\, \dot{m}_{fuel} \,.\, NCV} \quad (9)$$

Were,

RPM = revolutions per minute

$\dot{m}_{fuel}$ = mass flow rate of fuel per second

NCV = net calorific value of fuel

Heat release rate (HRR) is a measure illustrating how quickly energy is produced through fuel combustion. The generated heat is primarily transmitted via the piston and transformed into

mechanical energy. Following the principles of the first law of thermodynamics, the heat release rate can be computed using the model presented below.

$$\frac{dQ_n}{d\theta} = \frac{\gamma}{\gamma-1} P \frac{dV}{d\theta} + \frac{1}{\gamma-1} V \frac{dP}{d\theta} + \dot{Q}_{cr} + \dot{Q}_{HT} \qquad 10$$

$$\gamma = \frac{C_p}{C_v} \qquad 11$$

were,

$\frac{dQ_n}{d\theta}$: heat release rate

$\frac{dV}{d\theta}$: rate of change of cylinder volume with respect to crank angle

$\frac{dP}{d\theta}$: rate of change of in-cylinder pressure with respect to crank angle

P : in-cylinder pressure at each crank angle

V : cylinder volume at each crank angle

C_p : specific heat in constant pressure of the fuel

C_v : specific heat in constant volume of the fuel

$\dot{Q}_{cr}$: heat lost to crevices

$\dot{Q}_{HT}$: heat lost to cylinder walls

4.5 Vibration Analysis

Three Wilcoxson PC420V-EX series vibration sensors are utilized for the collection of engine vibration readings. The sensors have a transverse sensitivity of 20mA and are designed to endure vibration limitations of 250 g peak and shock limits of 2500 g peak. A low-frequency response range of 10 Hz - 1 kHz and a high-frequency response range of 4.0 Hz - 2.0 kHz are provided by

these sensors. Subsequently, they are programmed into the PLC ecockpit application for monitoring purposes. The vibration modules are installed on the cylinder head of the engine to measure vibrations in the x (longitudinal) (mm/s), y (lateral) (mm/s), and z-axis (vertical) (mm/s). The RMS (root-mean-square) formula is employed to compute the vibration values in the x, y, and z axes of the engine, which entails taking the square root of the arithmetic mean of the squares of these values.

$$X_{RMS} = \sqrt{\frac{1}{n}(\overline{x_1^2}\, x_2^2 + \cdots .\, x_n^2)}$$

FFT is a mathematical technique used to convert time-based signals into frequency-based signals. This transformation is essential in vibration analysis, as it allows for the identification and analysis of different frequency components within a vibration signal. When applied to vibration data, FFT decomposes the complex, time-varying signal into its constituent frequencies, revealing the different vibrational modes and intensities present. This process is crucial for diagnosing mechanical issues in machinery, as different fault conditions often manifest as changes in the frequency spectrum of vibrations. FFT results can yield to detection of anomalies, identify wear and tear, and predict potential failures in mechanical systems [166, 167].

4.6 Summary

The specifications of the Ajax DPC-81 engine are presented, followed by an overview of the data collection equipment, encompassing various sensors and data collection plans. Subsequently, the experimental setup and procedure are detailed. The discussion extended to analytical methods, including emission and combustion analysis. Lastly, the utilization and calculations involving vibration sensors are also addressed.

Chapter 5 Results and Discussion

This section presents a detailed analysis of the results from the tests performed on the AMS. The engine's performance is rigorously evaluated at various loads ranging from 40% to 75%. The bypass valve settings are adjusted according to the load; at 40% and 45% loads, the valve is opened to 80%, while at 50% and 55% loads, it is set to 70%. For loads of 60% and 65%, the bypass valve opening is capped at 60%, and at higher loads of 70% and 75%, it is limited to 20%. This part of the discussion will illuminate the optimal bypass valve positions identified for these different load levels.

Subsequently, vibration analysis is conducted to select load conditions—specifically 40%, 50%, 60%, and 75%. This involves employing Wilcoxon sensors mounted on the engine, supplemented by vibration sensors from Windrock, to capture the engine's vibrational dynamics under operational stresses followed by FFT analysis.

The final segment of this section delves into the findings from the machine learning models. These results, stemming from comprehensive data analysis, are expounded upon to shed light on their predictive accuracy and potential implications for engine performance optimization.

5.1. Emission Analysis for the Air Management System (AMS)

The advantage of using the AMS is that it does not hinder the incoming air so that the engine can run more efficiently. In current experiments the bypass is opened in 10% increments until the allowable exhaust temperature limit i.e., 700 ^{O}F is reached, and the emissions and combustion data are collected.

In Figure 25, a clear trend in emissions behavior is evident as the bypass valve position is varied. CH_4 emissions show a significant decrease, dropping from 8314 ppm to 2952 ppm, indicating

effective control over unburnt fuel emissions through the AMS. CO_2 emissions initially rise with the increase in bypass valve position up to 30%, followed by a gradual decline to 2.15% at 60% bypass valve position. In contrast, both NOx and VOC emissions peak early but then display a marked reduction after the 30% bypass point. CO emissions, although on an upward trajectory, remain relatively low. Notably, the data analysis reveals that most emissions attain their lowest levels at a 70% bypass valve position, suggesting an optimal setting for emissions reduction at a 40% engine load.

The observed emission trends in Figure 25 can be attributed to various factors. The substantial reduction in CH_4 emissions is likely a result of improved combustion efficiency achieved through the AMS, effectively reducing the amount of unburnt fuel. The initial increase and subsequent decrease in CO_2 emissions correlate with the bypass valve position, indicating more complete combustion at certain settings. The reduction in NOx and VOC emissions after the 30% bypass point could be due to higher exhaust temperatures, which facilitate more efficient combustion, thereby reducing these emissions. The high exhaust temperatures also result in less available O_2 in the exhaust, contributing to the reduction of NOx and VOC. The upward trend in CO emissions, despite remaining low, suggests an incomplete oxidation process, likely due to the lower concentration of O_2 available for converting CO to CO_2 [168, 169].

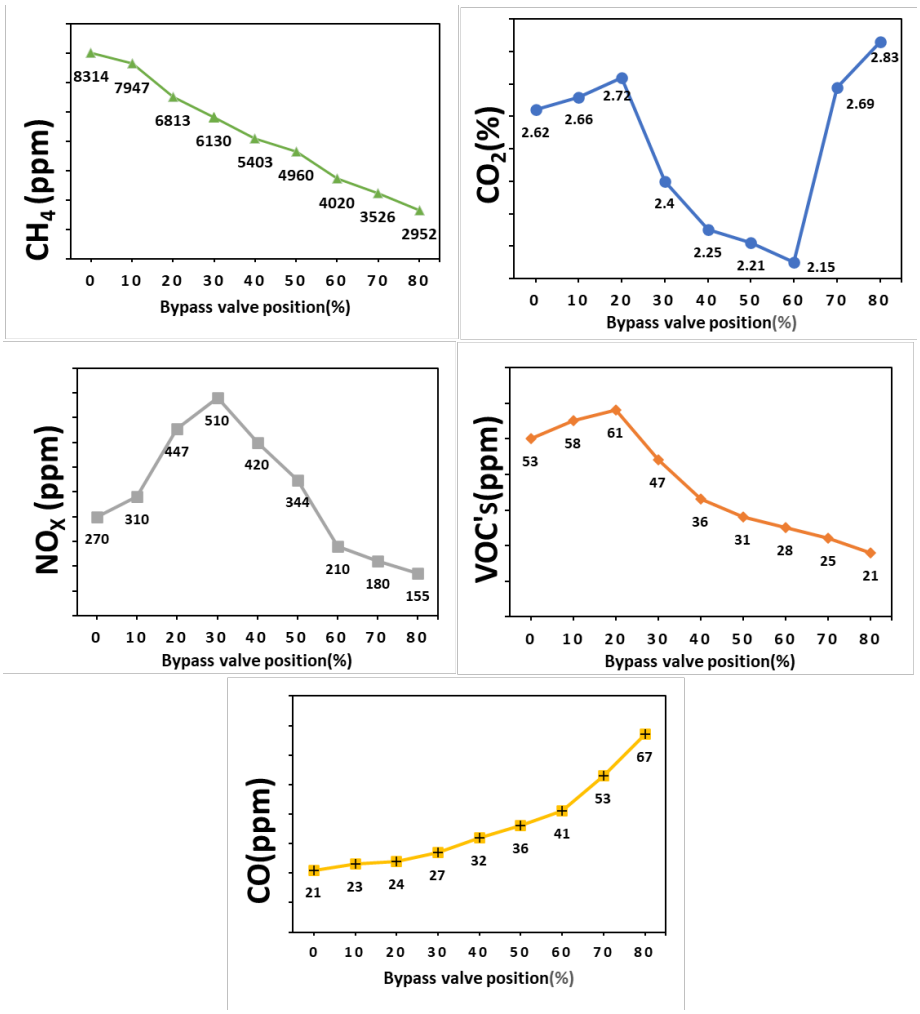

Figure 25. Emissions of 40% engine load and different bypass valve position

In Figure 26, displays emissions data for a 45% engine load, where CH_4 and VOC emissions significantly reduce at higher bypass openings, indicative of improved combustion and catalyst efficiency. NOx emissions initially increase due to a lean air-fuel ratio but subsequently decrease as the bypass valve opens further, enriching the mixture. CO_2 follows a similar trend, initially rising and then decreasing significantly after the 30% bypass point. Conversely, CO emissions start increasing beyond 60% bypass, likely due to insufficient oxygen for complete conversion to CO_2. The data suggests that a 60% bypass valve position optimally reduces most emissions, with a 70% bypass at 45% load being ideal for emission reduction.

The trends at a 45% load in Figure 26 are influenced by several factors. The reduction in CH_4 and VOC emissions is attributed to enhanced combustion and catalyst performance at higher exhaust temperatures. The initial NOx increase, followed by a decrease, is linked to changes in the air-fuel ratio: from leaner to richer with increased bypass opening. This adjustment also affects CO_2 emissions, which drop after an initial rise due to more complete combustion at richer mixtures. The rise in CO emissions at higher bypass positions indicates a lack of oxygen for full oxidation, underscoring the importance of bypass valve management for balancing engine performance and emissions [168].

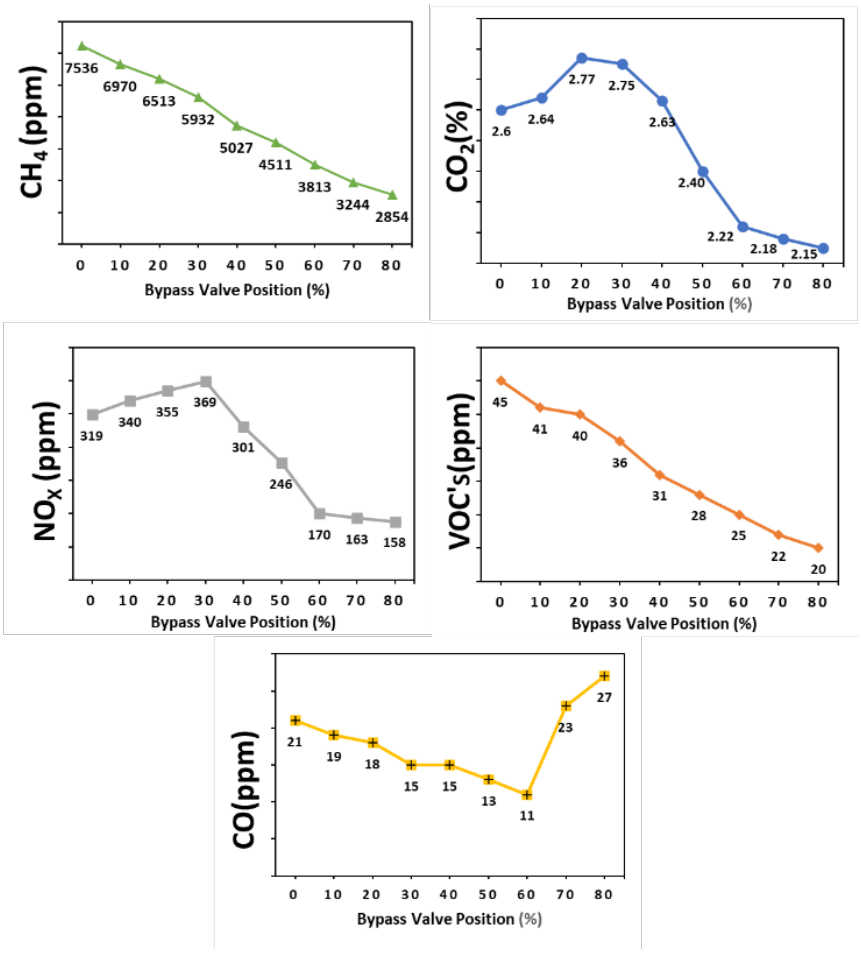

Figure 26. Emissions of 45% engine load and different bypass valve position

Figure 27 presents the emissions trends at a 50% engine load with the bypass valve utilized up to 70%. Notably, NOx emissions initially surge but then decrease by 43% at a 70% bypass, likely due to reduced O_2 concentration. CH_4 and VOC emissions show a marked downward trend, halving from 6022 ppm to 3104 ppm and from 36 ppm to 17 ppm, respectively. This reduction is attributed to increased catalyst efficiency and improved engine performance at higher exhaust temperatures. CO_2 emissions fluctuate slightly before sharply declining past the 50% bypass point. Conversely, CO emissions exhibit significant variations, peaking at a 60% bypass valve opening, possibly linked to fluctuating O_2 levels and air-fuel ratio changes. The data suggests that a 60% bypass valve opening is the most effective for minimizing emissions at this load.

At 50% engine load, the emissions behavior as depicted in Figure 27 can be explained by several engine dynamics. The initial NOx spike and subsequent reduction align with the changes in O_2 concentration due to bypass valve adjustments. The significant decrease in CH_4 and VOC emissions is a result of higher catalyst efficiency under increased exhaust temperatures, coupled with better engine performance. The fluctuating CO_2 emissions reflect the engine's response to varying combustion efficiencies, while the notable increase in CO emissions at a 60% bypass opening could be linked to a temporarily richer air-fuel mixture, affecting the CO to CO_2 conversion process. This analysis indicates that managing the bypass valve position is crucial for optimizing emissions, with 60% bypass emerging as an optimal setting at this load for balancing engine efficiency and environmental impact [168].

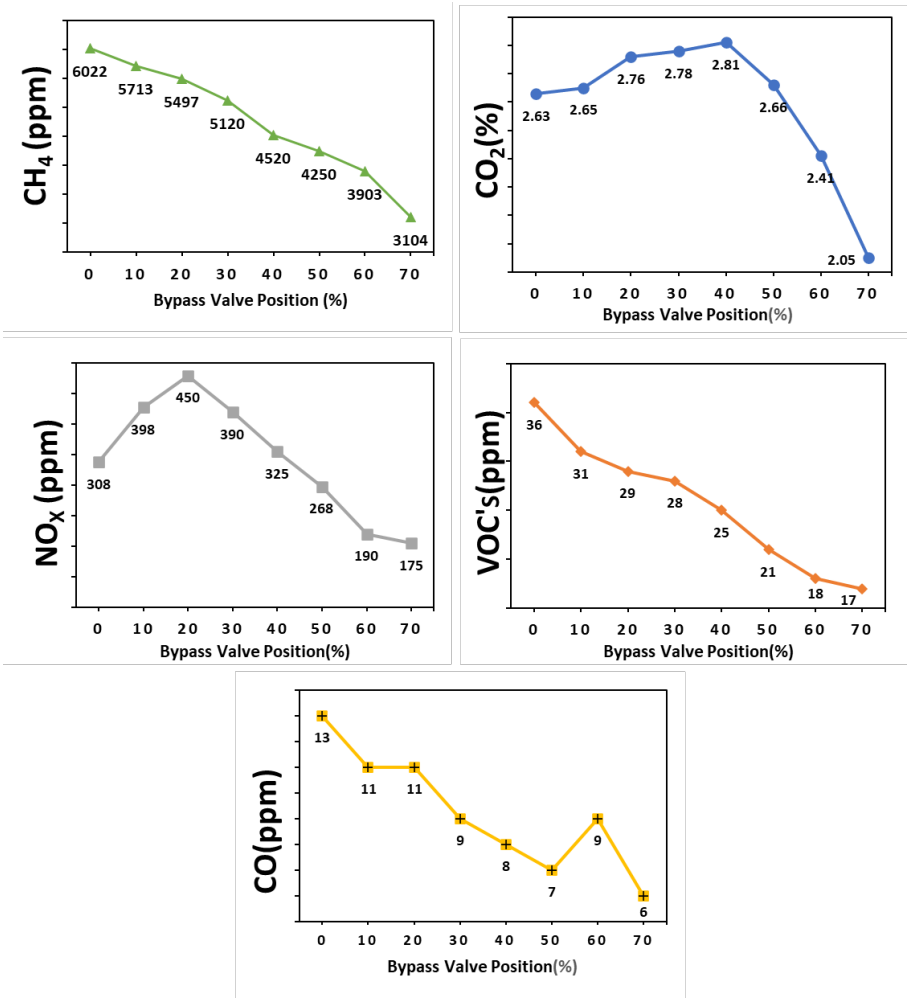

Figure 27. Emission of 50% engine load and different bypass valve position

Figure 28 showcases the emissions at a 55% engine load, with the bypass valve positions extended up to 70%. The data reveals a consistent decrease in CH_4 and VOC emissions, dropping significantly from 5013 ppm to 2457 ppm and 27 ppm to 7 ppm, respectively. NOx emissions, on the other hand, show an increase up to the 20% bypass position, likely due to the high Heat Release Rate (HRR) characteristic of this load. CO_2 emissions initially rise until the 40% bypass position, possibly due to increased O_2 presence, but subsequently undergo a sharp overall decrease, ending at 2.48%. This trend is attributed to the reduction in O_2 concentration at higher bypass positions. CO emissions, while generally following a downward trend, experience a slight uptick post the 50% bypass point, ultimately resulting in a 42% reduction at the highest bypass position. The

analysis suggests that a 50% bypass valve position optimally reduces emissions, striking a balance between performance and exhaust temperature constraints.

At a 55% engine load, as depicted in Figure 28, the emission trends reflect the complex interplay of engine dynamics and bypass valve settings. The steady decline in CH_4 and VOC emissions can be attributed to the enhanced efficiency of combustion and catalytic processes at this load. The initial rise in NOx emissions correlates with the increased HRR, a characteristic of this engine load, before tapering off due to richer air-fuel mixtures at higher bypass settings. The fluctuation in CO_2 emissions highlights the effect of varying O_2 levels on combustion, with a notable reduction observed as the bypass valve opening increases. Interestingly, the CO emissions' pattern at this load is more consistent than at 50% load, with a significant overall reduction, indicating improved combustion efficiency. The data points to a 50% bypass position as the ideal setting for emission reduction at this load, considering both the performance and the limitations imposed by exhaust temperatures [168].

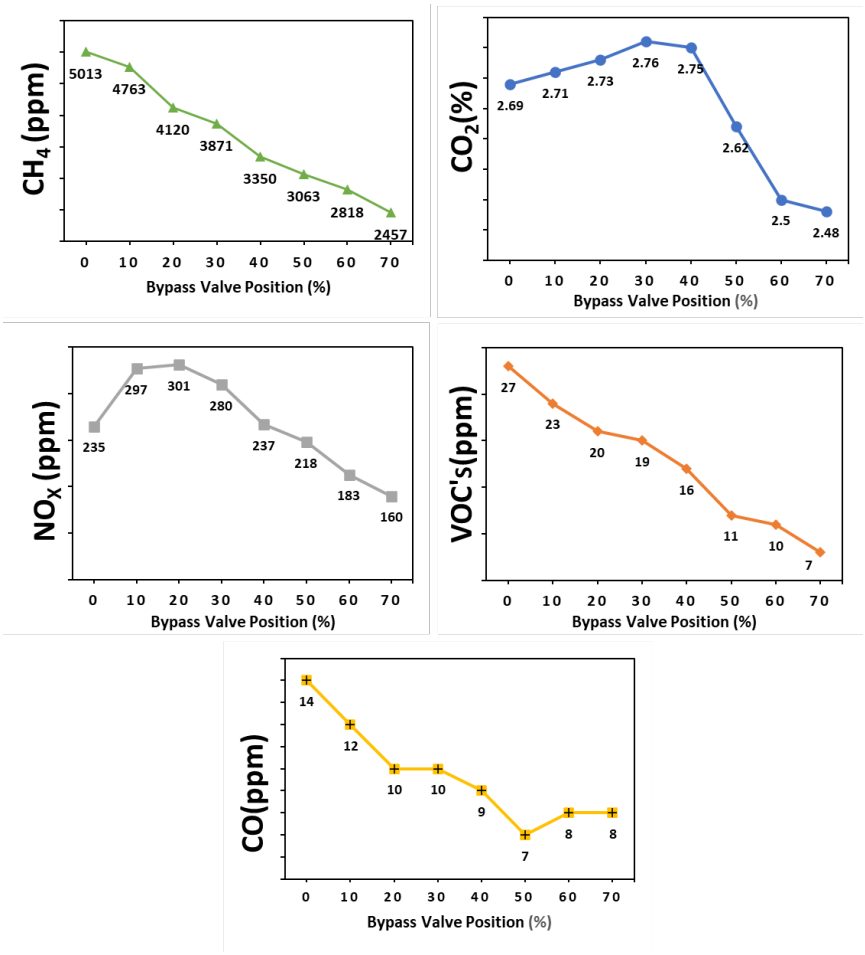

Figure 28. Emissions at 55% engine load and different bypass valve position

Figure 29 presents the emissions at a 60% engine load with a set 60% bypass position. At this higher load, bypass valve operation is restricted by exhaust temperature limits. The data shows a general downward trend in most emissions. CH_4 and NOx emissions see initial declines of 17% and 11%, respectively, with a more pronounced decrease past the 40% bypass position, mainly due to lower oxygen concentration and enhanced engine performance. CO emissions initially decrease steeply, recording the lowest levels at the 40% bypass setting, likely due to higher O_2 availability. However, CO increases again at 50% and 60% bypass positions, correlating with reduced O_2 levels. VOCs exhibit the lowest emissions at 30% and 60% bypass positions, benefiting from increased catalyst efficiency at higher exhaust temperatures. CO_2 emissions show an initial

increase up to the 40% bypass position, then drop to 2.86%, with further reductions being limited by exhaust temperatures. The analysis indicates that the most effective bypass position for reducing emissions at a 60% load is 50%.

The emission trends at a 60% engine load, as seen in Figure 29, are indicative of the interplay between bypass valve positions and engine operating conditions. The substantial decrease in CH_4 and NOx beyond the 40% bypass point can be attributed to the richer fuel mixture and reduced oxygen concentration, leading to more efficient combustion. The pattern of CO emissions, decreasing initially and then increasing at higher bypass settings, reflects the changing oxygen levels impacting the oxidation process. The varying emissions of VOCs at different bypass positions are linked to the catalyst's performance, which improves with the increase in exhaust temperature. Similarly, the initial rise and subsequent fall in CO_2 emissions highlight the engine's response to varying combustion conditions. These findings suggest that managing the bypass valve position is critical for optimizing engine performance and emissions, with a 50% setting emerging as optimal at this load [40, 168].

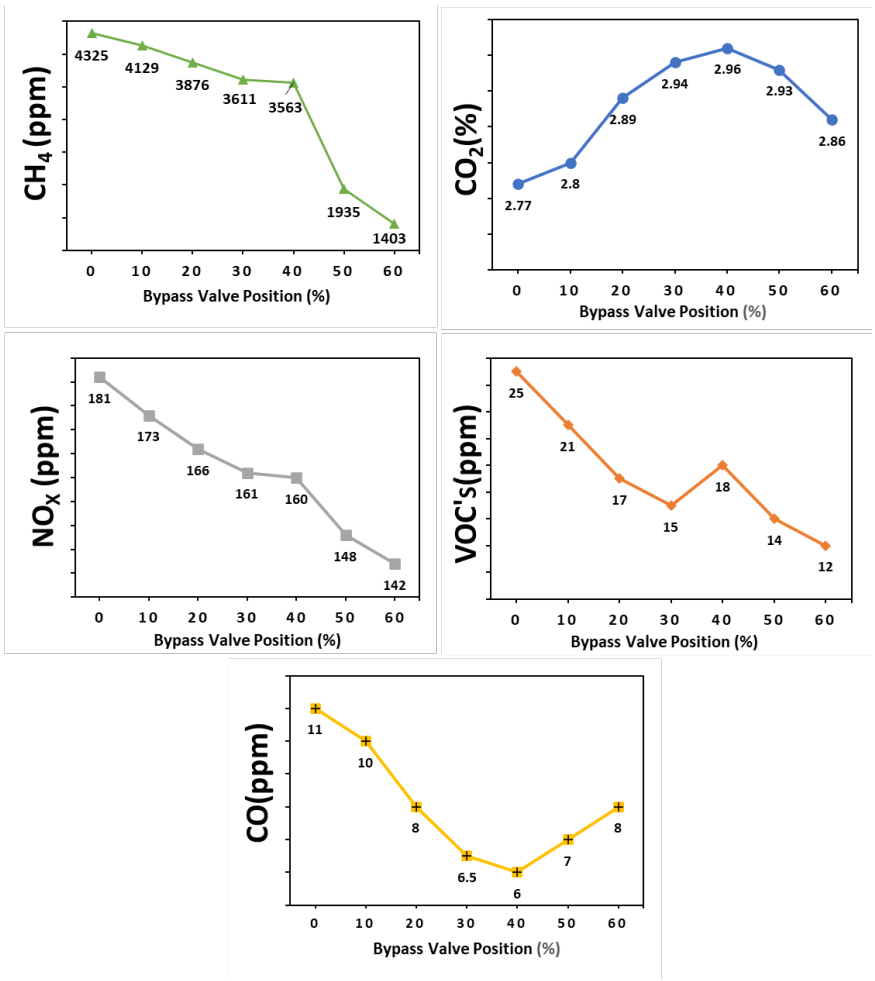

Figure 29. Emission at 60% engine load and different bypass valve position

Figure 30 displays the emission trends at a 65% engine load, with bypass valve adjustments up to 60%. The data reveals a general decline in most emissions. CH_4 emissions notably reduce by 70%, mainly due to decreased unburnt fuel. CO_2 also trends downward, moving from 2.98% to 2.4%, although the reduction is less marked at higher loads, likely due to the lower O_2 concentration impacting CO_2 conversion. VOC emissions initially decrease until the 30% bypass position, then spike at 40%, but eventually exhibit significant reductions at 60% and 70% bypass positions, attributable to improved catalyst efficiency. NOx emissions, which are high at 0% bypass, decrease as the bypass opens. However, both NOx and CO levels rise at 50% and 60% bypass positions,

probably due to reduced O_2 availability. Based on this analysis, a 40% bypass valve position emerges as the optimal setting for emissions reduction at this load.

The emission behavior at a 65% engine load, as depicted in Figure 30, can be explained through various engine dynamics. The significant drop in CH_4 emissions is likely due to improved combustion efficiency, reducing unburnt fuel presence. The downward trend in CO_2 emissions, although less pronounced at higher loads, points to challenges in achieving complete CO_2 conversion due to lower O_2 levels. The fluctuating VOC emissions, particularly the spike at 40% bypass, might be influenced by temporary inefficiencies in the catalyst, which is rectified at higher bypass settings. The initial high NOx levels and their subsequent decrease correlate with the richer fuel mixture achieved through bypass adjustments. However, the increase in both NOx and CO emissions at higher bypass settings highlights a potential imbalance in the air-fuel mixture, emphasizing the need for careful management of bypass valve positions. This trend analysis underlines the importance of optimizing the bypass valve position to achieve the best balance between engine performance and emission control, with 40% bypass being optimal at a 65% engine load [168, 170].

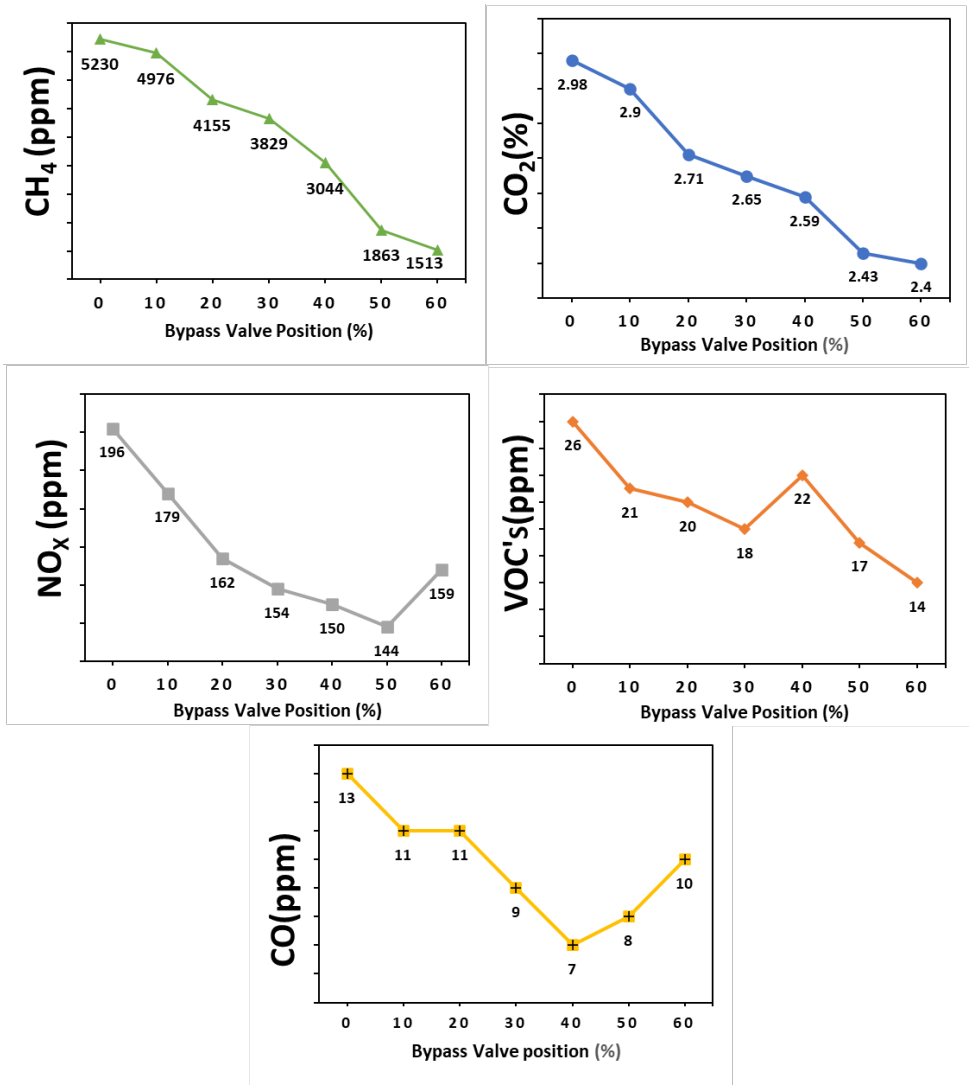

Figure 30. Emission at 65% engine load and different bypass valve position

Figure 31 highlights the emission trends at a 70% engine load with bypass valve settings up to 20%. This high load condition reveals a general trend of decreasing emissions, a sign of more efficient combustion processes. CH_4 emissions show a reduction from 1744 to 1466 ppm at the 20% bypass position, although the variation between 10% and 20% bypass positions is minimal. CO_2 emissions follow a steep downward trajectory, indicating reduced emissions due to a lower O_2 concentration hindering complete conversion. NOx emissions, starting at 96 ppm at 0% bypass, achieve their lowest levels at the 20% bypass setting, again linked to reduced O_2 concentration. VOCs also significantly decrease, with the 10% bypass position demonstrating the lowest

emissions, a result of improved catalyst efficiency at higher exhaust temperatures. While the bypass valve setting adversely affects CO levels, they remain within safe ranges. However, the 20% bypass position presents operational challenges, particularly in temperature management. The data suggests that a 10% bypass valve position is most effective for minimizing emissions at this high engine load.

In Figure 31, the emission patterns at a 70% engine load underscore the effectiveness of fine-tuning the bypass valve for emissions control. The reduced CH_4 emissions across both 10% and 20% bypass positions reflect a more efficient combustion, with little unburnt fuel. The sharp decline in CO_2 emissions can be attributed to the lower oxygen levels at higher loads, which affects the complete conversion of CO to CO_2. The pattern of NOx emissions reflects a direct correlation with O_2 concentration, where reduced levels lead to lower NOx emissions. The significant decrease in VOCs at the 10% bypass position highlights the optimal interplay between the catalyst efficiency and exhaust temperatures at this setting. Despite the bypass valve's negative impact on CO levels, they remain controlled, indicating an efficient combustion process. However, operational constraints, particularly related to temperature management at higher bypass settings, suggest that the 10% position is the most suitable for achieving both optimal performance and emission reduction at a 70% engine load.

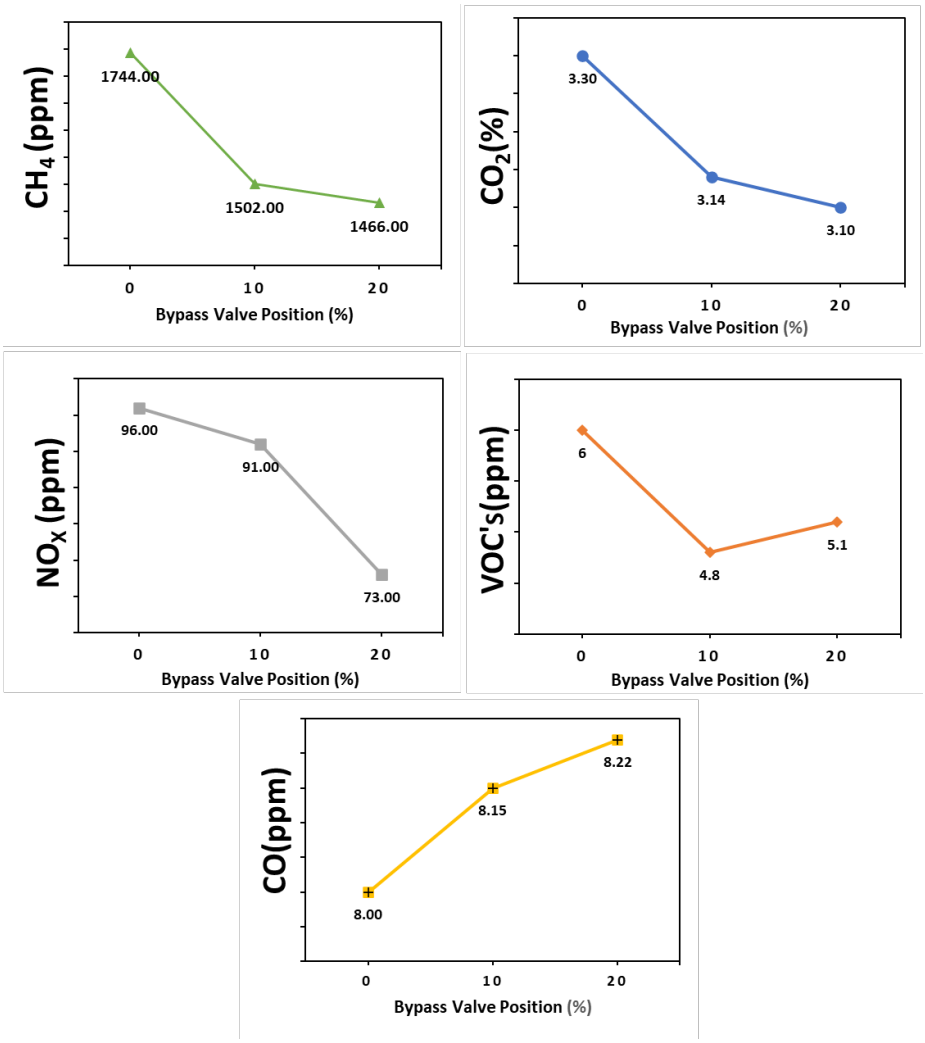

Figure 31. Emissions at 70% load and different bypass valve position

Figure 32 reveals the impact of the bypass system on emissions at a 75% engine load, with valve positions up to 20%. CH_4 emissions demonstrate a notable downward trend, dropping from 1811 to 1490 ppm, indicative of the AMS efficiency in enhancing performance and reducing unburnt fuel. CO_2 emissions show a decrease from 3.4% to 3.2% at a 10% bypass position, a trend that becomes more pronounced at higher loads, highlighting the bypass system's influence on emissions. However, CO_2 levels rise at the 20% bypass, suggesting increased O_2 accumulation in the exhaust. NOx emissions consistently decrease, with the lowest levels at 20% bypass. VOCs also follow a downward trend, reflecting the catalyst's effectiveness at higher loads. CO emissions,

in contrast to the 70% load, decrease with the lowest levels at 20% bypass. Despite the minimal differences between 20% and 30% bypass positions, a key limitation at 20% is managing exhaust temperatures. Thus, the optimal bypass position for a 75% load is determined to be 10%.

The emission data for a 75% engine load, as shown in Figure 32, underscores the AMS's role in reducing emissions across different bypass valve positions. The consistent decrease in CH_4 emissions across the load spectrum is a testament to the AMS's ability to improve combustion efficiency and minimize unburnt fuel. The trend in CO_2 emissions, with an initial decrease followed by an increase at higher bypass settings, indicates a complex interaction between combustion efficiency and O_2 concentration. NOx emissions' downward trajectory further illustrates the AMS's effectiveness in controlling emissions, particularly in reducing NOx levels at higher bypass positions. VOC emissions also decrease, albeit not as significantly as CH_4, showing the catalyst's increased efficiency at higher operational loads. The reduction in CO emissions at 75% load, differing from the pattern observed at 70% load, suggests variations in combustion processes and O_2 availability at different bypass settings. The analysis indicates that a 10% bypass position optimally balances emissions reduction and operational constraints like exhaust temperature at this high engine load [168].

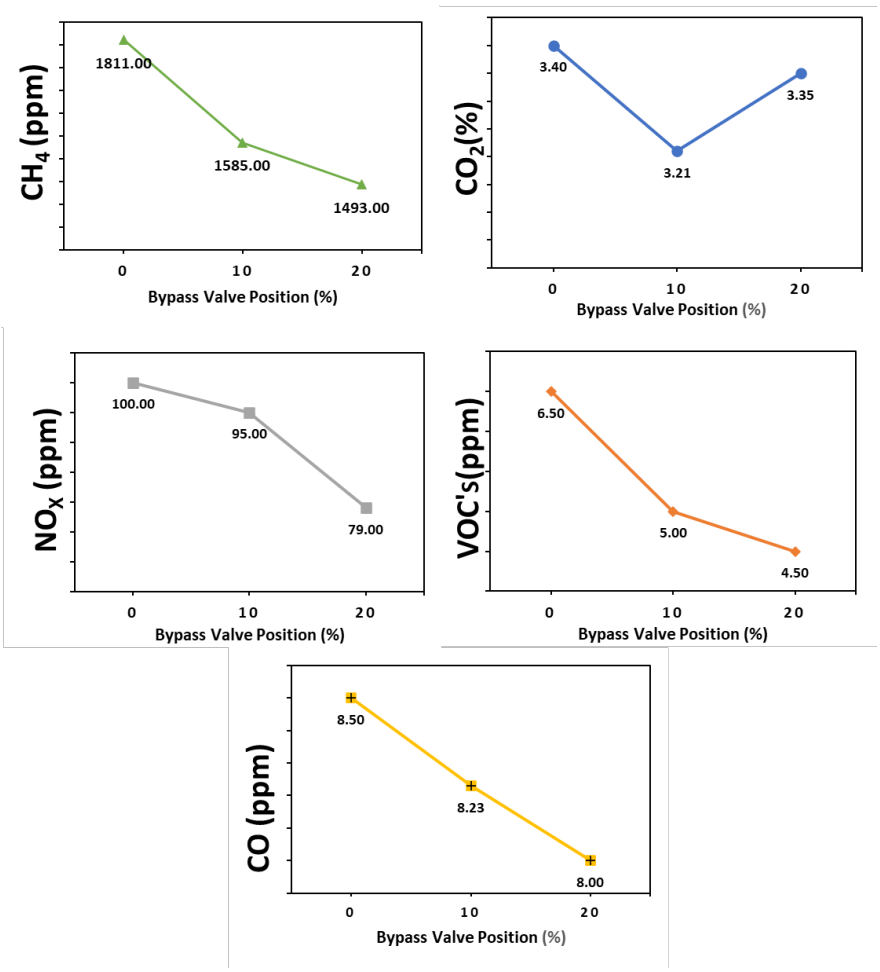

Figure 32. Emissions at 75% load and different bypass valve position

In conclusion, Emissions related to various engine loads are discussed in detail, revealing distinct impacts on emissions for each load condition. This highlights the critical need for optimizing the bypass valve position differently for various loads. It is worth noting that the highest bypass valve position recorded the least emissions; however, due to exhaust temperature limitations, this position cannot be conclusively considered as the optimum choice.

5.2 Combustion Performance

Figure 33 presents an empirical analysis of the Indicated Thermal Efficiency (ITE) at different engine loads (40% to 75%) and bypass valve positions. Initially, at lower bypass positions, ITE values are high for all loads, suggesting higher thermal efficiency due to richer air-fuel mixtures.

As bypass valve positions increase, ITE also rises across all loads, signifying better fuel utilization. The pattern varies with load; at 40% and 45% loads, ITE gradually decreases until a 40% bypass, then increases significantly as the bypass opens to 80%, indicative of more efficient combustion at these settings. At higher loads of 70% and 75%, ITE sees a steeper increase at a 20% bypass, reflecting more effective combustion and improved efficiency at these higher bypass settings. These variations highlight the engine's different operational characteristics at various loads and bypass valve positions.

The trends in ITE across different loads and bypass valve positions, as seen in Figure 33, provide valuable insights into engine performance under varying operational conditions. At lower loads (40% and 45%), the gradual increase in ITE at higher bypass positions suggests that the engine becomes more efficient in fuel utilization when the air-fuel mixture is richer. This indicates a balance between maintaining efficient combustion and managing airflow. The substantial increase in ITE at higher loads (70% and 75%) at a 20% bypass position indicates that these engines achieve optimal combustion efficiency at a specific bypass setting, which aligns with the engine’s design for higher load operations. The variation in ITE response to bypass valve adjustments underscores the importance of tailoring these settings to engine load for optimal performance, emphasizing the interplay between airflow, fuel utilization, and combustion efficiency [30, 37, 168].

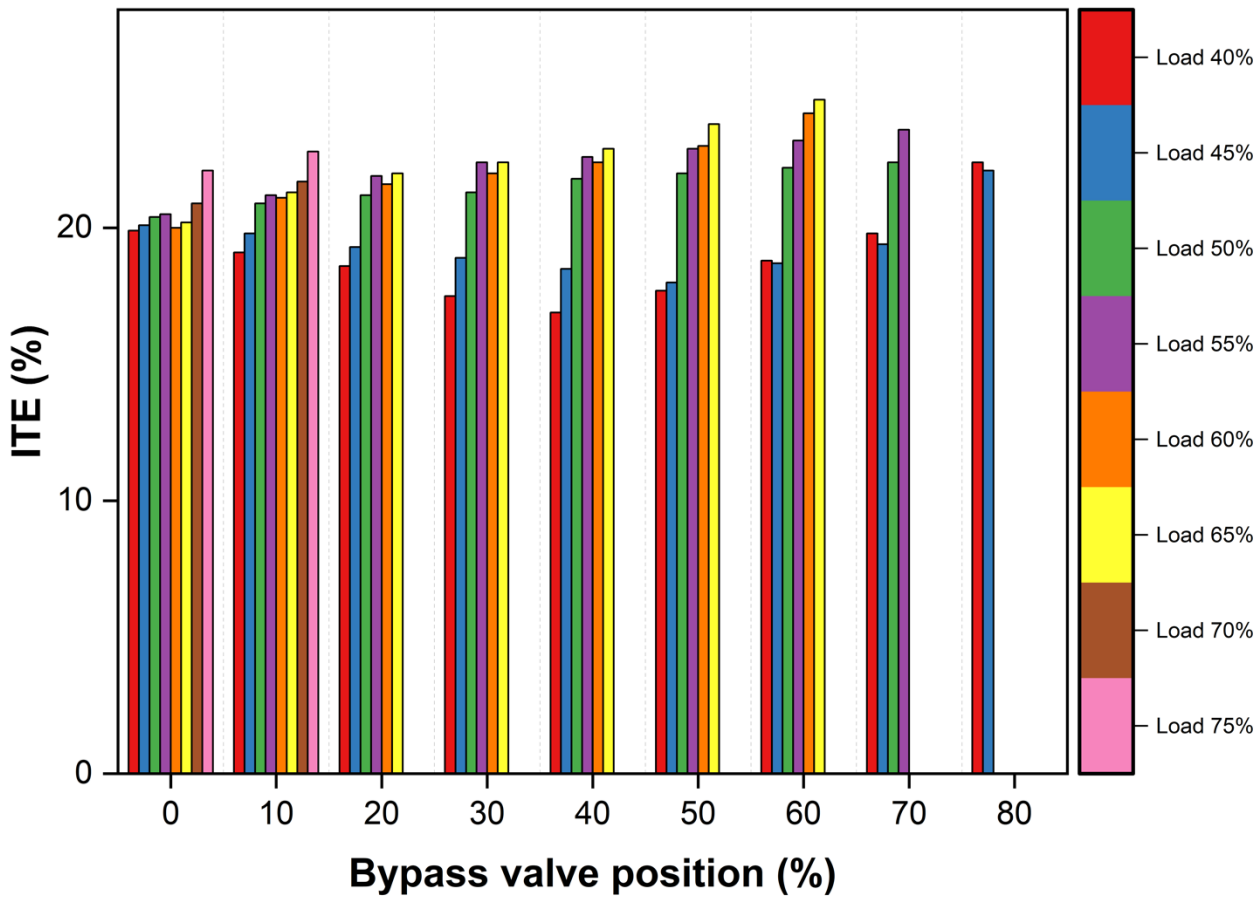

Figure 33. ITE for different loads and bypass valve positions

Figure 34 provides an analysis of the cycle-to-cycle variability (CCV) in terms of the standard deviation of peak pressure (σ_{Ppeak}) across different bypass valve positions for engine loads ranging from 40% to 75%. σ_{Ppeak} values, which indicate combustion stability, are shown on the y-axis, while bypass valve positions are on the x-axis. The results show a general trend of decreased σ_{Ppeak} values at wider bypass valve positions, suggesting more stable combustion due to greater air bypass. This observation is particularly apparent at bypass positions beyond 50%, where the engine tends to operate with a richer air-fuel mixture, leading to more stable combustion. At lower bypass positions, corresponding to leaner air-fuel mixtures, σ_{Ppeak} values are higher, indicative of less stable combustion. For the lower loads (40% and 45%), σ_{Ppeak} increases up to 50% bypass, signifying leaner mixtures and less stable combustion. Beyond 50% bypass, a steep decline in

σ_{Ppeak} values occurs as the mixture becomes richer. In contrast, higher loads show lower σ_{Ppeak} values, with a slight increase at maximum bypass, indicating better stability at these settings.

The trends in CCV and σ_{Ppeak} values across various bypass valve positions, as depicted in Figure 34, offer crucial insights into the combustion stability under different engine operating conditions. At lower bypass settings, the engine runs on leaner air-fuel mixtures, which, while efficient, can lead to higher CCV as reflected in increased σ_{Ppeak} values. This suggests a susceptibility to combustion efficiency fluctuations under these conditions. However, as the bypass valve opens wider (beyond 50%), allowing more air to bypass, the engine transitions to richer air-fuel mixtures, enhancing combustion stability as evidenced by the significant reduction in σ_{Ppeak} values. This trend is more pronounced at lower loads (40% and 45%), where the shift from a lean to a richer mixture markedly improves stability. For higher loads, the engine demonstrates inherently more stable combustion, with σ_{Ppeak} values remaining relatively low, even at maximum bypass. These findings highlight the importance of optimizing the air-fuel mixture through bypass valve adjustments to achieve stable and efficient engine operation across different load conditions [30, 168].

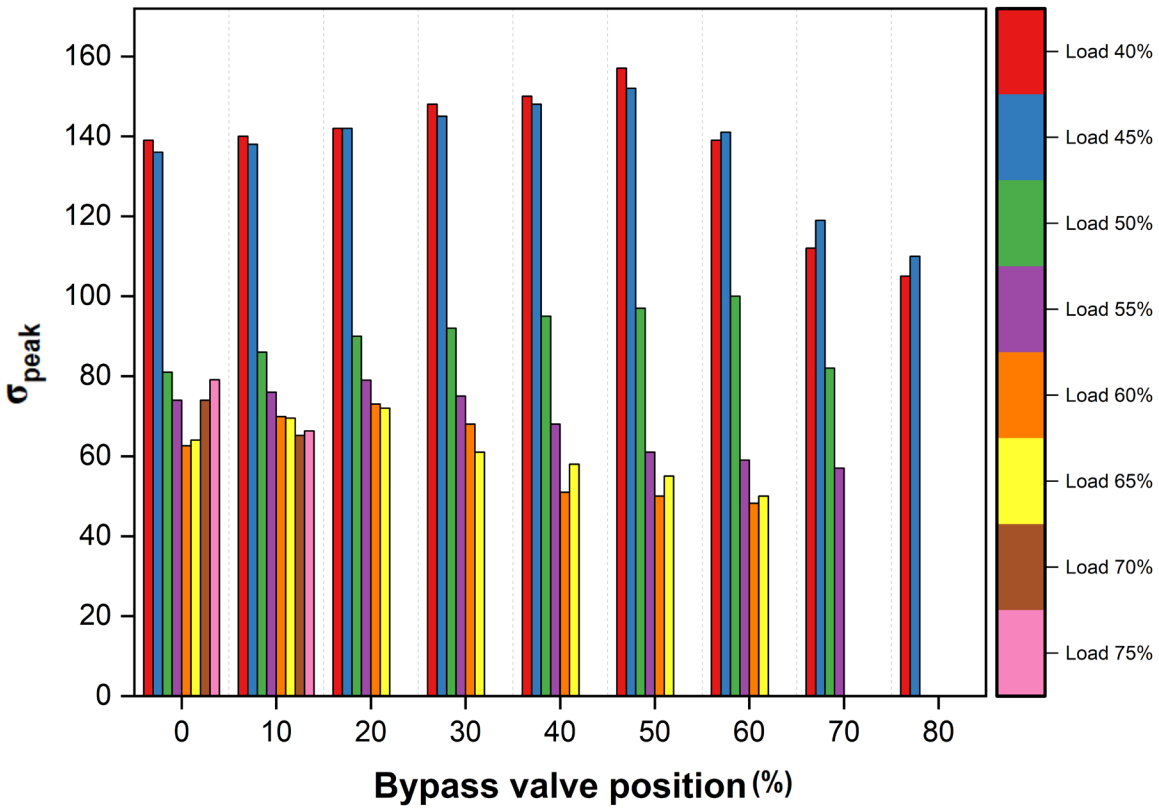

Figure 34. σ_{ppeak} for different loads and bypass valve position

Figure 35 presents the standard deviation of Mean Effective Pressure (σ_{MEP}) across different engine loads (40% to 75%) and bypass valve positions. σMEP, which measures cycle-to-cycle variations in combustion pressure, is shown on the y-axis, with bypass valve positions on the x-axis. The graph reveals a general trend where σ_{MEP} decreases as the bypass valve position increases, suggesting more consistent combustion cycles with richer mixtures achieved by allowing more air to bypass. This trend is more pronounced at lower loads (40% and 45%), where an increase in bypass position correlates with decreased σ_{MEP}, aligning with emission reduction trends. At higher loads, the decrease in σ_{MEP} is less significant, reflecting a less pronounced reduction in emissions at these loads.

The data in Figure 35 highlights the relationship between bypass valve positions, combustion stability, and engine load. At lower loads, the decrease in σ_{MEP} with increased bypass valve

positions indicates improved combustion stability due to richer air-fuel mixtures. This is consistent with the observed trend in emission reduction, where increased bypass leads to lower emissions, suggesting more efficient combustion. On the other hand, at higher loads, the impact of bypass valve position on σ_{MEP} and emissions is less dramatic. This suggests that at these higher loads, the engine operates more consistently, regardless of the air-fuel mixture changes. These observations underscore the importance of bypass valve adjustments in achieving optimal combustion stability and efficiency, particularly at varying engine loads [40].

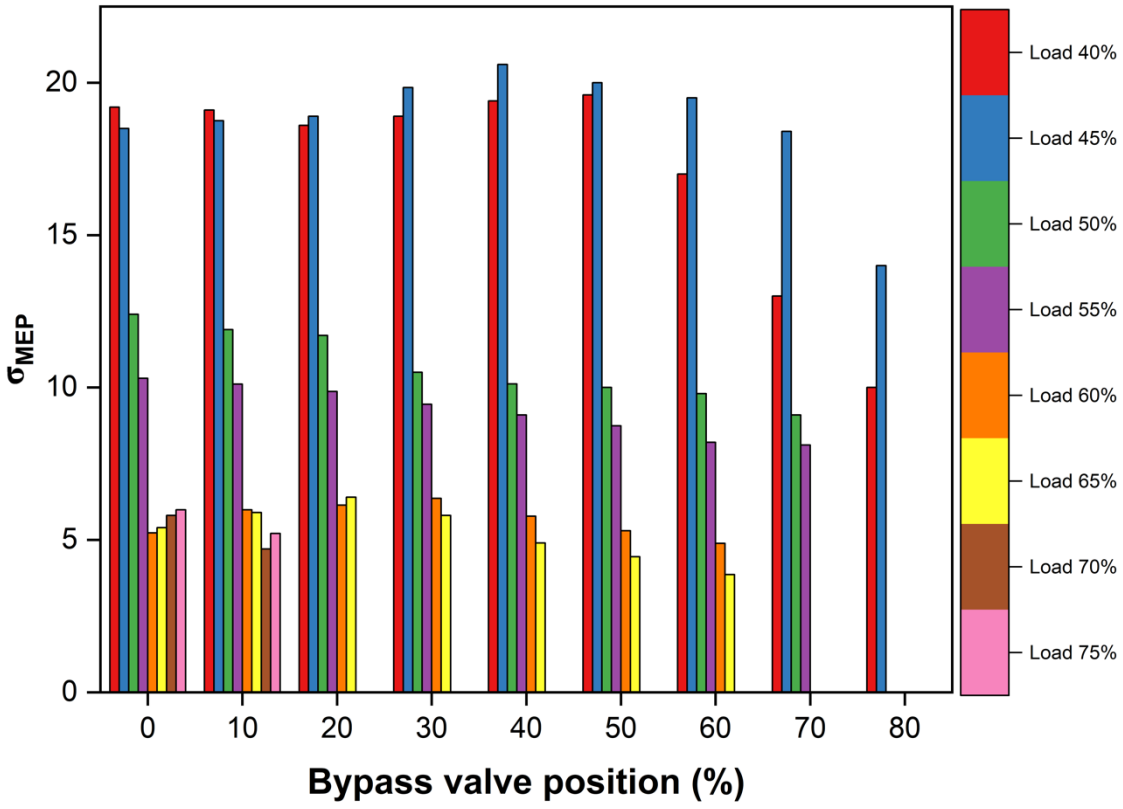

Figure 35. σ_{MEP} for different loads and bypass valve positions

5.3 Optimum Bypass Valve Positions

Figure 36 provides a visual comparison of the bypass valve positions as a function of engine load percentages. The horizontal axis represents the engine load in percentage terms, starting from 40% and increasing incrementally to 75%. The vertical axis denotes the bypass valve position, also in percentage terms. Each bar corresponds to a specific engine load percentage and reflects the optimum bypass valve position required at that load.

As the engine load increases, the bypass valve position generally appears to decrease. For example, at a 40% engine load, the bypass valve position is around 70%, indicating a higher opening. Conversely, at a 75% engine load, the bypass valve position is significantly lower, close to 10%, suggesting a much smaller opening. This pattern suggests that the need for bypassing air decreases as the engine load increases.

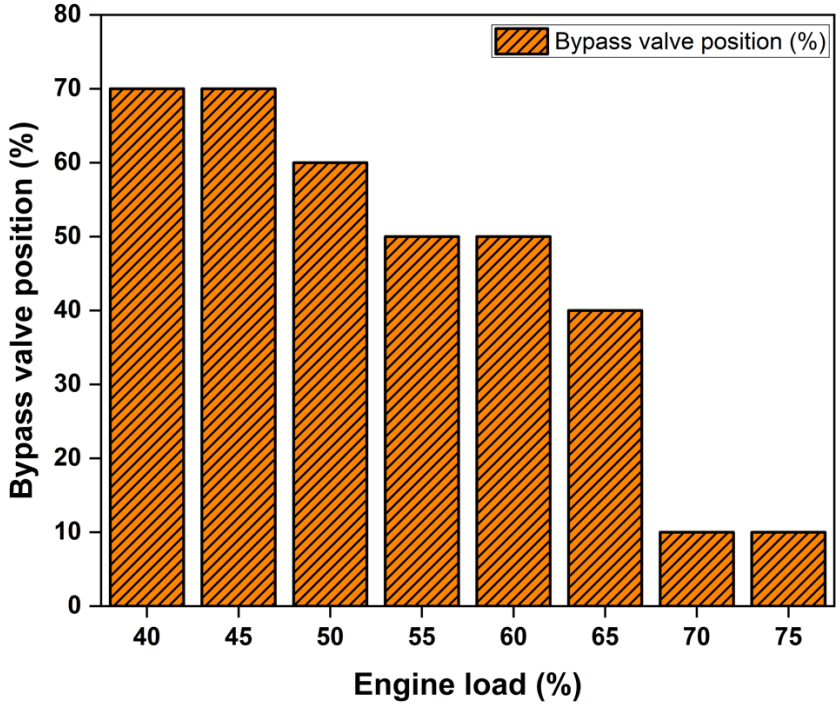

Figure 36 Optimum bypass valve position for different loads

5.4 Vibration Analysis

line graph in Figure 37 represents the Root Mean Square (RMS) vibration measurements in millimeters per second for three axes (X, Y, and Z) as a function of the bypass valve position at 40% engine load, expressed as a percentage. The X-axis of the graph represents the bypass valve position, while the Y-axis indicates the vibration RMS. Each line, marked with distinct colors, corresponds to one of the three axes of vibration measurement.

As the bypass valve position increased from fully closed (0%) to more open positions, the graph shows a downward trend in all these axes, reaching a minimum at around 60% valve position, and then a spike is observed for 70% bypass.

The peak vibration for the X and Y axis occurs at 20%, however the Z-axis peaks at 10% bypass this proves that vibration is independent of bypass. The lowest values observed are on the 60% bypass position for all the axes. At 70% bypass, all the vibrations spiked peaked due to the maximum opening of the bypass.

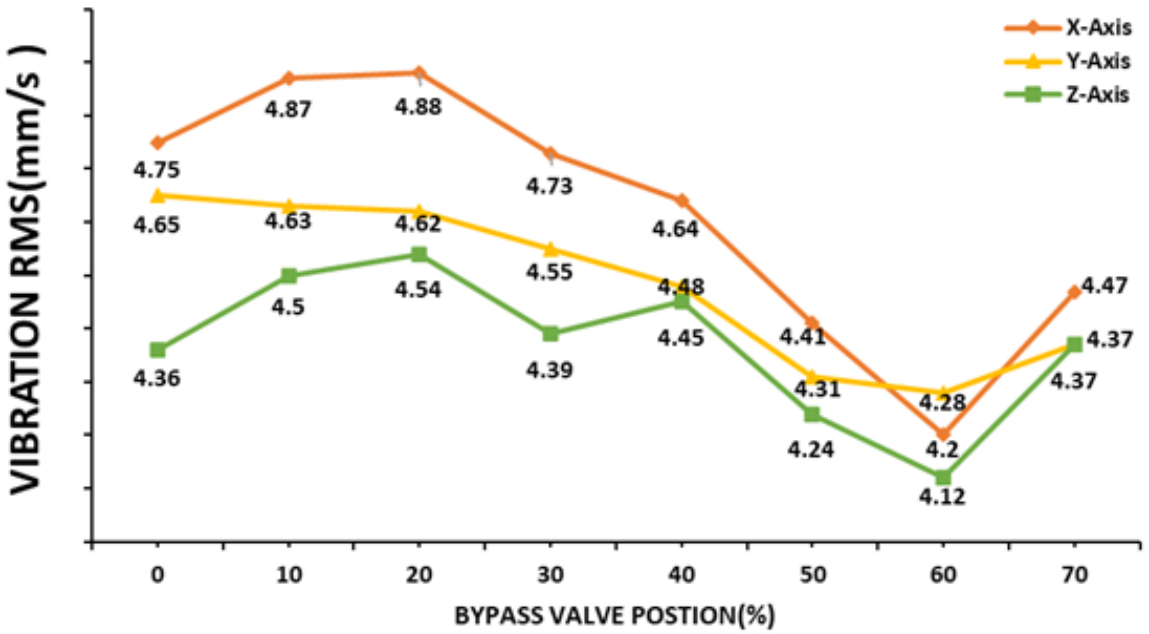

Figure 37. Line graph of Average RMS Vibration at 40% load and various bypass valve positions

Figure 38 shows the relationship between engine vibration (in millimeters per second) and engine load (expressed as a percentage). The x-axis displays the vibration intensity, while the y-axis represents the engine load. Each data point corresponds to a specific instance of engine operation, capturing the load at a given level of vibrational intensity.

The plot reveals a dispersion of vibration data across a broad range of engine loads, without a clear or consistent pattern to suggest no correlation between the two variables. As vibration intensities increase, there is a wide spread of engine load percentages, indicating that higher vibrations do not necessarily correspond to higher or lower engine loads predictably.

The data suggests that engine load is influenced by factors beyond just the measured vibration intensity. This could imply that vibration, while an important parameter for engine health monitoring, may not be a standalone indicator of engine load. For engine diagnostics and

performance optimization, this graph indicates the need to consider additional parameters alongside vibration to accurately assess engine load [131, 132].

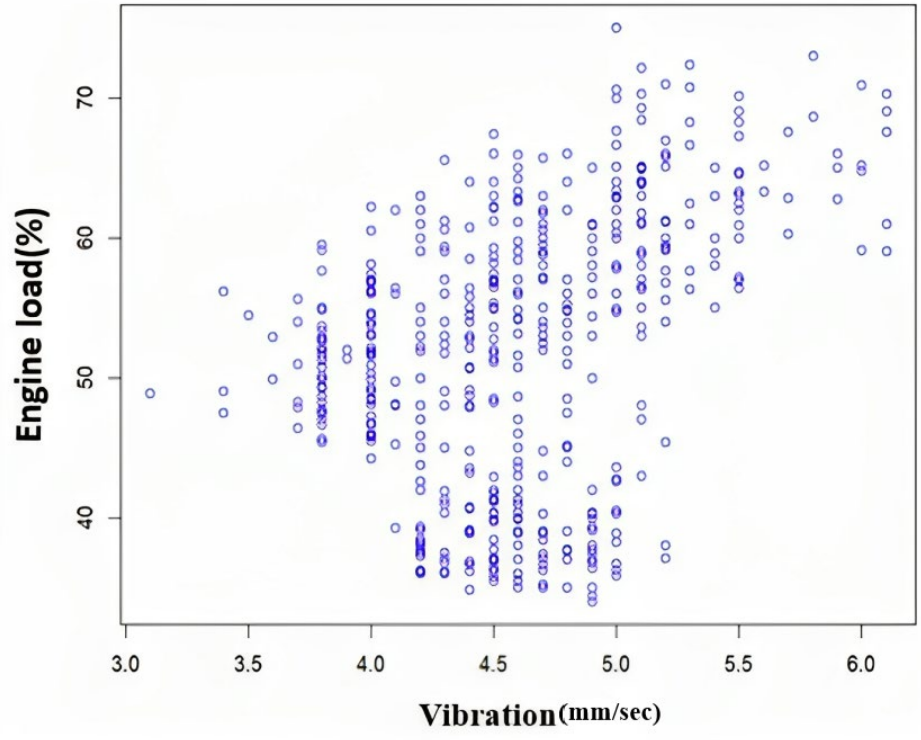

Figure 38 Scatter plot of vibration for different engine load

Figure 39 comprises three pairs of graphs, each depicting vibration data from an AJAX DPC-60 Engine Frame at 40% load and three different bypass positions (0%, 40%, and 80%). Each pair consists of a time waveform and an accompanying FFT graph. The time waveform plots show the raw vibration signal over time, illustrating the engine's dynamic behavior through its operating cycle. FFT is a mathematical technique used to transform time-domain data into frequency-domain data. In these FFT plots, the X-axis represents frequency in cycles per minute (CPM), and the Y-axis indicates the vibration amplitude. The top-left graph (a) displays a time waveform representing vibration in the axial direction, with amplitude measured in inches per second plotted against time in milliseconds. The irregular waveform suggests a complex vibration signature with notably high amplitude, indicating significant axial engine movement. In the (b) middle-left graph,

a frequency spectrum is derived from the axial time waveform data, presenting dominant vibration frequencies in CPM (cycles per minute). The spectrum data for the 0% bypass position exhibits spikes at starting points, indicating normal engine conditions. In contrast, the spectra for the 40% and 80% bypass positions reveal spikes indicating prolonged and substantial variations in vibration, particularly evident in the second and third pairs of graphs (c).

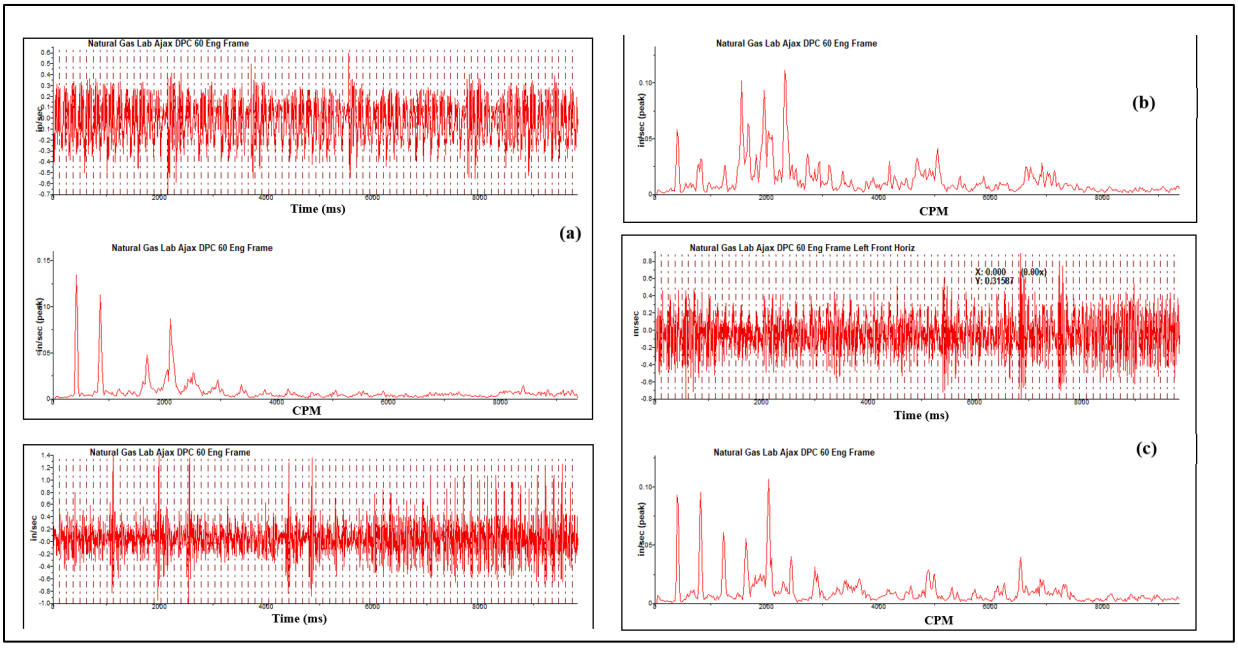

Figure 39. Time wave and FFT graph of 40% load and different bypass valve positions. a) 0% bypass. b) 40% bypass and c) 80% bypass.

Figure 40 comprises three pairs of graphs, each illustrating vibration data from an AJAX DPC-60 Engine Frame at 50% load and three distinct bypass positions (0%, 40%, and 70%). Each pair includes a time waveform and a corresponding FFT graph a, b and c. Notably, the time waveform for the 0% bypass position displays a few spikes. The accompanying spectral graph (a) represents FFT data, where spikes are primarily concentrated at the starting frequency, indicating relatively low vibration levels. However, the spectral graphs on the top right and bottom left (b) shows a multitude of spikes, indicating higher and more variable vibrations at increased bypass positions.

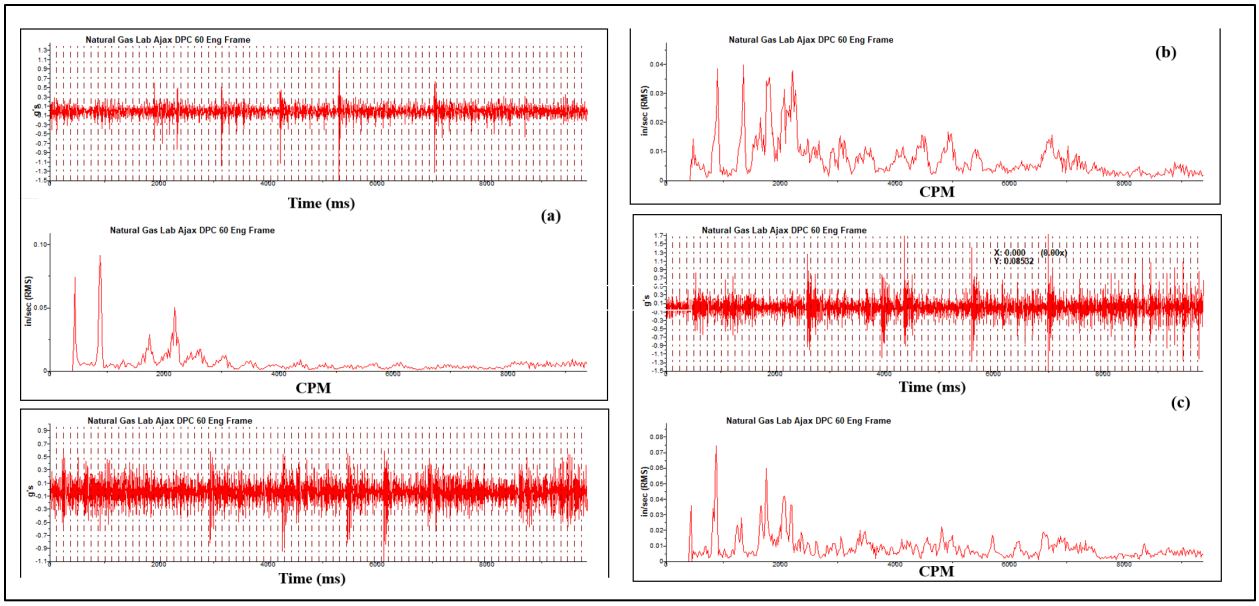

Figure 40. Time wave and FFT graph of 50% load and different bypass valve positions. a) 0% bypass. b) 40% bypass and c) 70% bypass.

Figure 41 shows engine vibrations at a 60% load with three different bypass valve positions: 0%, 30%, and 60%. The time waveform at the top left of the figure for the 0% bypass valve position reveals an array of vibration spikes, suggesting considerable engine movement in the axial direction. This is an indication of less stable engine operation.

The (b) shows the vibration at 40% bypass valve position. Here, a significant reduction in vibration spikes suggests improved combustion and a more stable engine operation. This is in stark contrast to the (c) 70% bypass valve position, where an increase in vibration spikes is observed once again. The pattern of spikes at different bypass valve positions indicates that while some bypassing is beneficial for reducing vibrations and optimizing engine performance, there is a threshold beyond which further bypassing can degrade engine stability. This highlights the delicate balance that must be maintained when adjusting the bypass valve to ensure optimal engine performance.

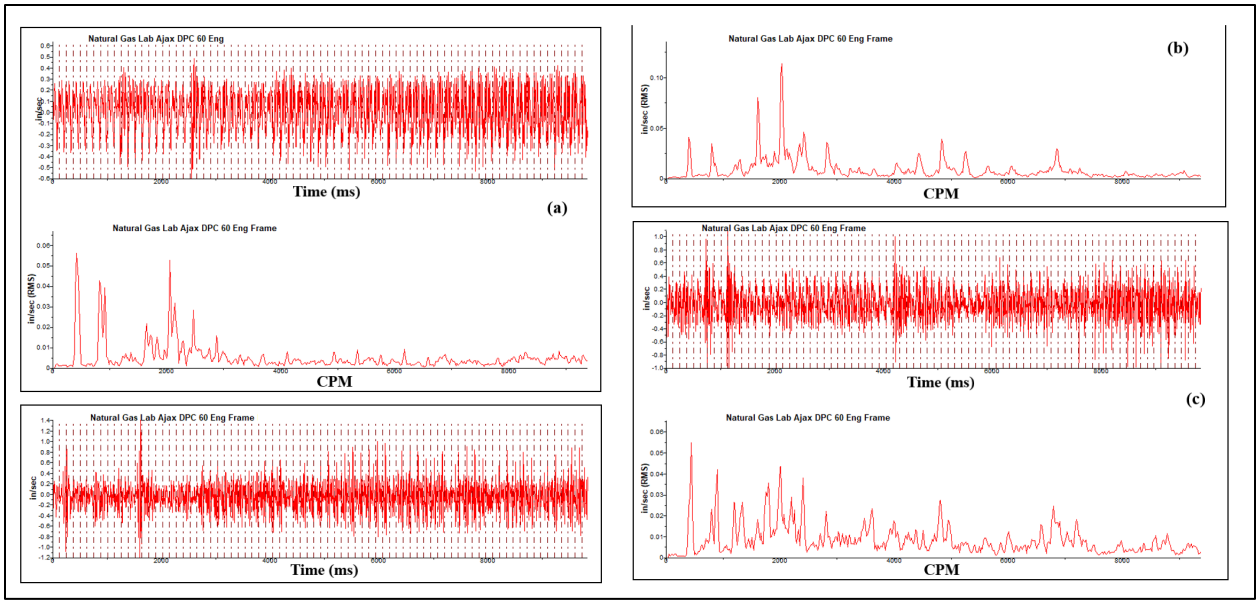

Figure 41. Time wave and FFT graph of 60% load and different bypass valve positions. a) 0% bypass. b) 40% bypass and c) 70% bypass.

Figure 42 features three pairs of comprehensive graphs, each offering a detailed glimpse into the vibration data stemming from an AJAX DPC-60 Engine Frame operating at a substantial 75% load. These pairs thoughtfully encompass a trio of bypass positions 0%, 10%, and 20%, providing a comprehensive exploration of the engine's vibrational dynamics. In each pair, there is a precise time waveform artfully paired with a corresponding FFT graph. These graphs effectively illustrate the distinct impact of heightened load conditions. Notably, at the (a) 0% bypass position, the spectral graph displays common spikes, indicative of typical vibrations. However, upon closer inspection of the (b) 10% bypass scenario, the time waveform (bottom left) reveals pervasive fluctuations throughout the recorded data, while the spectral graph (top-right) highlights a profusion of spikes across the entire dataset, implying inconsistent engine speeds over time. In contrast, the (c) 20% bypass configuration presents an entirely different story, where the time waveform exhibits strikingly prominent spikes, dwarfing those in other scenarios. Furthermore, the corresponding spectral graph (bottom right) unmistakably highlights pronounced and sustained vibrations, reflecting the engine's substantial oscillations throughout the entire cycle.

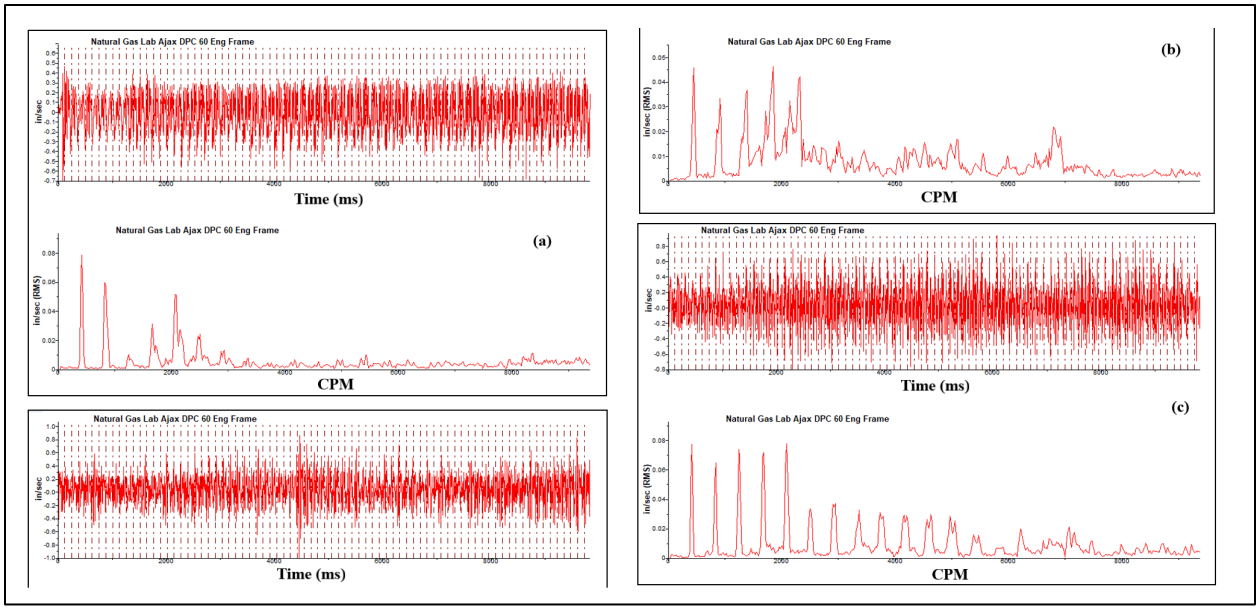

Figure 42. Time wave and FFT graph of 75% load and different bypass valve positions. a) 0% bypass. b) 10% bypass and c) 20% bypass.

In summary, FFT analysis has unveiled a noteworthy insight: vibration patterns vary across different bypass valve positions and tend to escalate with heightened bypass valve positions and engine loads. This crucial knowledge would have remained concealed without the application of FFT. This underscores the importance of not relying solely on vibration data for predictive purposes, emphasizing the necessity of a well-rounded setup for accurate predictions beyond vibration metrics alone.

5.5 Machine Learning

Figure 43 presents a heatmap a correlation matrix of various engine parameters, providing a visual summary of how each variable potentially influences the others. Dark blue cells indicate a strong positive correlation, suggesting a direct and proportional relationship between parameters, such as between Suction Pressure and Discharge Pressure, where an increase in one is associated with an increase in the other. Light blue to white cells represents a weaker positive correlation. The shades of red illustrate negative correlations, with dark red indicating a strong inverse relationship, such

as between O_2 and Load, implying that higher engine loads tend to have lower oxygen levels. Cells closer to white indicate a negligible or no correlation, as observed between Vibrations and most other parameters, suggesting that vibrations do not significantly correlate with engine performance metrics like RPM, NOx, and Load. This heatmap is a powerful diagnostic tool, enabling quick identification of relationships that could be leveraged for optimizing engine performance and developing predictive maintenance schedules.

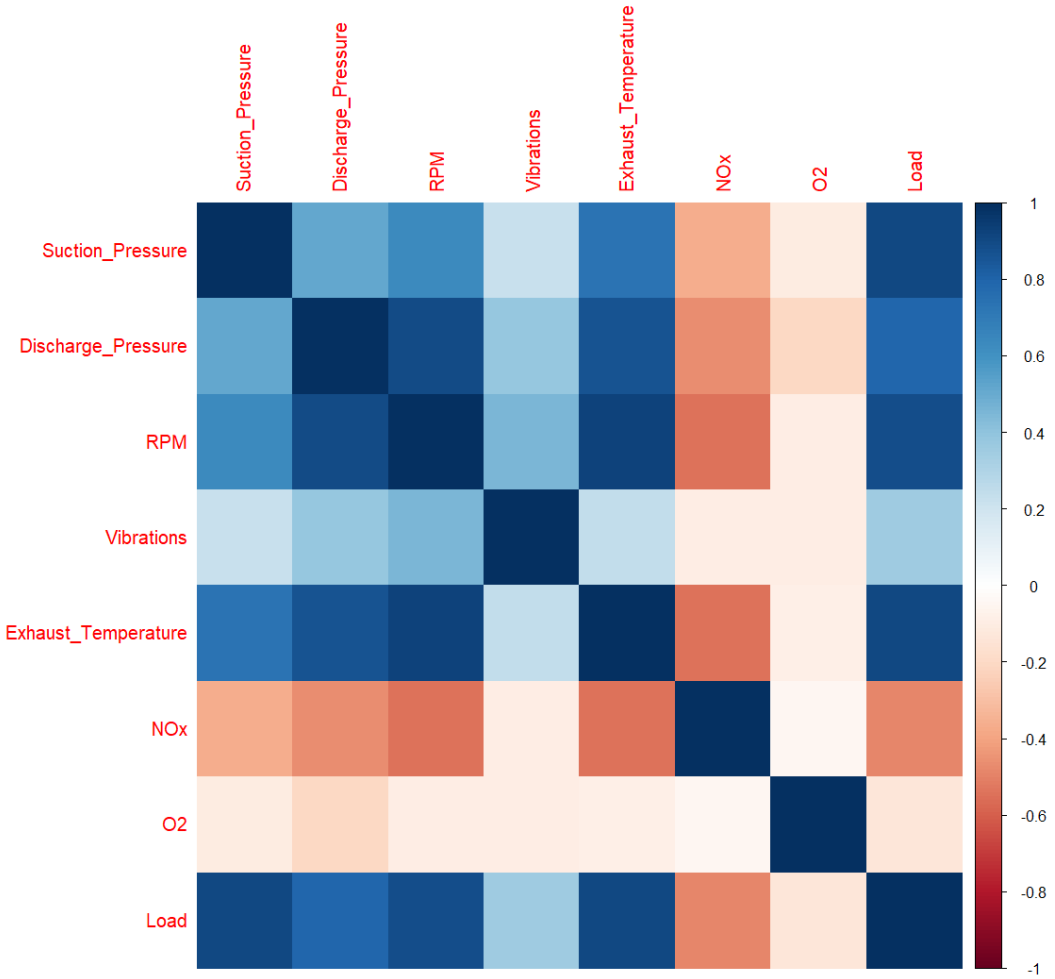

Figure 43. Correlation plot of the data

This scatter plot in Figure 44 visualizes the relationship between the suction pressure (in psi) and the loa, where each dot represents an individual observation of the engine's performance at varying conditions. The suction pressure is plotted along the x-axis, and the engine load is plotted along

the y-axis. The plot is color-coded based on the engine load ranges, from 40 to 75%, allowing for a visual segmentation of data points across the load spectrum. A fitted line, likely representing a linear regression model, is drawn through the data points, indicating a positive correlation between suction pressure and engine load—suggesting that as suction pressure increases, the engine load tends to increase as well. The spread of the data points reveals that at lower loads (blue points), the data are more tightly clustered around the fitted line, implying a more consistent relationship between suction pressure and load. As the load increases (green to yellow points), the spread becomes wider, indicating more variability in the engine load at higher suction pressures. This plot is essential for understanding how suction pressure affects engine load, and the linear model provides a predictive tool for estimating load based on suction pressure readings.

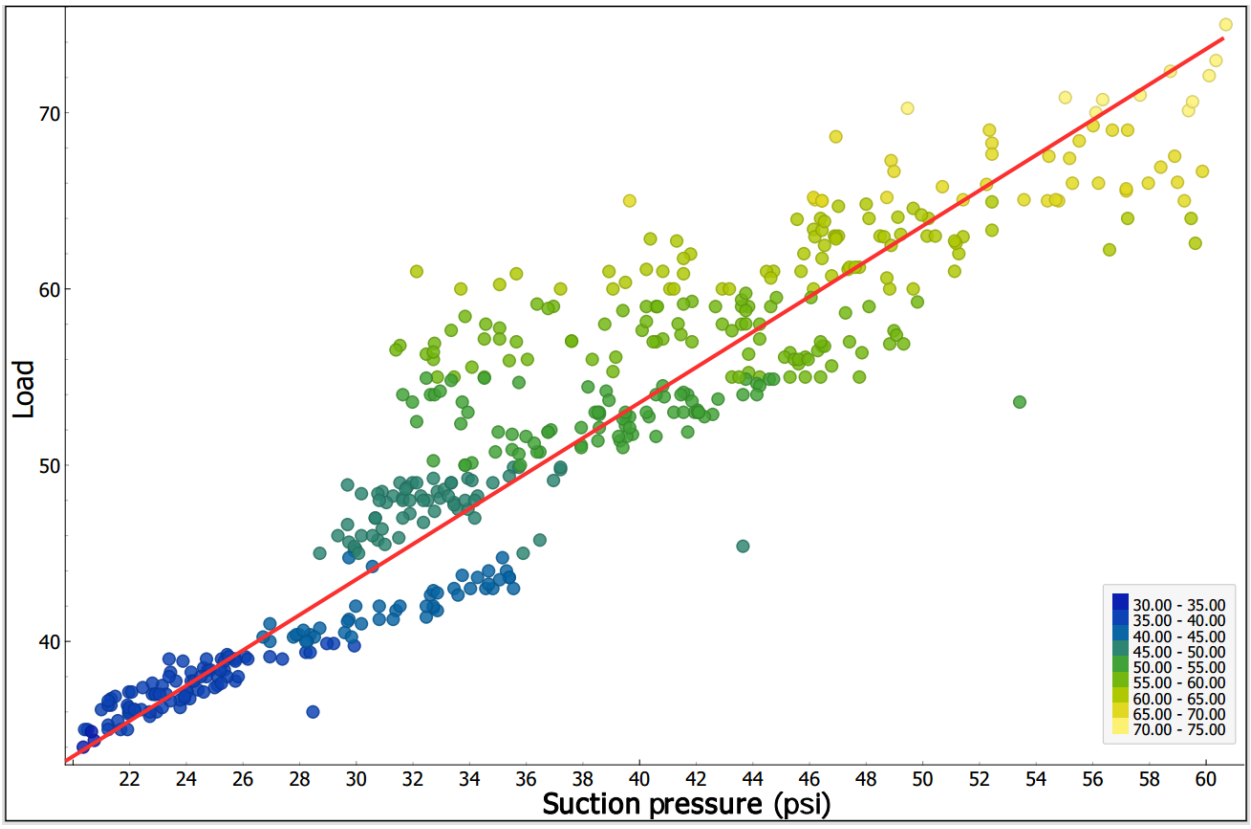

Figure 44 Correlation of suction pressure with engine load

The scatter plot Figure 45 illustrates the positive correlation between discharge pressure (measured in psi) and engine load, with discharge pressure plotted on the x-axis and engine load displayed on the y-axis. The data is color-coded, representing load ranges from 30.00 to 75.00, allowing for visual segmentation by operational conditions. A linear regression line in red indicates the relationship trend, showing that as discharge pressure increases, engine load generally increases as well. The clustering of data points is tighter at lower discharge pressures, suggesting a more consistent relation to engine load, while at higher discharge pressures, the data points disperse more, suggesting other factors may also be influencing engine load. This visual analysis is vital for optimizing engine performance based on discharge pressure, and the linear model provides a predictive baseline for engine load estimations.

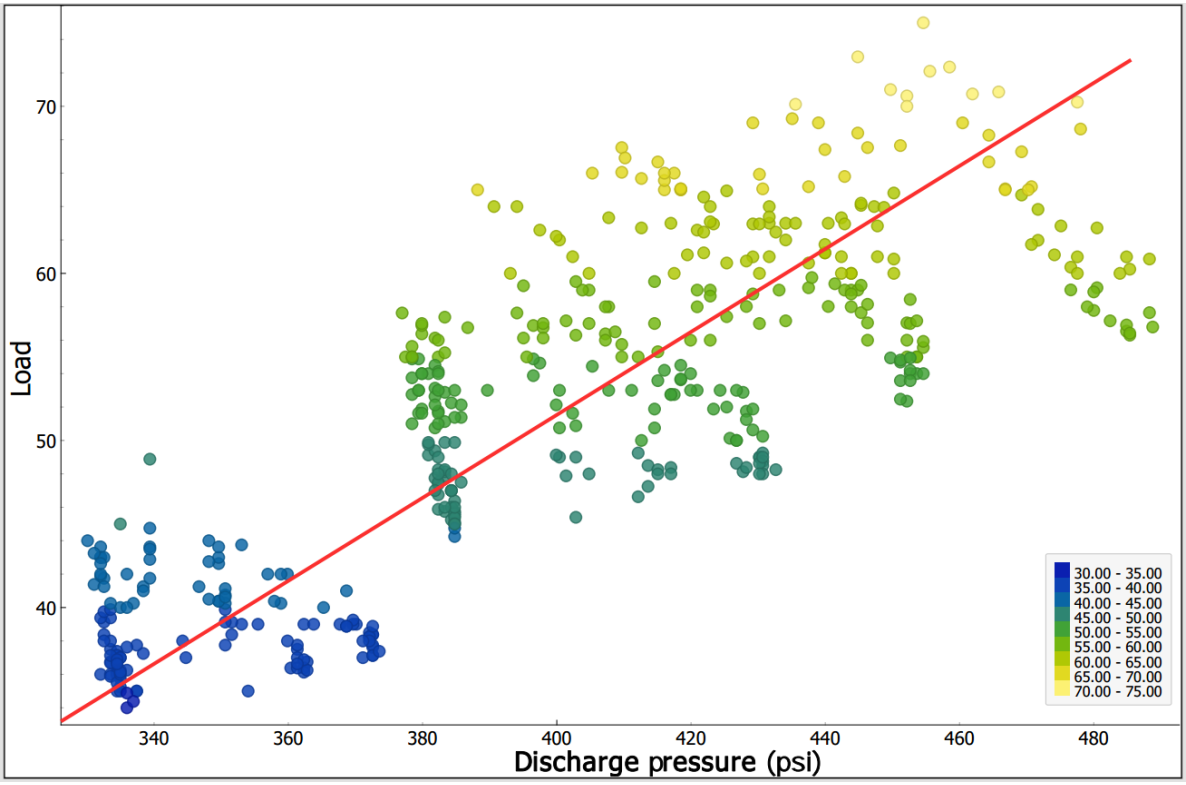

Figure 45 Correlation of discharge pressure vs engine load

Figure 46 shows a scatter plot graphically representing the relationship between the engine's speed (RPM) and its load (%). Each point on the plot corresponds to a specific measurement, with the color indicating the range of the engine load. The blue points represent the lower load ranges (30-45%), green indicates middle load ranges (45-60%), and yellow shows the higher load ranges (60-75%). The red line depicts the trend line, showing a positive correlation between engine speed and load; as the engine speed increases, the load also tends to increase. This trend suggests that at higher RPM, the engine is under greater load, which could be due to higher gas throughput or increased resistance within the engine system. The spread of the points, particularly the vertical dispersion at specific RPMs, could indicate variability in the engine's load capacity at those speeds or reflect changes in operational conditions such as fuel quality or environmental factors. Overall, the graph provides a clear visualization of how these two parameters interact across different operating conditions.

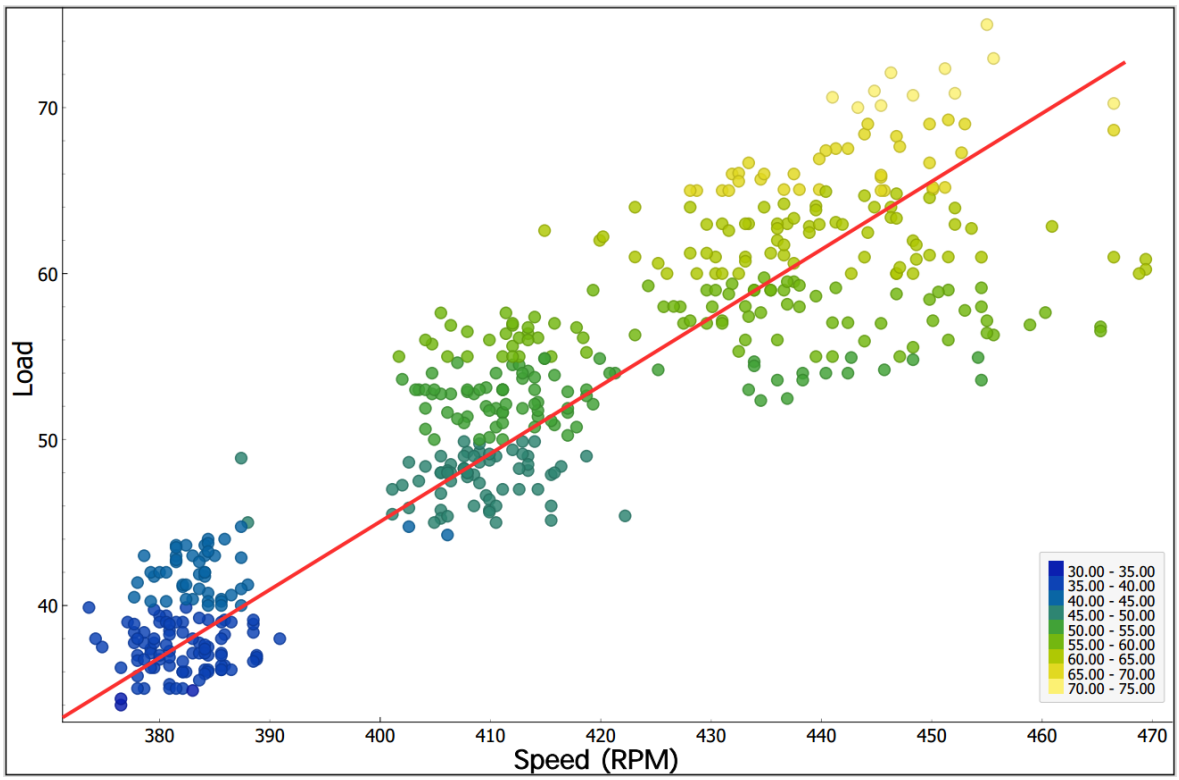

Figure 46 Correlation of speed with engine load

Figure 47 displays the relationship between the coefficient of determination, denoted as R-squared (R^2), and the number of predictors used in a statistical model. The R-squared value is a statistical measure that represents the proportion of the variance for a dependent variable that's explained by an independent variable or variables in a regression model.

On the x-axis, the number of predictors used in the model increases from 1 to 3. On the y-axis, the R-squared values are plotted, which range approximately from 0.85 to just above 0.95.The graph shows that as the number of predictors increases, there is an initial sharp increase in the R-squared value, indicating a significant improvement in the model's explanatory power with the addition of the first predictor. The subsequent increase in the number of predictors results in a more gradual rise in the R-squared value. This suggests that each additional predictor contributes to a smaller increase in the variance explained by the model.

The highest R-squared value observed is with three predictors, which indicates the best model performance among the ones presented. However, without additional context on the nature of the predictors and the model, the implications of this increase cannot be fully understood.

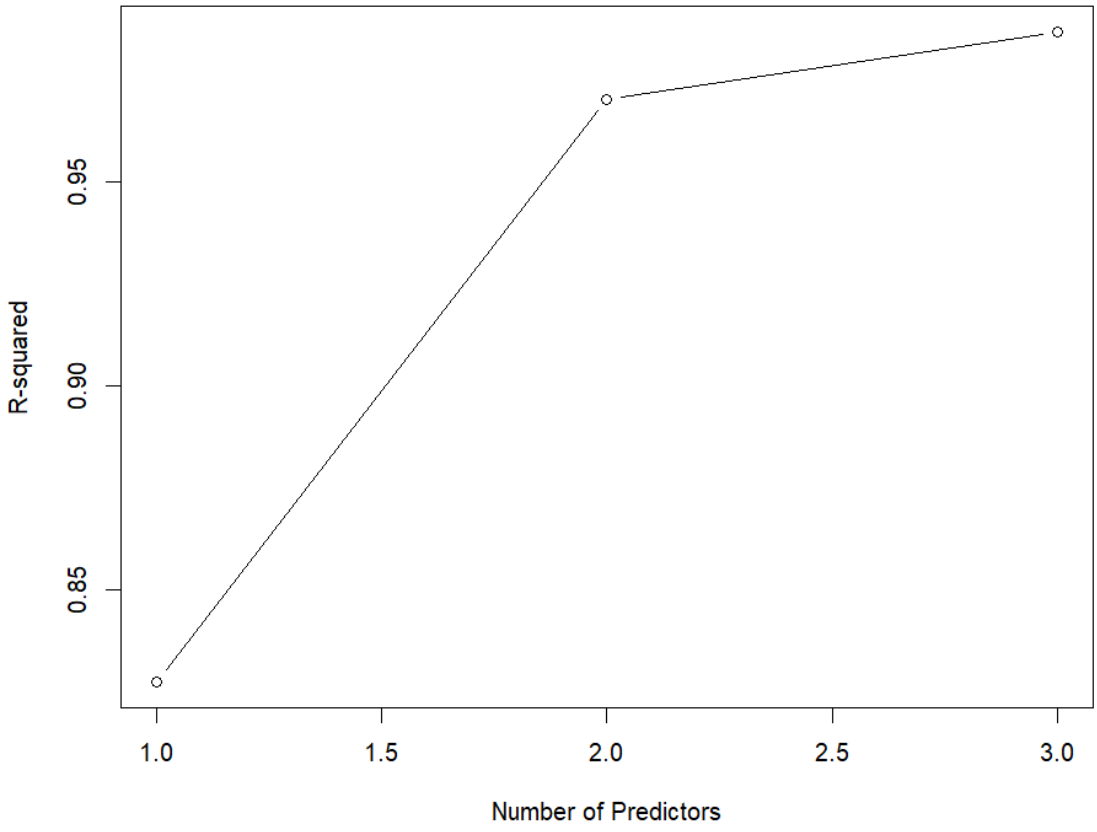

Figure 47. Effects of R-square with the number of predictors

Figure 48 shows a comparative analysis is presented between the actual engine load and the load predicted by the SVR model. The data points predicted by the SVR model are depicted in cyan, offering a visual correlation with the actual engine load measurements. This graph effectively illustrates the alignment of the SVR-predicted data with the real engine load, underscoring the model's accuracy.

While the presence of outliers is noted, which is a common occurrence in machine learning models, their quantity is minimal, suggesting a high level of precision in the model's predictive capabilities. Overall, this graph serves as a clear indicator of the SVR model's performance in accurately forecasting engine load, demonstrating its potential utility in practical applications.

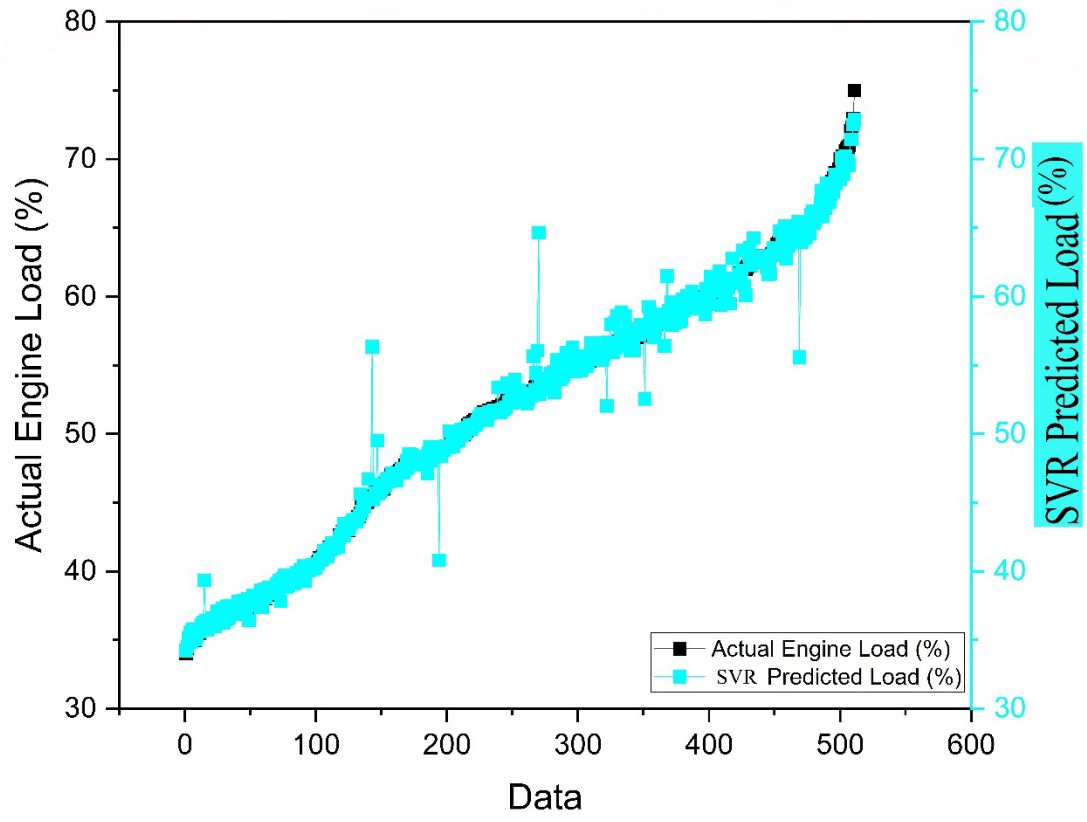

Figure 48 Prediction comparison of Actual engine load and load predicted by SVR model

Figure 49 presents a comparison between the actual engine load and the load predicted by the ANN model. In the graph, the actual load data, calculated using the PowerFlow model, is represented by black-colored data points, while the load predictions made by the ANN model are shown in purple. The graphical representation indicates that while the ANN model achieves a high degree of accuracy, as evidenced by the proximity of the purple points to the black ones, the predictions do not entirely mirror the pattern of the actual load. The data points, although closely packed, show a

slight deviation from the actual load pattern. This divergence can be attributed to the ANN model's accuracy, which stands at 92%. Due to this level of accuracy, the predicted data does not align perfectly with the actual engine load. The graph highlights the capability of the ANN model to predict engine load with reasonable accuracy, although it indicates that the model has a slightly lower precision compared to other methods like SVM.

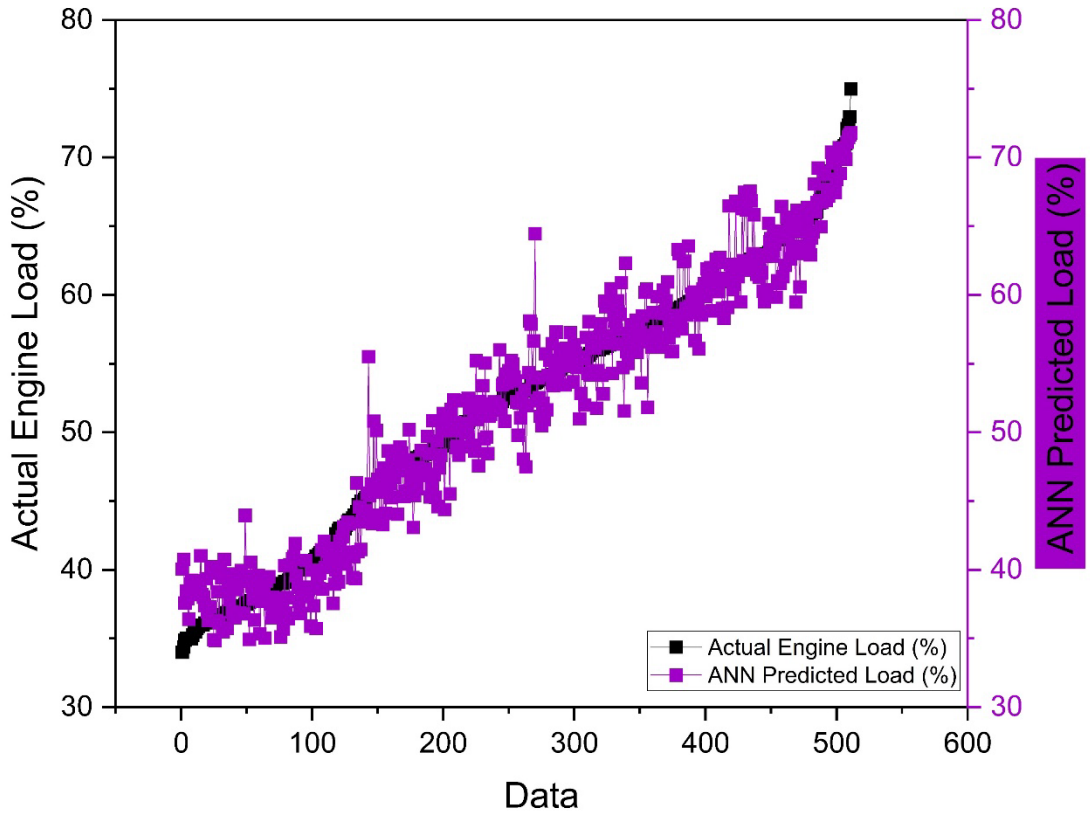

Figure 49 Prediction comparison of Actual engine load and load predicted by ANN model

In Figure 50, the x-axis of the graph is labeled "Predicted Engine Load (%) and y-axis is labeled "Actual Engine Load (%)" and has a similar range. The predicted load is the load which is predicted by the linear regression algorithm, the actual engine load is the load which is calculated using the powerflow model.

This range suggests that the model is being evaluated over a variety of engine loads, providing a comprehensive assessment of its predictive capability. The graph includes a line of best fit,

indicating the relationship that the multiple linear regression model has found. The dots are closely clustered around this line, which suggests a strong correlation between the predicted and actual values, indicating the model's high accuracy.

Above the scatter plot, the model's performance metrics is provided: an R-squared (R^2) value of 0.9868 and an adjusted R-squared of 0.9867. These value is close to 1, which signifies that the model explains a very high proportion of the variance in the actual engine load, considering the number of predictors used. The closeness of the R-squared and adjusted R-squared values also indicates that the model is not overfitted, as the adjustment for the number of predictors has not significantly reduced the R-squared value.

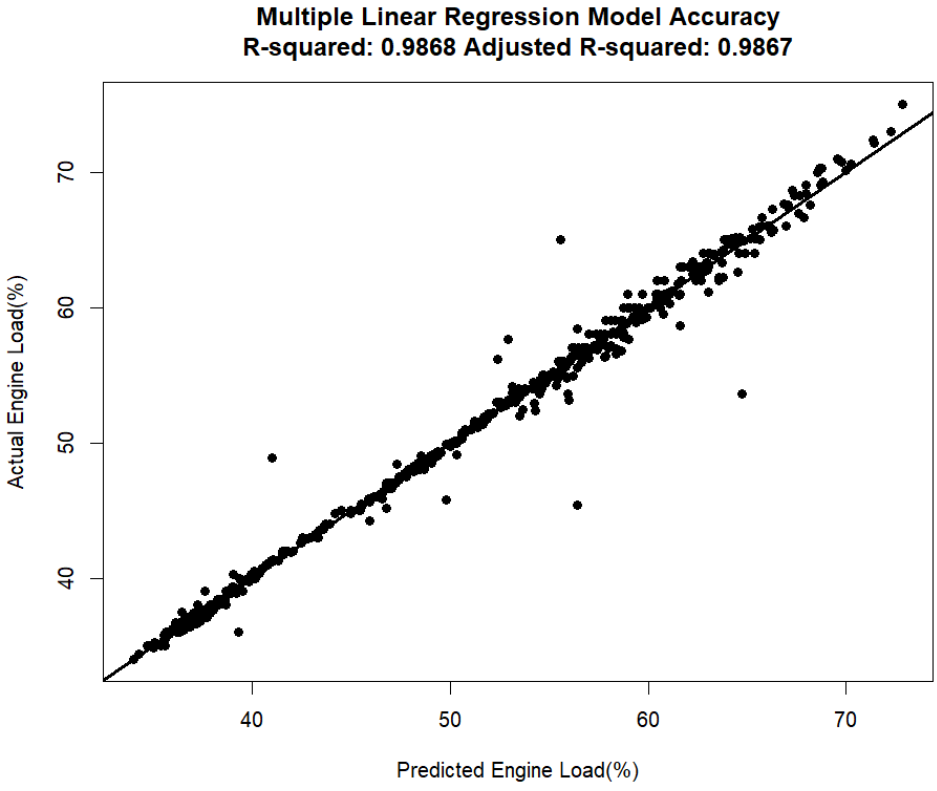

Figure 50. Prediction comparison of actual engine load and load predicted by linear regression model

Table 5, compares the performance of three different machine learning models: SVM, ANN, and Linear Regression. The performance of each model is evaluated using four metrics: Mean Squared Error (MSE), Root Mean Squared Error (RMSE), Mean Absolute Error (MAE), and R-squared (R^2).

For the linear regression model, the MSE is 1.280, the MSE is 1.131, the MAE is 0.532, and the R^2 is 0.986. These values suggest that the SVM model has a high degree of accuracy, with a strong correlation between the predicted and actual values, as indicated by the R^2 value close to 1.

The ANN shows significantly higher error metrics with an MSE of 7.383, RMSE of 2.717, and MAE of 2.103. Its R^2 value is 0.922, which is lower than the SVM and Linear Regression models, indicating a lower fit to the data.

The SVM model has an MSE of 1.313, RMSE of 1.145, MAE of 0.544, and an R^2 of 0.986. These metrics are similar to those of the SVM model, suggesting that both models have a similar degree of accuracy and predictive capability.

The R^2 values for both the SVM and linear regression models are extremely high, suggesting that these models are highly effective at predicting the outcomes they are designed to predict. The Neural Network model, while still useful, is less accurate according to these metrics.

Table 5. Accuracy of machine learning models

Model	MSE	RMSE	MAE	R^2
Linear Regression	1.280	1.131	0.532	0.986
ANN	7.383	2.717	2.103	0.922
SVM	1.313	1.145	0.544	0.986

Equation 12 represents the formula that is derived from linear regression. The equation has the bias of the parameter which needs to be multiplied and then lastly it has a constant that needs to be subtracted. This equation is directly incorporated into the PLC.

$$\text{Engine Load} = 0.583*\text{suction\_pressure} + 0.043313*\text{discharge\_pressure} + 0.1294*\text{speed} - 41.178 \quad (12)$$

Chapter 6 Conclusions

6.1 Air Management System (AMS)

The AMS was experimentally investigated on the AJAX DPC-81 NGFRE in terms of emissions and combustion analysis. The experiments were conducted at load varying from 40-75% with the bypass valve positions varied depending upon the exhaust temperature limitation for instance on 40% the max bypass position was 80% whereas for 75% load, the max bypass was 30%.

6.1.1 40% Load

- The optimal reduction in emissions, including CH_4, VOC, and NOx, was observed at a bypass valve position of 70%. At this position, CH_4 and VOC emissions decreased by 64% and 52%, respectively. Conversely, an increase in CO emissions was noted as the bypass valve opened further, reaching the highest level at an 80% bypass valve position.
- Combustion stability showed improvement as the bypass valve opened, with a 2% increase in ITE noted at a 70% bypass. The highest ITE was recorded at an 80% bypass valve position, indicating enhanced fuel efficiency and engine performance.

6.1.2 45% Load

- A significant reduction in NOx, CO_2, VOC, and CO emissions was achieved at a 70% bypass valve position. A slight increase in CO was noted post-60% bypass. A steep decrease in NOx emissions was recorded between 30% to 60% bypass, reaching the lowest at 80% bypass.
- Combustion stability was suboptimal at a 40% bypass but showed marked improvements beyond a 60% bypass, peaking at an 80% bypass. An increase in ITE of 3% was observed at a 70% bypass position.

6.1.3 50% Load

- At a 60% bypass valve position, there was a minimum in emissions for CH_4, CO_2, NOx, and VOC, with reductions of 54%, 38%, and 50%, respectively, indicating a general downward trend in emissions.
- Improved combustion stability was noted with increases in bypass, with the most stable condition at a 60% bypass valve position.

6.1.4 55% Load

- At a 50% bypass valve position, a downward trend was observed for CH_4, CO_2, NOx, VOC, and CO emissions, with methane showing the largest decrease at 43%. Other emissions also saw substantial reductions.
- Combustion stability improved with increases in bypass, and a noticeable 1.8% improvement in ITE was observed at a 50% bypass valve position.

6.1.5 60% Load

- A significant reduction in CH_4, NOx, VOC, and CO emissions was observed at a 50% bypass valve position, with CH_4 decreasing by a notable 55%. Emissions of NOx and VOC were lowest at the highest bypass valve position. However, CO_2 emissions increased alongside the opening of the bypass valve, with CO levels rising post-30% bypass.
- Combustion stability experienced substantial improvements at a 50% bypass, reaching optimal levels at a 60% bypass. An increase in ITE was also associated with the widening of the bypass.

6.1.6 65% Load

- At a 40% bypass valve position, emissions of CH_4 and CO_2 showed a downward trend with reductions of 41% and 13%, respectively. NOx emissions were minimized at a 50% bypass but spiked at a 60% bypass position, while CO levels were lowest at a 40% bypass but increased at higher bypass settings.
- Combustion stability showed a 3% improvement at a 40% bypass, with the highest stability observed at a 50% bypass. ITE displayed an upward trend with the increase in bypass valve opening.

6.1.7 70% Load

- At the minimal 10% bypass setting, there was a downward trend for CH_4, CO_2, and NOx emissions, with reductions of 16% for CH_4 and 24% for NOx. CO_2 also followed a similar downward pattern. CO emissions, however, showed an upward trend with increased bypass valve positions. VOC emissions appeared relatively unaffected at the maximum bypass.
- The ITE improved significantly at higher loads, indicating enhanced combustion performance and overall smoother engine operation.

6.1.8 75% Load

- At a 10% bypass valve position, a downward trend in CH_4, NOx, VOC, and CO emissions was noted. A 13% reduction in methane was observed at a 10% bypass, with the lowest levels recorded at a 20% bypass. NOx saw a 20% reduction at a 10% bypass, with the lowest observed at a 20% bypass.
- Combustion stability was bolstered by the incremental opening of the bypass valve, with a 2.3% increase in ITE noted at the maximum bypass position.

6.2 Vibration Analysis

Vibration analysis was conducted across three axes of the engine with 40, 60, and 75% load and different bypass valve positions. The average RMS (mm/sec) indicated that vibration levels fluctuated at various bypass valve positions. Vibration measurements mostly fell within the 4-5 mm/sec range, suggesting that at given loads, vibrations are typically within this bandwidth due to which a linear relation was hard to establish. Further, FFT analysis illustrated that while time waveform vibrations were present, spectral analysis confirmed the engine operated ideally at 40% load. As the load increased, spectral spikes suggested variations in engine speed, leading to an increased frequency of spikes in the FFT data. At 75% load, a high frequency of spikes was recorded, reinforcing that vibration does not directly correlate with load linearly. Nevertheless, vibration data are valuable for engine monitoring and fault detection purposes.

6.3 Machine Learning

The research collected data across engine loads ranging from 40% to 75%, including variables such as suction pressure, discharge pressure, engine speed, NOx, O_2, and exhaust temperature. An analysis to evaluate linearity between these variables and engine load revealed that suction pressure, discharge pressure, and speed had a significant correlation with engine load, indicating their potential as predictive indicators. Contrarily, vibration analysis demonstrated that vibrations did not exhibit a clear correlation suitable for the machine learning model.

Three machine learning models were employed: Linear Regression, SVR, and ANN, with R-squared values of 0.98, 0.96, and 0.92, respectively. These models were validated against the thermodynamic model generated in the PowerFlow software. From the linear regression model,

the development of a formula for load prediction was developed that can be seamlessly integrated into a PLC for real-time engine performance prediction, monitoring, and optimization.

6.4 Future Work

Future work will focus on incorporating the determined optimal bypass valve positions into the PLC, along with the established load prediction formula. This integration will empower the PLC to autonomously predict engine load and adjust the bypass valve accordingly, ensuring peak performance for varying load conditions. Such enhancements will render the system self-sustaining and self-regulating. Additionally, the integration of advanced AI and ML techniques will be explored to bolster predictive maintenance strategies and facilitate accurate methane emission predictions, further enhancing the system's efficiency and environmental compliance.

Appendix

Table 6 Table of uncertainties

Variables	Uncertainty
NOx	± 5.35 ppm
CO	± 0.12 ppm
CO_2	± 0.013 %
CH_4	± 59.10 ppm
VOCs	± 0.18 ppm
O_2	± 0.69 %
H_2O	± 0.72 %
T	± 4.23 °F
P	± 10.03 psi
MEP	± 27.75psi
HRR	± 30.27 J/^{o}
ITE	± 3.47 %
AFR	± 0.86

References

1. Hafner, M. and S. Tagliapietra, *The Globalization of Natural Gas Markets-New Challenges and Opportunities for Europe*. 2013: Claeys & Casteels.
2. Nersesian, R., *Energy for the 21st century: a comprehensive guide to conventional and alternative sources*. 2014: Routledge.
3. Kalair, A., et al., *Role of energy storage systems in energy transition from fossil fuels to renewables.* Energy Storage, 2021. **3**(1): p. e135.
4. Asif, M. and T. Muneer, *Energy supply, its demand and security issues for developed and emerging economies.* Renewable and sustainable energy reviews, 2007. **11**(7): p. 1388-1413.
5. Friedemann, A., *Life after fossil fuels.* A Reality Check on Alternative Energy. Cham (Suiza): Springer-Lecture Notes in Energy, 2021.
6. Ryerson, W.N., *Population: The multiplier of everything else.* The post carbon reader: Managing the 21st century's sustainability crises, 2010: p. 153-75.
7. Ediger, V.Ş. and I. Berk, *Geostrategic challenges in the oil and gas sectors.* Energy economy, finance and geostrategy, 2018: p. 173-197.
8. Bp, S., *BP Statistical review of world energy 2002.* http://www. bp. com/, 2002.
9. Soldo, B., et al., *Improving the residential natural gas consumption forecasting models by using solar radiation.* Energy and buildings, 2014. **69**: p. 498-506.
10. Yue, T., et al., *Gaseous emissions from compressed natural gas buses in urban road and highway tests in China.* Journal of Environmental Sciences, 2016. **48**: p. 193-199.
11. Chen, H., J. He, and X. Zhong, *Engine combustion and emission fuelled with natural gas: a review.* Journal of the Energy Institute, 2019. **92**(4): p. 1123-1136.
12. Kojima, M., C. Brandon, and J. Shah, *Improving urban air quality in South Asia by reducing emissions from two-stroke engine vehicles*. 2000, World Bank Washington, DC.
13. Kundert, D. and M. Mullen. *Proper evaluation of shale gas reservoirs leads to a more effective hydraulic-fracture stimulation*. SPE.
14. Aguilera, R.F. and M. Radetzki, *The shale revolution: Global gas and oil markets under transformation.* Mineral Economics, 2014. **26**: p. 75-84.
15. Khosrokhavar, R., S. Griffiths, and K.-H. Wolf, *Shale gas formations and their potential for carbon storage: opportunities and outlook.* Environmental Processes, 2014. **1**: p. 595-611.
16. Speight, J.G., *Natural gas: a basic handbook*. 2018: Gulf Professional Publishing.
17. John, R.P., et al., *Micro and macroalgal biomass: a renewable source for bioethanol.* Bioresource technology, 2011. **102**(1): p. 186-193.
18. Singh, N.R., E. Pandey, and E. Gnansounou, *Biofuels.* Speight James G, editor. The biofuels handbook. RSC energy series, 2011(5): p. 160-98.

19. Singh, K. and M.K.S. Sastry, *Production of fuels from landfills*, in *The Biofuels Handbook*. 2011, Royal Society of Chemistry London, UK. p. 408-453.

20. Ahmadi, P., A. Chapoy, and B. Tohidi, *Density, speed of sound and derived thermodynamic properties of a synthetic natural gas.* Journal of Natural Gas Science and Engineering, 2017. **40**: p. 249-266.

21. Cho, H.M. and B.-Q. He, *Spark ignition natural gas engines—A review.* Energy Conversion and Management, 2007. **48**(2): p. 608-618.

22. King, S.R., *The impact of natural gas composition on fuel metering and engine operational characteristics*. 1992, SAE Technical Paper.

23. Borges, L.H., C. Hollnagel, and W. Muraro, *Development of a Mercedes-Benz natural gas engine M 366 LAG, with a lean burn combustion system*. 1996, SAE Technical Paper.

24. Sobiesiak, A. and S. Zhang, *The first and second law analysis of spark ignition engine fuelled with compressed natural gas*. 2003, SAE Technical Paper.

25. Ting, D.S.K. and M.D. Checkel, *The effects of turbulence of spark-ignited, ultra lean, premixed methane-air flame growth in a combustion chamber*. 1995, SAE Technical Paper.

26. Mtui, P.L. and P.G. Hill, *Ignition delay and combustion duration with natural gas fueling of diesel engines*. 1996, SAE Technical Paper.

27. Tilagone, R., et al., *Development of a high efficiency, low emission SI-CNG bus engine*. 1996, SAE Technical Paper.

28. Kato, K., et al., *Development of engine for natural gas vehicle.* SAE transactions, 1999: p. 939-947.

29. Wang, J., et al., *Combustion behaviors of a direct-injection engine operating on various fractions of natural gas–hydrogen blends.* International Journal of Hydrogen Energy, 2007. **32**(15): p. 3555-3564.

30. da Costa, R.B.R., et al., *Combustion, performance and emission analysis of a natural gas-hydrous ethanol dual-fuel spark ignition engine with internal exhaust gas recirculation.* Energy Conversion and Management, 2019. **195**: p. 1187-1198.

31. Farzaneh-Gord, M., et al., *Thermodynamic analysis of natural gas reciprocating compressors based on real and ideal gas models.* international journal of refrigeration, 2015. **56**: p. 186-197.

32. Ali, S.M., et al., *Automated valve fault detection based on acoustic emission parameters and support vector machine.* Alexandria Engineering Journal, 2018. **57**(1): p. 491-498.

33. Qi, G., et al., *Fault-diagnosis for reciprocating compressors using big data and machine learning.* Simulation Modelling Practice and Theory, 2018. **80**: p. 104-127.

34. Xiao, S., et al., *Fault diagnosis of a reciprocating compressor air valve based on deep learning.* Applied Sciences, 2020. **10**(18): p. 6596.

35. Zimmerle, D.J., et al., *Methane Emissions from the Natural Gas Transmission and Storage System in the United States.* Environmental Science & Technology, 2015. **49**(15): p. 9374-9383.

36. Ishibashi, Y. and M. Asai, *Improving the exhaust emissions of two-stroke engines by applying the activated radical combustion.* SAE transactions, 1996: p. 982-992.

37. Korakianitis, T., A.M. Namasivayam, and R.J. Crookes, *Natural-gas fueled spark-ignition (SI) and compression-ignition (CI) engine performance and emissions.* Progress in energy and combustion science, 2011. **37**(1): p. 89-112.

38. *Overview of Greenhouse Gases. Available from: .*

39. Yang, W., et al., *Global Warming Potential of CH4 uptake and N2O emissions in saline–alkaline soils.* Atmospheric Environment, 2018. **191**: p. 172-180.

40. Sevik, J., et al., *Performance, efficiency and emissions assessment of natural gas direct injection compared to gasoline and natural gas port-fuel injection in an automotive engine.* SAE International Journal of Engines, 2016. **9**(2): p. 1130-1142.

41. United States. Environmental Protection Agency. Office of, P., *Inventory of US Greenhouse Gas Emissions and Sinks: 1990-1994*. 1995: US Environmental Protection Agency.

42. EPA, *GHGRP Petroleum and Natural Gas Systems*. 2016.

43. Townsend, J. and M.A. Badar, *Impact of condition monitoring on reciprocating compressor efficiency.* Journal of Quality in Maintenance Engineering, 2018. **24**(4): p. 529-543.

44. Hassan, H.A., et al., *Integrated System to Reduce Emissions from Natural Gas-Fired Reciprocating Engines—Performance Assessment of Amperometric NOx/O 2 Sensors*. 2022, SAE Technical Paper.

45. Ladommatos, N. and R. Stone, *Conversion of a diesel engine for gaseous fuel operation at high compression ratio.* SAE transactions, 1991: p. 416-424.

46. Iodice, P., A. Amoresano, and G. Langella, *A review on the effects of ethanol/gasoline fuel blends on NOX emissions in spark-ignition engines.* Biofuel Research Journal, 2021. **8**(4): p. 1465-1480.

47. Normann, F., et al., *Emission control of nitrogen oxides in the oxy-fuel process.* Progress in Energy and Combustion Science, 2009. **35**(5): p. 385-397.

48. Keller, J.O. and I. Hongo, *Pulse combustion: The mechanisms of NOx production.* Combustion and Flame, 1990. **80**(3-4): p. 219-237.

49. Muzio, L.J. and G.C. Quartucy, *Implementing NOx control: research to application.* Progress in Energy and Combustion Science, 1997. **23**(3): p. 233-266.

50. Nicol, D.G., et al., *The importance of the nitrous oxide pathway to NOx in lean-premixed combustion.* 1995.

51. Chong, J.-J., et al., *Enhancing the NO2/NOx ratio in compression ignition engines by hydrogen and reformate combustion, for improved aftertreatment performance.* International Journal of Hydrogen Energy, 2010. **35**(16): p. 8723-8732.

52. Masum, B.M., et al., *Effect of ethanol–gasoline blend on NOx emission in SI engine.* Renewable and Sustainable Energy Reviews, 2013. **24**: p. 209-222.

53. Shahir, N.S., et al., *Performance and emission assessment of diesel–biodiesel–ethanol/bioethanol blend as a fuel in diesel engines: A review.* Renewable and Sustainable Energy Reviews, 2015. **48**: p. 62-78.

54. Kouremenos, D.A., C.D. Rakopoulos, and D.T. Hountalas, *Experimental investigation of the performance and exhaust emissions of a swirl chamber diesel engine using JP-8 aviation fuel.* International journal of energy research, 1997. **21**(12): p. 1173-1185.

55. Heywood, J.B., *Internal combustion engine fundamentals*. 2018: McGraw-Hill Education.

56. Chuah, L.F., et al., *A review of performance and emission characteristic of engine diesel fuelled by biodiesel.* Chemical Engineering Transactions, 2022. **94**: p. 1099-1104.

57. Novak, J.M. and P.N. Blumberg, *Parametric simulation of significant design and operating alternatives affecting the fuel economy and emissions of spark-ignited engines.* SAE Transactions, 1978: p. 3485-3511.

58. Iodice, P., G. Langella, and A. Amoresano, *Ethanol in gasoline fuel blends: Effect on fuel consumption and engine out emissions of SI engines in cold operating conditions.* Applied Thermal Engineering, 2018. **130**: p. 1081-1089.

59. Abdel-Rahman, A.A., *On the emissions from internal-combustion engines: a review.* International Journal of Energy Research, 1998. **22**(6): p. 483-513.

60. Weaver, C.S., *Natural gas vehicles—a review of the state of the art.* SAE transactions, 1989. **98**: p. 1190-1210.

61. Carlson, D.A., et al., *Large-scale convex optimization methods for air quality policy assessment.* Automatica, 2004. **40**(3): p. 385-395.

62. Reis, L.A., et al., *Developing a fast photochemical calculator for an integrated assessment model.* International Journal of Environment and Pollution, 2012. **50**(1-4): p. 140-150.

63. Jaecker-Voirol, A., *VOC: Volatile Organic Compounds: Formation and Emission*, in *Pollutants from Combustion: Formation and Impact on Atmospheric Chemistry*. 2000, Springer. p. 241-261.

64. Zimmerle, D.J., et al., *Methane emissions from the natural gas transmission and storage system in the United States.* Environmental science & technology, 2015. **49**(15): p. 9374-9383.

65. Rutherford, J.S., et al., *Closing the methane gap in US oil and natural gas production emissions inventories.* Nature communications, 2021. **12**(1): p. 4715.

66. Camuzeaux, J.R., et al., *Influence of methane emissions and vehicle efficiency on the climate implications of heavy-duty natural gas trucks.* Environmental science & technology, 2015. **49**(11): p. 6402-6410.

67. Pan, D., et al., *Methane emissions from natural gas vehicles in China.* Nature communications, 2020. **11**(1): p. 4588.

68. Mitchell, A.L., et al., *Measurements of methane emissions from natural gas gathering facilities and processing plants: Measurement results.* Environmental science & technology, 2015. **49**(5): p. 3219-3227.

69. Chapman, K.S. and S.R. Nuss-Warren, *Cost-Effective Reciprocating Engine Emissions Control and Monitoring for E&P Field and Gathering Engines*. 2007, Kansas State Univ., Manhattan, KS (United States).

70. Agency, U.S.E.P., *Compliance Requirements for Stationary Engines*. 2023.

71. Heywood, J.B., et al., *The performance of future ICE and fuel cell powered vehicles and their potential fleet impact*. 2004, SAE Technical Paper.

72. Baratta, M., et al., *Combustion chamber design for a high-performance natural gas engine: CFD modeling and experimental investigation.* Energy Conversion and Management, 2019. **192**: p. 221-231.

73. Yan, B., et al., *The effect of combustion chamber geometry on in-cylinder flow and combustion process in a stoichiometric operation natural gas engine with EGR.* Applied Thermal Engineering, 2018. **129**: p. 199-211.

74. Feist, M.D., M. Landau, and E. Harte, *The effect of fuel composition on performance and emissions of a variety of natural gas engines.* SAE International Journal of Fuels and Lubricants, 2010. **3**(2): p. 100-117.

75. Kuczyński, S., et al., *Impact of liquefied natural gas composition changes on methane number as a fuel quality requirement.* Energies, 2020. **13**(19): p. 5060.

76. Mahla, S.K., L.M. Das, and M.K.G. Babu, *Effect of EGR on performance and emission characteristics of natural gas fueled diesel engine.* Jordan Journal of Mechanical and Industrial Engineering, 2010. **4**(4).

77. Economides, M.J. and D.A. Wood, *The state of natural gas.* Journal of Natural Gas Science and Engineering, 2009. **1**(1-2): p. 1-13.

78. Hickman, D.A. and R. Milum. *Reciprocating Compressor Performance Predictions: Control Methodologies from the PLC to the PC*.

79. Castaing-Lasvignottes, J. and S. Gibout, *Dynamic simulation of reciprocating refrigeration compressors and experimental validation.* International journal of refrigeration, 2010. **33**(2): p. 381-389.

80. Elhaj, M., et al., *Numerical simulation and experimental study of a two-stage reciprocating compressor for condition monitoring.* Mechanical Systems and Signal Processing, 2008. **22**(2): p. 374-389.

81. Winandy, E., C. Saavedra, and J. Lebrun, *Simplified modelling of an open-type reciprocating compressor.* International journal of thermal sciences, 2002. **41**(2): p. 183-192.

82. Farzaneh-Gord, M., A. Niazman, and M. Deymi, *Optimizing reciprocating air compressors design parameters based on first law analysis.* UPB Scientific Bulletin, Seriese D: Mechanical Engineering, 2013: p. 13-26.

83. Henningsson, M., P. Tunestål, and R. Johansson, *A Virtual Sensor for Predicting Diesel Engine Emissions from Cylinder Pressure Data.* IFAC Proceedings Volumes, 2012. **45**(30): p. 424-431.

84. Yap, W.K., T. Ho, and V. Karri, *Exhaust emissions control and engine parameters optimization using artificial neural network virtual sensors for a hydrogen-powered vehicle.* International Journal of Hydrogen Energy, 2012. **37**(10): p. 8704-8715.

85. EIA, *AEO2014 Early Release Overview*.

86. Pétron, G., et al., *Hydrocarbon emissions characterization in the Colorado Front Range: A pilot study.* Journal of Geophysical Research: Atmospheres, 2012. **117**(D4).

87. Energy, U.S.D.o., *Combined heat and power technology fact sheet series.* 2016.

88. Wu, D. and R. Wang, *Combined cooling, heating and power: A review.* progress in energy and combustion science, 2006. **32**(5-6): p. 459-495.

89. Pachauri, R.K., et al., *Climate change 2014: synthesis report. Contribution of Working Groups I, II and III to the fifth assessment report of the Intergovernmental Panel on Climate Change*. 2014: Ipcc.

90. Myhre, G., D. Shindell, and J. Pongratz, *Anthropogenic and natural radiative forcing.* 2014.

91. Mahdevari, S., *Coal mine methane: Control, utilization, and abatement*, in *Advances in Productive, Safe, and Responsible Coal Mining*. 2019, Elsevier. p. 179-198.

92. Chai, X., D.J. Tonjes, and D. Mahajan, *Methane emissions as energy reservoir: context, scope, causes and mitigation strategies.* Progress in Energy and Combustion Science, 2016. **56**: p. 33-70.

93. Yusuf, R.O., et al., *Methane emission by sectors: a comprehensive review of emission sources and mitigation methods.* Renewable and Sustainable Energy Reviews, 2012. **16**(7): p. 5059-5070.

94. Elhaj, M.A., *Condition monitoring of reciprocating compressor valves*. 2005, The University of Manchester (United Kingdom): England. p. 282.

95. Heimburger, A.M.F., et al., *Assessing the optimized precision of the aircraft mass balance method for measurement of urban greenhouse gas emission rates through averaging.* Elem Sci Anth, 2017. **5**: p. 26.

96. Atherton, E., et al., *Mobile measurement of methane emissions from natural gas developments in northeastern British Columbia, Canada.* Atmospheric Chemistry and Physics, 2017. **17**(20): p. 12405-12420.

97. Robertson, A.M., et al., *Variation in methane emission rates from well pads in four oil and gas basins with contrasting production volumes and compositions.* Environmental Science & Technology, 2017. **51**(15): p. 8832-8840.

98. Brandt, A.R. and G. Petron, *Fugitive emissions and air quality impacts of US natural gas systems.* The Bridge, 2015. **45**: p. 22-31.

99. Kemp, C.E., A.P. Ravikumar, and A.R. Brandt, *Comparing natural gas leakage detection technologies using an open-source "virtual gas field" simulator.* Environmental science & technology, 2016. **50**(8): p. 4546-4553.

100. Abd-Alla, G.H., *Using exhaust gas recirculation in internal combustion engines: a review.* energy conversion and management, 2002. **43**(8): p. 1027-1042.

101. Zheng, M., G.T. Reader, and J.G. Hawley, *Diesel engine exhaust gas recirculation—a review on advanced and novel concepts.* Energy conversion and management, 2004. **45**(6): p. 883-900.

102. Abdelaal, M.M. and A.H. Hegab, *Combustion and emission characteristics of a natural gas-fueled diesel engine with EGR.* Energy conversion and management, 2012. **64**: p. 301-312.

103. Hohn, K. and S.R. Nuss-Warren, *Cost-Effective Reciprocating Engine Emissions Control and Monitoring for E&P Field and Gathering Engines*. 2011, Kansas State Univ., Manhattan, KS (United States).

104. Shi, W., et al., *Effect of spark timing on combustion and emissions of a hydrogen direct injection stratified gasoline engine.* International Journal of hydrogen energy, 2017. **42**(8): p. 5619-5626.

105. Elsemary, I.M.M., et al., *Spark timing effect on performance of gasoline engine fueled with mixture of hydrogen–gasoline.* International Journal of Hydrogen Energy, 2017. **42**(52): p. 30813-30820.

106. Zhang, B., C. Ji, and S. Wang, *Combustion analysis and emissions characteristics of a hydrogen-blended methanol engine at various spark timings.* International Journal of Hydrogen Energy, 2015. **40**(13): p. 4707-4716.

107. Venkateswarlu, K., et al., *Modeling and fabrication of catalytic converter for emission reduction.* Materials Today: Proceedings, 2020. **33**: p. 1093-1099.

108. Brown, P.M., *Design of a Pilot Plant to Leach Platinum from Catalytic Converters.* Chemical Engineering Education, 1994. **28**(4): p. 266-268.

109. Cornejo, I., P. Nikrityuk, and R.E. Hayes, *The influence of channel geometry on the pressure drop in automotive catalytic converters: Model development and validation.* Chemical Engineering Science, 2020. **212**: p. 115317.

110. Akansu, S.O., et al., *Internal combustion engines fueled by natural gas—hydrogen mixtures.* International Journal of Hydrogen Energy, 2004. **29**(14): p. 1527-1539.

111. Bourn, G.D., J.W. Gingrich, and J.A. Smith, *Advanced compressor engine controls to enhance operation, reliability and integrity*. 2004, Southwest Research Institute (US).

112. Chandroth, G.O., *Diagnostic classifier ensembles: enforcing diversity for reliability in the combination.* 1999.

113. Gu, Z., et al., *Methods for large reciprocating compressor capacity control: A review based on pulse signal concept.* Chinese Science Bulletin, 2011. **56**(19): p. 1967-1974.

114. Williams, J.P., *Predicting process systems.* Hydrocarbon Engineering, 2001. **6**.

115. Vidian, F., D.H. Putra, and A. Kholis, *A short review and development of rope brake dynamometer for measurement of brake power on small scale engine.* Journal of Mechanical Engineering Research and Developments, 2020. **43**(2): p. 144-153.

116. Menon, S.K., *The scaling of performance and losses in miniature internal combustion engines*. 2010: University of Maryland, College Park.

117. Gierke, D., *Part 1: Dynamometer and Engine Performance Analysis.* Flying Models, 1973(6): p. 21-25.

118. Nightingale, C.R., *24 - Telecommunication power systems*, in *Telecommunications Engineer's Reference Book*, F. Mazda, Editor. 1993, Butterworth-Heinemann. p. 24-1-24-17.

119. Espadafor, F.J., J.B. Villanueva, and M.T. García, *Analysis of a diesel generator crankshaft failure.* Engineering Failure Analysis, 2009. **16**(7): p. 2333-2341.

120. Kock, F., et al., *The free-piston linear generator potentials and challenges.* MTZ worldwide, 2013. **74**(10): p. 38-43.

121. Goto, S., et al., *Development of free piston engine linear generator system part 2-investigation of control system for generator*. 2014, SAE Technical Paper.

122. Van Blarigan, P. *Advanced internal combustion electrical generator*. Citeseer.

123. Hanachi, H., et al., *A physics-based modeling approach for performance monitoring in gas turbine engines.* IEEE Transactions on Reliability, 2014. **64**(1): p. 197-205.

124. Rakopoulos, D.C., et al., *Effects of butanol–diesel fuel blends on the performance and emissions of a high-speed DI diesel engine.* Energy conversion and management, 2010. **51**(10): p. 1989-1997.

125. Verma, A., N.S. Dugala, and S. Singh, *Experimental investigations on the performance of SI engine with Ethanol-Premium gasoline blends.* Materials Today: Proceedings, 2022. **48**: p. 1224-1231.

126. Talikoti, B.S., S.N. Kurbet, and V.V. Kuppast, *A review on vibration analysis of crankshaft of internal combustion engine.* International Research Journal of Engineering and Technology (IRJET), 2015. **2**(02): p. 2395-0056.

127. Taghizadeh-Alisaraei, A., et al., *Vibration analysis of a diesel engine using biodiesel and petrodiesel fuel blends.* fuel, 2012. **102**: p. 414-422.

128. Ghemari, Z., S. Salah, and R. Bourenane, *Resonance Effect Decrease and Accuracy Increase of Piezoelectric Accelerometer Measurement by Appropriate Choice of Frequency Range.* Shock and Vibration, 2018. **2018**: p. 1-8.

129. Rao, S.S., *Mechanical vibrations fifth edition*. 2011.

130. Zhao, X., et al., *Real time identification of the internal combustion engine combustion parameters based on the vibration velocity signal.* Journal of Sound and Vibration, 2017. **390**: p. 205-217.

131. Gravalos, I., et al., *Detection of fuel type on a spark ignition engine from engine vibration behaviour.* Applied Thermal Engineering, 2013. **54**(1): p. 171-175.

132. Ghazaly, N.M., et al., *Prediction of misfire location for SI engine by unsupervised vibration algorithm.* Applied Acoustics, 2022. **192**: p. 108726.

133. Hickman, D.A., et al., *Development, Field Testing and Implementation of Automated, Hydraulically Controlled, Variable Volume Loading Systems for Reciprocating Compressors*. 2002. p. 1109-1117.

134. Shalev-Shwartz, S. and S. Ben-David, *Understanding machine learning: From theory to algorithms*. 2014: Cambridge university press.

135. Osisanwo, F.Y., et al., *Supervised machine learning algorithms: classification and comparison.* International Journal of Computer Trends and Technology (IJCTT), 2017. **48**(3): p. 128-138.

136. Badillo, S., et al., *An Introduction to Machine Learning.* Clinical Pharmacology & Therapeutics, 2020. **107**(4): p. 871-885.

137. Newton, J., *Analysis of microarray gene expression data using machine learning techniques.* CMPUT 606: Computational Molecular Biology and Bioinformatics, 2002.

138. James, G., et al., *An introduction to statistical learning*. Vol. 112. 2013: Springer.

139. MacQueen, J. *Some methods for classification and analysis of multivariate observations*. Oakland, CA, USA.

140. Hastie, T., et al., *The elements of statistical learning: data mining, inference, and prediction*. Vol. 2. 2009: Springer.

141. Ng, A., M. Jordan, and Y. Weiss, *On spectral clustering: Analysis and an algorithm.* Advances in neural information processing systems, 2001. **14**.

142. Jiang, T., J.L. Gradus, and A.J. Rosellini, *Supervised Machine Learning: A Brief Primer.* Behavior Therapy, 2020. **51**(5): p. 675-687.

143. Salian, I., *NVIDIA Blog: Supervised Vs. Unsupervised Learning.* The Official NVIDIA Blog, 2018.

144. Nasteski, V., *An overview of the supervised machine learning methods.* Horizons. b, 2017. **4**: p. 51-62.

145. Kotsiantis, S.B., I.D. Zaharakis, and P.E. Pintelas, *Machine learning: a review of classification and combining techniques.* Artificial Intelligence Review, 2006. **26**: p. 159-190.

146. Singh, A., N. Thakur, and A. Sharma. *A review of supervised machine learning algorithms*. in *2016 3rd International Conference on Computing for Sustainable Global Development (INDIACom)*. 2016.

147. Kotsiantis, S.B., I. Zaharakis, and P. Pintelas, *Supervised machine learning: A review of classification techniques.* Emerging artificial intelligence applications in computer engineering, 2007. **160**(1): p. 3-24.

148. Demšar, J., *Statistical comparisons of classifiers over multiple data sets.* The Journal of Machine learning research, 2006. **7**: p. 1-30.

149. Dong, J. and S.-x. Hu, *The progress and prospects of neural network research.* Information and Control, 1997. **26**(5): p. 360-368.

150. Jenkins, B.K. and A.R. Tanguay, *Handbook of neural computing and neural networks*. 1995, Boston: MIT Press.

151. Luo, Z., Y. Xie, and C. Zhu, *A study of the convergence of the CMAC learning process.* Acta Automatica Sinica, 1997. **23**: p. 455-461.

152. Balcázar, J.L., R. Gavalda, and H.T. Siegelmann, *Computational power of neural networks: A characterization in terms of Kolmogorov complexity.* IEEE Transactions on Information Theory, 1997. **43**(4): p. 1175-1183.

153. Setiono, R. and W.K. Leow, *FERNN: An algorithm for fast extraction of rules from neural networks.* Applied Intelligence, 2000. **12**: p. 15-25.

154. Krose, B., *An introduction to neural networks*. 1996.

155. Alpaydin, E., *Introduction to machine learning*. 2020: MIT press.

156. Gallant, S.I., *Neural network learning and expert systems*. 1993: MIT press.

157. Vapnik, V. and A.J. Lerner, *Generalized portrait method for pattern recognition.* Automation and Remote Control, 1963. **24**(6): p. 774-780.

158. Cortes, C. and V. Vapnik, *Support-vector networks.* Machine learning, 1995. **20**: p. 273-297.

159. Norouzi, A., M. Aliramezani, and C.R. Koch, *A correlation-based model order reduction approach for a diesel engine NOx and brake mean effective pressure dynamic model using machine learning.* International Journal of Engine Research, 2021. **22**(8): p. 2654-2672.

160. Norouzi, A., et al. *Machine learning-based diesel engine-Out NOx reduction using a plug-in PD-type iterative learning control*. IEEE.

161. Niu, X., et al., *Investigation of ANN and SVM based on limited samples for performance and emissions prediction of a CRDI-assisted marine diesel engine.* Applied Thermal Engineering, 2017. **111**: p. 1353-1364.

162. Mohammad, A., et al., *Hybrid physical and machine learning-oriented modeling approach to predict emissions in a diesel compression ignition engine*. 2021, SAE Technical Paper.

163. Aliramezani, M., A. Norouzi, and C.R. Koch, *Support vector machine for a diesel engine performance and NOx emission control-oriented model.* IFAC-PapersOnLine, 2020. **53**(2): p. 13976-13981.

164. Hoard, J. and L. Rehagen, *Relating subjective idle quality to engine combustion*. 1997, SAE Technical Paper.

165. Selamet, A., et al., *An experimental study on the effect of intake primary runner blockages on combustion and emissions in SI engines under part-load conditions*. 2004, SAE Technical Paper.

166. Somashekar, V., et al., *Vibration signature analysis of ic engine.* 2013.

167. Patil, N.A. and L.P. Raut, *vibration analysis of CI engine using FFT analyzer.* IJRET: International Journal of Research in Engineering and Technology, 2016.

168. Hassan, H.A., et al., *Integrated system to reduce emissions from natural gas-fired reciprocating engines.* Journal of Cleaner Production, 2023. **396**: p. 136544.

169. Toof, J.L., *A model for the prediction of thermal, prompt, and fuel NOx emissions from combustion turbines.* 1986.

170. Emiroğlu, A.O. and M. Şen, *Combustion, performance and emission characteristics of various alcohol blends in a single cylinder diesel engine.* Fuel, 2018. **212**: p. 34-40.